TlBr raw material purification, crystal growth, annealing, detector fabrication and characterisation for gamma-ray detector applications

Vasilij Kozlov

Laboratory of Inorganic Chemistry

Department of Chemistry

Faculty of Science

University of Helsinki

Finland

Academic Dissertation

To be presented, with the permission of the Faculty of Science of the University of Helsinki, for public criticism in Auditorium A110 of the Department of Chemistry, A. I. Virtasen Aukio 1, on March 12th 2010 at 12 o'clock noon.

Helsinki, 2010

Supervisor Prof. Markku Leskelä
Laboratory of Inorganic Chemistry
Department of Chemistry
University of Helsinki
Helsinki, Finland

Reviewers Prof. Stanislav Pospisil
Institute of Experimental and Applied Physics
Czech Technical University in Prague
Czech Republic

Dr. Keitaro Hitomi
Department of Electronics
Tohoku Institute of Technology
Japan

Opponent Prof. Juozas Vaitkus
Department of Semiconductor Physics,
Institute of Materials Science and Applied Research
Vilnius University
Lithuania

ISBN 978-952-92-6915-0 (paperback)
ISBN 978-952-10-6104-2 (PDF version)
http://ethesis.helsinki.fi

Yliopistopaino
Helsinki 2010

Abstract

The research reported in this thesis dealt with single crystals of thallium bromide grown for gamma-ray detector applications. The crystals were used to fabricate room temperature gamma-ray detectors. Routinely produced TlBr detectors often are poor quality. Therefore, this study concentrated on developing the manufacturing processes for TlBr detectors and methods of characterisation that can be used for optimisation of TlBr purity and crystal quality.

The processes under concern were TlBr raw material purification, crystal growth, annealing and detector fabrication. The study focused on single crystals of TlBr grown from material purified by a hydrothermal recrystallisation method. In addition, hydrothermal conditions for synthesis, recrystallisation, crystal growth and annealing of TlBr crystals were examined. The final manufacturing process presented in this thesis deals with TlBr material purified by the Bridgman method. Then, material is hydrothermally recrystallised in pure water. A travelling molten zone (TMZ) method is used for additional purification of the recrystallised product and then for the final crystal growth. Subsequent processing is similar to that described in the literature.

In this thesis, literature on improving quality of TlBr material/crystal and detector performance is reviewed. Aging aspects as well as the influence of different factors (temperature, time, electrode material and so on) on detector stability are considered and examined. The results of the process development are summarised and discussed. This thesis shows the considerable improvement in the charge carrier properties of a detector due to additional purification by hydrothermal recrystallisation. As an example, a thick (4 mm) TlBr detector produced by the process was fabricated and found to operate successfully in gamma-ray detection, confirming the validity of the proposed purification and technological steps. However, for the complete improvement of detector performance, further developments in crystal growth are required.

The detector manufacturing process was optimized by characterisation of material and crystals using methods such as X-ray diffraction (XRD), polarisation microscopy, high-resolution inductively coupled plasma mass (HR-ICPM), Fourier transform infrared (FTIR), ultraviolet and visual (UV-Vis) spectroscopy, field emission scanning electron microscope (FESEM) and energy-dispersive X-ray spectroscopy (EDS), current-voltage (*I-V*) and capacity voltage (CV) characterisation, and photoconductivity, as well direct detector examination.

Preface

The experimental work presented in this thesis was done in the Laboratory of Inorganic Chemistry at the University of Helsinki during the years 2000-2008. The work has been funded by the European Space Agency (ESA) and Finnish Research Programme for Space Research (ANTARES), and supported by the University of Helsinki, the Academy of Finland, the Finnish National Technology Agency (TEKES) and the Finnish Inorganic Materials Chemistry Graduate Program.

Firstly, I wish to thank my supervisor, Prof. Markku Leskelä, for the opportunity to work with him in the field of materials science, and for providing the topic for this research. His expert advice and guidance during the work gave new perspectives to my project. I am grateful to my co-workers from Oxford Instruments Analytical Oy (Finland) for their support and help in creating the TMZ installation and degassing system, and especially to Heikki Sipilä, Seppo Nenonen and Hans Andersson for fruitful talks, meetings and collaboration. Long term cooperation with Heikki Sipilä resulted in productive discussions with great impact on the experimental work.

I would also like to sincerely thank the entire personnel of the Inorganic Chemistry Laboratory for helpful discussions and technical assistance. Ilpo Mutikainen and Jarno Kansikas are acknowledged for their quick guidance and technical solutions for many problems. I'd like to express my gratitude to Marianna Kemell, Marko Vehkamäki and Mikko Heikkilä for their patient help in imaging with SEM, deposition of metallic electrodes and XRD 2Θ-Ω scan measurements, respectively. I'd like to also express appreciation to Jaana Valo for her interest in the topic and general discussions. I am especially grateful to collaborators from the Institute of Chemistry (Vienna, Austria) and particularly to Thomas Prohaska for performing the ICPMS measurements and trace element analysis. Vladimir Gostilo and his colleagues (Bruker Baltic, Latvia) are thanked for their cooperation with sample production and measurement of detector properties. I'd like to express gratitude to Igorj Lisitsky and his co-workers (GIREDMET, Russia) for supplying TlBr raw material and a series of samples, and to Pasi Kostamo (HUT, Finland) for fruitful collaboration.

Finally, I want to embrace my wonderful family, especially my wife Natalia, my children Irina and Peter, and our mummi – they all encouraged and gave me additional strength to perform this work. Also, many thanks to our dog Lordik, whose bright life and emotions charged me during the whole process of this work.

Espoo/Helsinki, 17 August 2009 Vasilij Kozlov

List of Original Publications

This thesis is based on 7 original publications, which are referred in the text by Roman numerals.

I V. Kozlov, M. Leskelä, T. Prohaska, G. Schultheis, G. Stingeder, H. Sipilä, *TlBr crystal growth, purification and characterisation*, Nucl. Instr. and Meth. A 531 (2004) 165 – 173.

II V. Kozlov, M. Leskelä and H. Sipilä, *Annealing and characterisation of TlBr crystals for detector applications*, Nucl. Instr. and Meth. A 546 (2005) 200 – 204.

III V. Kozlov, M. Leskelä, M. Kemell, H. Sipilä, *Effects of polishing and etching on TlBr single crystals*, Nucl. Instr. and Meth. A 563(1) (2006) 58 – 61.

IV V. Kozlov, M. Leskelä, M. Vehkamäki, H. Sipilä, *Effects of metallisation of TlBr single crystals for detector applications*, Nucl. Instr. and Meth. A 573 (2007) 212 – 215.

V V. Kozlov, M. Kemell, M. Vehkamäki, M. Leskelä, *Degradation effects in TlBr single crystals under prolonged bias voltage*, Nucl. Instr. and Meth. A 576 (2007) 10 – 14.

Va V. Kozlov, M. Kemell, M. Vehkamäki, M. Leskelä, *Erratum to "Degradation effects in TlBr single crystals under prolonged bias voltage" [Nucl. Instr. and Meth. A 576 (2007) 10–14]*, Nucl. Instr. and Meth. A 602 (2009) 625.

VI V. Kozlov, H. Andersson, V. Gostilo, M. Leskela, A. Owens, M. Shorohov, H. Sipila, *Improved process for the TlBr single-crystal detector*, Nucl. Inst. and Meth. A 591/1 (2008) 209-212.

VII V. Kozlov, H. Andersson, V. Gostilo, M. Kemell, P. Kostamo, M. S. Kouznetsov, M. Leskelä, H. Lipsanen, I. S. Lisitsky, M. Shorohov and H. Sipilä, *Improvements and problems of Bridgman–Stockbarger method for fabrication of TlBr single crystal detectors*, Nucl. Instr. and Meth. A 607 (2009) 126–128.

Related conference presentations by the same author

V. Kozlov, M. Leskelä, T. Prohaska, G. Shultheis, G. Stingeder and H. Sipilä, TlBr crystal growth, purification and characterisation, 5th International Workshop on Radiation Imaging Detectors, Riga, Latvia, 7-11 September 2003, Abstract Book, p. 50 (talk).

V. Kozlov, M. Leskelä, and H. Sipilä, Characterisation of TlBr crystals for detector applications, The 6th International Workshop on Radiation Imaging Detectors, Glasgow, Scotland, 25-29 July 2004, Abstracts, p.33 (talk).

V. Kozlov, M. Leskelä, M. Kemell, H. Sipilä, Effects of polishing and etching on TlBr single crystals, 7th International Workshop on Radiation Imaging Detectors, ESRF, Grenoble, France, 4-7 July 2005, Programme and Abstracts, p. 103 (poster).

V. Kozlov, M. Leskelä, M. Vehkamäki, H. Sipilä, Effects of metallization of TlBr single crystals for detector applications, 7th International Conference on Position Sensitive Detectors, University of Liverpool, 12-16 September 2005, Conference Programme, p. 21 (talk).

V. Kozlov, M. Leskelä, M. Kemell, M. Vehkamäki, Degradation effects in TlBr single crystals under prolonged bias voltage, 8th International Workshop on Radiation Imaging Detectors, Pisa, Italy, 2-6 July 2006, Programme and Abstracts, p. 37 (talk).

V. Kozlov, H. Andersson, M. Leskelä, H. Sipilä, Improved process for the detector grade TlBr single crystals, 2006 IEEE Room-Temperature Semiconductor Detector (RTSD) Workshop, October 30 - November 3, San Diego, CA, US, R06-27 (poster).

V. Kozlov, H. Andersson, V. Gostilo, M. Leskelä, M. Shorohov, H. Sipilä, A. Owens, Improved process for the TlBr single crystal detector, 9th International Workshop on Radiation Imaging Detectors, Erlangen, Germany, 22-26 July 2007, Abstracts, p. 42 (poster).

V. Kozlov, H. Andersson, V. Gostilo, P. Kostamo, M. S. Kouznetsov, M. Leskelä, H. Lipsanen, I. S. Lisitsky, M. Shorohov and H. Sipilä, Improved Bridgman-Stockbarger method for the TlBr single crystal detector, The 10th International Workshop on Radiation Imaging Detectors, June 29 - July 3, 2008, Helsinki, Finland, Abstract Book, p. 89 (poster).

Publications relevant to the current field of study

N. Darovskikh, E. I. Zabidarov, V. I. Kozlov, G. A. Krutov, A. I. Kurbakov, A. A. Loshmanov, E. E. Rubinova, V. A. Trunov, Investigations of monocrystalline structure perfections by means of a gamma-diffractometer, Preprint LINP, # 614, 1980. (rus)

V. I. Kozlov, A. A. Loshmanov, A. L. Malyshev, V. A. Trunov, V. A. Ulianov, The small-angle scattering of neutrons on the type A zeolite at its thermal destruction, Preprint LINP, # 862, 1983. (rus)

G. Gukasov, I. A. Zobkalo, V. I. Kozlov, V. P. Plakhty, Search for the effects of P-parity non-conservation in the crystals with the spiral magnetic structure, Preprint LINP, # 896, 1983. (rus)

V. I. Fedorov, A. G. Gukasov, V. Kozlov, S. V. Maleyev, V. P. Plakhty, I. A. Zobkalo, Interaction between the spin chirality and the elastic torsion, Physics Letters A 224 (1997) 372-378.

V. Kozlov, M. Leskelä, M. Kuznetsov, and I.S. Lisitsky, TlBr crystal characterisation using x-ray rocking curve method, 18th Nordic Structural Chemistry Meeting, Gustavelund Conference Center, Tuusula, Helsinki, Finland, 11-13 June 2004, Programme-Abstracts, p. P10 (poster).

P. Kostamo, M. Shorohov, V. Gostilo, H. Sipilä, V. Kozlov, I. Lisitsky, M. Kuznetsov, A. Lankinen, A.N. Danilewsky, H. Lipsanen, M. Leskelä, Characterization of TlBr for X-ray and γ-ray detector applications, Nucl. Instr. and Meth. A 607/1 (2009) 129-131.

List of Abbreviations

ΔG	Free energy of Gibbs
μ	Carrier mobility
τ	Trapping time constant
□Tl	Vacancy in Tl site of lattice
ATR	Attenuated total reflectance
CERAC	Trade mark of company
CHEMPUR	Trade mark of company
CSD	Compound semiconductor detector
E	Electric field
E μ τ	Mean drift length before trapping
EB	Electron beam
EDS	Energy-dispersive X-ray spectroscopy
Eg	Bandgap
EPR	Electron paramagnetic resonance
(FE)-SEM	(Field emission) scanning electron microscope
(FT)IR	(Fourier transform) infrared spectroscopy
FWHM	Full width at half maximum
GIREDMET	State Institute of rear earth metals (Russia)
HR-ICPMS	High-resolution inductively coupled plasma mass spectrometry
HSC	HSC Chemistry 5.1 for Windows, software
I-V	Voltage-current characteristics
KRS-5	Mixture of TlBr and TlI: Br (46%) and I (54%)[55]
mp	Melting point
ND	No data
PDF	Powder diffraction file
PTFE	Polytetrafluorethylen
SIMS	Secondary ion mass spectrometry
TMZ	Travelling molten zone
UV-Vis	Ultraviolet and visual spectroscopy
XRD	X-ray diffraction methods

Table of contents

1 Introduction

Among wide bandgap semiconductor materials single crystals of TlBr (2.68 eV) are the most promising for use in room temperature gamma-ray detectors.[1] The high stopping-power of its elements [Z_{eff} = (81+35)/2 = 58] and its density (7.56 g/cm^3) make it unique and suitable for space astrophysics, medicine and military applications. Unfortunately, TlBr is toxic and soft, and both these properties considerably impede the development of TlBr as single crystals. In addition, the use of TlBr crystals for gamma-ray detectors is still limited by the quality of this material.[2] Two characteristics of TlBr material, purity and crystal quality, which are attributes of gamma-ray detectors,[3] are still far from perfect.[I, II]

The aim of this thesis was to obtain the single crystals of high-purity and highest crystal quality, which were suitable for X-ray and gamma-ray detection. When the experimental work of this thesis was started, TlBr detectors were known to perform poorly, and their mobility-lifetime products ($\mu\tau$) were still impurity limited.[4] Therefore, optical grade material, which is purified by commonly used methods, crystallisation from vapour and melt, was firstly applied for gamma-ray detectors. However, the produced detectors showed low performance,[I] because material aimed for optics is not good enough for radiation detectors.[51] The purity of TlBr could be improved in the zone refining process, since increasing the number of refining passes from 20 to 50, increases resistivity and $\mu\tau$ by an order of magnitude.[5] On the other hand, the performance of TlBr material purified by 200-300 passes has been limited by crystal imperfections that probably is originated during crystal growth or/and detector fabrication.[6] Thus, purity and crystal quality of TlBr are the most important problems in the detector manufacturing process.

Two basic concepts were used in this thesis for solving these problems. For purification, in addition to traditional methods used for obtaining optical grade materials, the crystallisation from water solutions was applied. The basis of this is that TlBr samples produced by melt methods and from water solutions were different with respect to impurity composition, and removing soluble components was effective in pure water.[I] For crystal quality improving, the annealing was used during the manufacturing process, because TlBr as extremely soft material easily became damaged and contaminated.

Different methods were used for the preparation of high-purity TlBr material and single crystals made from it. Since TlBr is sparingly soluble in water, the hydrothermal conditions were applied. In general, the use of the hydrothermal method for synthesis, recrystallisation,

crystal growth and annealing is innovation for TlBr, the details of which are considered in corresponding chapters.

This thesis consists of 7 publications and a summary text, in which the factors affecting the purity of the TlBr material, crystal quality, and detector performance were studied. In paper I, TlBr single crystals of different origins were studied by trace element analysis, and hydrothermal methods were for the first time used for purification purpose. In paper II, different types of annealing were used to improve the crystal quality of TlBr crystals; and annealing effects on the electrical, optical and X-ray response properties were studied as well. The effect on crystal quality of mechanical and chemical treatments, which are typically used for detector fabrication, was studied in paper III. Different electrode materials and their roles in TlBr-metal interfaces were described and examined in paper IV. Degradation of TlBr devices and their electrical stability under prolonged bias voltage were studied in paper V.

The results of papers I-V were used in improvement of the total process for the TlBr single-crystal detector, as it was reported[77] and described in paper VI. The complete improvement of detector performance was shown to require further developments in crystal growth of TlBr. Several improvements in Bridgman-Stockbarger method and corresponding failures in detector performance were discussed and analysed in paper VII.

The summary text of the thesis is organised as follows. In chapter 2 Background, the properties of Tl halides and general information relevant to gamma-ray detectors are considered and reviewed. TlBr purity and crystal quality are the most important characteristics for room temperature gamma-ray detectors. Therefore, in this work special attention has been paid to these qualities during TlBr purification, crystal growth and annealing (chapter 3), as well, during detector fabrication (chapter 4). These characteristics are also followed and treated in chapter 5, where instrumental methods used for optimisation of the total manufacturing process are summarised. The summary text does not contain separate chapters for literature review and experiments. These topics are included in the other chapters. The results of the work and view to the future developments and applications of TlBr single crystal detectors are presented in chapter Conclusion.

2 Background

2.1 Chemical properties

Several specific features of the element thallium influence the chemical behaviour of TlBr during the detector manufacturing process, and they are considered below.

2.1.1 Electronic configuration and oxidation states of thallium

As expected from the electronic configuration (s^2p^1) of elements in Group 13, the great majority of the compounds of Group 13 elements contain the element in oxidation state 3+. However, the univalent state becomes progressively more stable as one descends down the group[7a] and Tl(I) compounds are numerous.[7c] For thallium chemistry the Tl(I) – Tl(III) relationship is a dominant feature.[8] This phenomenon is associated with the so-called Sidgwick *inert electron pair* effect.[9] The term refers to the resistance of a pair of s electrons to participation in covalent bond formation,[8] and is much more pronounced for the heavier $6s^2$-elements Hg, Tl, Pb and Bi, which form stable compounds with an oxidation state two units less than would be expected. A more complete discussion of the *inert electron pair* effect is given in Ref.[10a] For thallium, the 6s-shell stabilises Tl(I) compounds, which often resemble the corresponding compounds of the alkali metals.[7c]

Although the oxidation state 3+ is less stable for thallium than for higher members of Group 13, when all three electrons of thallium are used, the bonding is always covalent.[7b] When the ionic character is pronounced for Tl(I) compounds, the impurity-admixture of oxidation state 3+ should be considered as well. For example, when oxygen, nitrogen, or sulphur bind to organic groups and also to Tl(I), the Tl-X bond appears to be more covalent than the bond to alkali metal ions in similar compounds.[8b]

In solutions, complexation increases the probability of the Tl^{3+} state. As expected from the high positive value of the redox potential (see Eq. 1), the Tl^+ state is quite stable in aqueous solutions. However, the potential decreases to +0.770 V in 1M HCl solution, due to the presence of the complexing anion Cl^-, which stabilises Tl^{3+} more than Tl^+.[8b]

$$Tl^{3+} + 2e = Tl^+, +1.26\ V \text{ in } 1M \text{ of } HClO_4 \qquad \text{(Eq. 1)}$$

The next trend influencing the Tl^+/Tl^{3+} ratio in aqueous chemistry is the extensive hydrolysis of Tl(III) ion to $TlOH^{2+}$, from which it becomes the colloidal oxide even at pH values from 1 to 2.5.[8b] In this work, the hydrolysis of Tl(I) was studied under hydrothermal conditions. A black precipitate of Tl_2O_3 formed easily in alkali solutions (see Fig. 1). The reaction was found to be favoured by increasing the temperature and/or pH. The minimum pH

value at which the black traces were found under the microscope was ~7.08 after hydrolysis at 180°C.

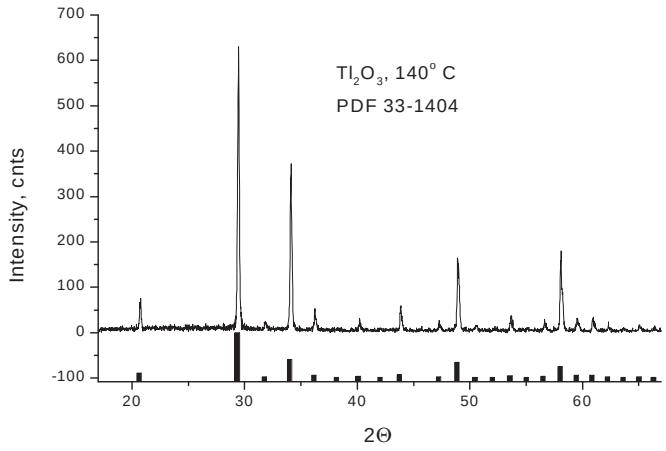

Fig. 1. X-ray powder diffraction pattern of the black material formed by hydrolysis of TlBr at 140 °C, shown by solid line, and reference pattern of Tl_2O_3 (PDF 33-1404), shown by bars.

Thus, the formation of the Tl(III) compound in Tl(I) aqueous solution is possible due to complexation or hydrolysis. Separate Tl(III) compounds or Tl^{3+}-ions can consequently be incorporated into the Tl(I) compound as impurities. Both mechanisms should be taken into account during synthesis, purification and crystal growth of Tl(I) compounds in water solution.

2.1.2 Tl(I) chemistry

The chemistry of the Tl(I) ion is briefly summarized based on Cotton.[8b] In crystalline salts, the Tl^+ ion is usually 6- or 8-coordinate. The colourless Tl^+ ion has a radius of 1.54 Å, which, when compared to the radii of K^+, Rb^+ and Ag^+ (1.44, 1.58, and 1.27 Å), explains why Tl(I) chemistry resembles that of both the alkali and silver ions. Thus, the Tl(I) hydroxide is readily soluble in water to give strongly basic solutions that absorb carbon dioxide from the air, like alkali. Many Tl(I) salts (for example, cyanide, nitrate, carbonate, sulphate, phosphates, perchlorate and acetate) are isomorphous with the corresponding alkali salts, although their solubilities are somewhat lower. In other salts, such as the chromate, sulphide and halides (except for the very soluble TlF), which are sparingly soluble in water, the Tl(I) ion resembles Ag^+. For example, TlCl darkens on exposure to light. However, unlike AgCl, TlCl is insoluble in ammonia.

The photosensitivity of Tl is used in scintillation radiation detectors, which are made from alkali halide crystals. Incorporation of Tl(I) halides into alkali halides gives rise to new absorption and emission bands, thus, salts activated with thallium become phosphors. The NMR signals of Tl(I) and Tl(III) are readily detected both in solutions and in solids. The resonances are very sensitive to the environment and have large solvent-dependent shifts. For Tl^+ it is possible to correlate shifts with solvating ability.

2.1.3 Tl(I) – Tl(III) mixed halides

Thallium (I) halides are quite stable. Tl(III) compounds are reduced to Tl(I) compounds in solution and decompose with heating. However, thallium readily gives rise to intermediate compounds which contain both Tl(I) and Tl(III).[11a] The action of bromine and chlorine on the Tl(I) halide yields the Tl(III) compound, but well-defined intermediate compounds may be isolated, as shown in Eq. 2:

$$Tl(I)\,[Tl(III)A_4] = 2\,TlA_2 \text{ and } Tl(I)_3\,[Tl(III)A_6] = 2\,Tl_2A_3, \qquad \text{(Eq. 2)}$$

where A is Cl or Br.[7d] Bromine gives these type of compounds more easily than chlorine. The tri-iodide compound, however, is $Tl(I)I\cdot I_2$, but in water solution there is an equilibrium between two isomeric forms of the tri-iodide: $Tl(I)\,[I\cdot I_2] <=> Tl(III)\,[I]_3$.[11b] Therefore, the formation of intermediate compounds can occur in Tl(I) halides if oxidant impurities are present or can be formed during synthesis, purification or crystal growth from the vapour or molten state.

2.1.4 Tl(I) halides and impurities

One of the most important impurities in Tl halides is thallium itself which has been oxidized during processing by the mechanisms described above. The oxidation can occur due to environmental conditions, tools and materials used, or oxidant impurities present during processing. The oxidised impurity can be in the form of a Tl(III) substance or Tl(I)-Tl(III) intermediate compound, or the Tl^{3+}-ion can be directly incorporated in a host lattice. If a Tl(III) compound decomposes, the corresponding compound of Tl(I) contaminates the thallium halide, as in case of Tl_2O_3, which is reduced to Tl_2O during thermo-treatment.

A second source of impurities is the substitution of ions in the host lattice. Ions, which are in the same oxidation state and with a radius similar to that of the ion they are replacing, substitute easily for each other, since they produce less distortion of the lattice. Thus, the Tl^+-ion, which has radii of 1.50 Å in NaCl-type or 1.59 Å in CsCl-type lattices[34b], can be replaced by alkali, silver (see 2.1.2) and ammonium ions. Tl^+ is a rather large ion and many other cations can occupy its place. Substitution with ions in other oxidation states also inserts

vacancies because electro-neutrality must be maintained. For example, one Cd^{2+}_{Tl} $\square_{Tl}$ Br^{-}_{2} substitutes for two TlBr. Halide anions can substitute for each other, which is a serious purity problem for Tl halides. Since Cl^{-}, Br^{-} and I^{-} anions are large ions with the radii of 1.81 Å, 1.96 Å and 2.2 Å,[34b] respectively, many other anions and molecular groups can be incorporated into the halide lattice.[12] Impurity phenomena and theoretical explanations based on molecular vibrations in crystals have been considered by Decius and Hexter.[13a]

The next source of impurities is the processing of a Tl halide in water solutions, where insoluble compounds contaminate it. The elements of insoluble halides are located near one another in the periodic table and act similarly chemically, particularly if their oxidation states are the same.[14] In Table 1, the solubilities of the halides decrease in the order Cl > Br > I. Sn,[15b] Sb and Bi[15c] halides are hydrolysed in dilute solution. If Si and W impurities are present in acidic dilute solutions of halides, silicic $Si(OH)_4$ and tungstic H_2WO_4 insoluble acids can precipitate.[14] Thus, in Tl halide obtained from solutions the possible impurities are AgX, Hg_2X_2, PbX_2 halides (where X – halide-anion), oxy-halides of Bi and Sb, and hydroxides of Si and W. The other elements considered in Table 1 will precipitate from solution only under specific conditions.

Table 1. A portion of the periodic table of elements, showing metals which form insoluble halides. The underlined elements have a tendency to be in oxidation state 2+, halides of which are only slightly insoluble. Elements in parentheses are normally present in the oxidation state whose halides are soluble or form complexes. Insoluble chlorides of elements in oxidation state 1+ are shown in grey.[14]

			(Cu)					
(Ru)	(Rh)	(Pd)	Ag				Sn	Sb
(Os)	(Ir)	(Pt)	(Au)	Hg		Tl	Pb	Bi

Therefore, during processing of Tl halide, impurities can be easily incorporated or Tl(I) can be partly oxidised to the Tl(III), and both processes cause a deviation in the stoichiometry of the compound. Non-stoichiometry is a problem in Tl halides, since it influences conductivity of the material[16] and, in turn, detector performance. Carefully maintaining the proper conditions and the use of clean room techniques preserves the stoichiometry and purity of the compound. In addition, all thallium compounds are highly toxic. They cause damage to the nervous system and digestive organs[11a] and in trace amounts cause loss of hair.[15a]

2.2 Physical properties

In the field of the detection of the hard X- and gamma-ray radiation, Tl halides are attractive as materials for gamma-ray detectors because of their physical properties, see Table 2. A wide bandgap of Tl halides (~3 eV) makes them as potential room temperature detectors.

Table 2. General properties of Tl halides

General properties	TlCl	TlBr	TlI	Ref.
Lattice parameter, Å	3.834	3.97	4.18*	11a
Melting point, ºC	431	460	442	175a
density ρ, g cm^{-3}	7.00	7.557(17.8º)	7.09	38a
solubility product constant, 25 C	1.86 x 10^{-4}	3.71 x 10^{-6}	5.54 x 10^{-8}	34a
Optical transparency				
Vis-IR edges, μm	0.38-36	0.44-48	0.56-60**	44d
Defect formation	**energy**			
by Schottky, eV	0.79	0.69	0.64	89
by Frenkel, eV	1.55	0.86	0.21	89

* yellow rhombic α-form exists below 168ºC
** data given for KRS-5: mixture of TlBr (46%) and TlI (54%)[55]

Tl halides form simple TlX compounds (where X – halide-anion) with a cubic CsI-type lattice. They have relatively low temperatures of melting that facilitate the single crystal growth from melt. Both the high stopping-power of Tl (Z=81) and density of its halides allow to make compact detection devices with high efficiency of radiation absorption. TlI has stopping-power higher than TlBr and TlCl [$Z_{eff} = (Z_{Tl}+Z_{Hal})/2$ is equal to 67, 58 and 49, respectively], but this compound transfers from cubic to rhombic form below 168ºC that impedes its crystal growth from the melt. All halides (excluding fluoride) are sparingly soluble in water that makes easy manipulations with them. The thallium halides are widely used in optical elements for IR devices[44g] due to their transparency over a wide spectral range, and are actively studied as promising materials for fibre IR waveguides because of their low transmittance loss and softness permitting easy extrusion.[45] The optical properties of TlBr are known to be used in scintillation detectors.[40, 41, 42, 43]

2.2.1 History

Thallium halides have been known since the early days of photography due to their photosensitivity to light, and only their toxic character prevented their use as photographic material. Lehfieldt (1933) studied the electrical conductivity of single crystals of alkali halides, AgCl, AgBr, TlCl and TlBr,[17] and the photo-conducting properties of silver and thallium halides, and found many similarities between them.[18]

A halide crystal counter was first described in Van Heerden's dissertation[19] (1945), which showed that silver chloride crystals at low temperature may detect gamma rays and α- / β-particles. Hofstadter[1] (1947), knowing about Lehfieldt's work, then extended Van Heerden's work to the Tl(I) halides. He found that, if mixed crystal $TlBr_{0.4}I_{0.6}$ (~KRS-5) was properly prepared and annealed, it was able to detect gamma-radiation of Ra. He suggested the same result for pure thallium bromide and thallium iodide. In 1949 Hofstadter published his work on crystal counters using theoretical approaches[20] to experiments with halide crystals.[3] At that time, halide compounds were thought to be the most promising materials for gamma-ray detection, and nobody understood that the elemental semiconductors (Si and Ge) were available for this purpose.

During the same time, in the field of semiconductor physics, Bardeen and Brattain (1948) discovered the Ge transistor[21] and described the nature of its contacts,[22] and Shockley and Pearson[23] considered theoretically and studied experimentally conductance modulation by surface charges. In 1949 McKay[24] used Bardeen and Brattain's results for making a barrier layer in germanium and very successfully measured α-ray pulses of Po. During the further rapid development of the Ge and Si semiconductor industry, in fact, they were anticipated to be primary radiation detectors.[2] The compound semiconductors, such as the alkali-metal halides, CdTe, CdZnTe and HgI_2, received very little attention until the 1960s.[25]

At that time the optics industry was developing Tl halide materials for IR and night vision devices. Therefore, optical transmittance and clarity were the main parameters for optimization, for which other characteristics, such as purity and crystal quality, were sacrificed. After the 1960s, progress in fabrication of compound semiconductor detectors (CSDs) has been incremental.[26] Nowadays, with regular missions into space, studies of the universe generated the problem of cosmic ray detection without the use of special cryogenic systems. As a result, attention once again turned to wide bandgap CSDs. CdTe, CdZnTe and HgI_2 radiation detectors were made commercially available; however, the individual devices were mostly restricted to small sizes.[26] Such quality factors as micro-crystallinity, high defect densities, purity and stoichiometric imbalances considerably limited the carrier transport properties of compound semiconductors.[2]

For future planetary and astrophysics missions, the development of high-resolution imaging X-ray spectrometers is needed. Silicon-based imaging detectors are already well developed, but their efficiency is limited in practice to 20 keV.[27] Therefore, the search for and improvement of CSD materials for the energy range 30-500 keV and higher, and for

specialized applications in which Ge, Si or scintillation detectors are unsuitable, is a current task for CSD development.

2.2.2 Criteria for the compound semiconductor as a gamma-ray detector

Since Hofstadter's work,[3] many researchers have formulated the requirements for materials to be used as gamma and X-ray detectors. The material characteristics[28] are restricted by the type of radiation, detector construction, and limitations of measuring techniques. The detection of various types of radiation by CSDs has been carefully considered in the classical works of Dearnaley[29] and Bertolini.[30] There are several reviews[25, 31, 32] of materials for radiation detectors at elevated temperatures, from which some general criteria for CSDs are summarised in Table 3.

Prince and Polishuk emphasised that a CSD should be a large uniform single crystal without polarisation effects, and that the mobility-trap time product $\mu\tau$ should be stable over operating temperatures. Among other features, they mentioned that a detector has to be low cost, reproducible, reliable, and resistant to environmental conditions, with the 1st stage of a preamplifier being included with the detector's package.[25] The CSD must be capable of operating in the energy range 50 – 100 keV and have about 2% FWHM resolution.[31]

Table 3. Material and device requirements for gamma-ray CSDs to be used at elevated temperatures.

Evaluation parameter	(1967)[25]	(1968),[30] (1975)[32]
Depletion depths	> 1mm	
Active area	> 1 cm^2	
Thickness	…	~2 mm
Material	high Z	Z~40
Bandgap E_g, eV	> 1.3	~1
Min carrier mobility μ, $cm^2/(V\ s)$	100	100
$\mu\ \tau$, cm^2/V	10^{-5}	
Ionised dopant density, cm^{-3}	$< 10^{12}$	$\leq 5x10^{11}$
Trapping centre density	…	$\leq 5x10^{12}$ cm^{-3}
Temperature range, ^oC	-50 to 300	
Contacts	non-injecting	non-injecting
Noise	Noise free	
Leakage current	$< 10^{-5}$ A	

In a simplified model of CSD in Fig. 2, a planar detector is operated by applying a voltage across contacts on opposite sides of the device. Ionising radiation (gamma rays or charged particles) produces at the absorption point a compact plasma cloud of the excited electron-hole pairs in proportion to the energy of the radiation deposited in the detector. For a period of time known as the *plasma time*, the plasma is inactive under the applied voltage, since any

opposite movements of electrons and holes are blocked by the appearance of an opposite inner electric field. The delay effects are generally decreased by an increase in the electric field.[32] During the second stage, the plasma cloud is enlarged by diffusion and split by the electric field to give free electrons and holes. These free charges then drift through the applied electric field, creating an induced charge at the terminals of the device. The charges formed by radiation are collected during this stage, and completeness of the collection determines the efficiency of the detection. Unfortunately, impurities and imperfections in a crystal lattice catch the carriers (both electrons and holes), then free them up. The uncertainty of the trapping and de-trapping events decreases the collection efficiency and the energy resolution.

This model shows that the material must to be of highest purity and crystal quality in order to minimise the trapping effects. In general, the collection efficiency is related to the $E\mu\tau$ product, which is often associated with the mean drift length before trapping. For a given material, an electric field E is limited by coronal breakdown.[31] Both the carrier mobility (μ) and lifetime (τ) terms, reflect the quality of the crystal. In this regard, the most useful figure of merit when comparing compounds is the mobility-lifetime product $\mu\tau$.[2]

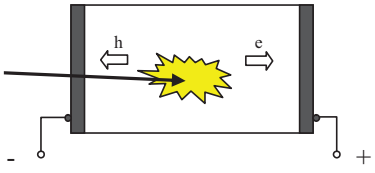

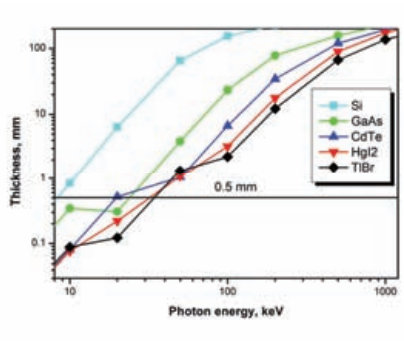

Fig. 2 (left). Formation of the plasma cloud by adsorption of a gamma quant or charged particle (density of electron and hole pairs on the order of 10^{-19} cm^{-3} for α-particles[32]), expansion of the cloud and the split to give free electrons (e) and holes (h).

Fig. 3 (right). Depth of various wide bandgap materials and Si for attenuation of 1000 (ratio of incident and passed photon radiation). Data calculations are based on Ref.[169] and attenuation coefficients of elements for photons of different energies.[34d]

For CSDs, the mobility-lifetime products for electrons are several orders of magnitude lower than those for elemental semiconductors. The product $\mu\tau$ for holes is worse yet by at minimum one order of magnitude, and therefore, the value of $\mu\tau_h$ for holes characterises the quality of the material and is often used in physicochemical considerations of CSDs.[33] Hence for minimisation of trapping, crystal thickness is decreased in order to achieve the mean drift

length of holes. For example, a thin crystal and a high electric field were used in the first Ge detector.[24]

Thus, the quality of the material limits the maximum detector thickness, which is determined by the mean drift length of holes. For many wide bandgap materials, a thickness of 0.5 mm is mostly technically attainable. On the other hand, the attenuation of radiation depends on material thickness (h) as $\exp(-\mu\rho h)$, where μ is the mass attenuation coefficient and ρ is material density. The attenuation efficiency of wide bandgap materials has been evaluated by several authors.[6, 35, 36] Plotted for a thickness of 0.5 mm it increases from Si to GaAs, CdTe, HgI_2 and TlBr.[176] The depths of these high-Z materials presented in Fig. 3 as a function of a photon energy at fixed 1000-fold attenuation show that the 0.5-mm thickness limit should be considerably increased for hard X- and gamma-rays. Thus, improved quality of materials is needed in order to make detectors of high energy photons.

The next problem is connected to the energy bandgap E_g: CSDs with a larger bandgap have lower dark current and higher spectroscopic resolution,[37] but they tend to have relatively small carrier mobilities due to greater polar lattice carrier scattering.[31] For room-temperature radiation CSDs, the lower limit for E_g is set to ~1.4 eV, since in materials with a smaller bandgap the carriers are thermally generated at room temperature. The highest bandgap is set to ~3.5 eV, since for larger bandgap materials an increase in energy is required for the electron-hole formation. Larger E_g values may also allow large values for the electrical resistivity (R), allowing the application of larger electrical fields (E). However, in CSDs the value of R itself depends additionally on stoichiometry, purity and the possible mixed oxidation state of the metal in the compound, for example in halides of Tl^+ and Tl^{3+}, Pb^{2+} and Pb^{4+}, and Hg^+ and Hg^{2+}. [33]

In a recent review on compound semiconductor radiation detectors, various wide bandgap materials and the influence of their characteristics on detection and detector performance are summarised and analysed.[2] The wide bandgap is important for space astrophysics because it allows device operation at near room temperature using a Peltier cooler. Among wide bandgap semiconductor materials, single crystal TlBr (2.68 eV) was chosen for the current work. The high stopping power and density[38a] of TlBr make this material the leader among other materials in completeness of gamma-ray absorption, as it is shown in Fig. 3. Both these properties could be utilised in the kinds of compact and mobile devices that are needed for express analysis and military applications. Moreover, the completeness of absorption could decrease the dose deposited in a patient during X-/ gamma-ray medical courses. The recent achievement of an inter-pixel resistance of ~500 GΩ with a gap of 100μm between the

electrodes at 50V in a small-format TlBr array[39] makes TlBr an attractive material for manufacturing a compact 2D-array detector in the field of hard X-ray imaging spectroscopy. The high transparency of TlBr over a wide spectral range is utilised as well in this field, and several scintillation and photo detectors using TlBr have been successfully manufactured.[40, 41, 42, 43] Therefore, TlBr is a promising material for X-ray and gamma-ray room temperature detectors, with many potential applications.

2.2.3 Quality of industrial TlBr

As noted previously, the quality of Tl halides was improved for decades to enhance optical transmittance. Tl halides transmit light over a wide range of visible and IR spectra (Table 2). The short wavelength boundary has been found to be dependent on bandgap (E_g) of the material, and long wavelength transmittance is limited by vibrations of the crystal lattice.[44b] Attenuation and scattering losses have been studied in optical fibre materials[45, 46, 47] since these losses are, for example in KRS-5, three orders of magnitude above the intrinsic bulk absorption at 10 μm.[47] The losses have been associated with impurity absorption[45] and as well with residual strain resulting from the manufacturing process.[46] The most rational parametrisation and numerical estimations of this problem have been done by Lines.[48, 49]

Experimental absorption coefficients in the long wavelength region are some what higher than expected based on theory. When an impurity is built into the host lattice, scattering of phonons increases, as a result, the attenuation of light enlarges with increasing impurity content. When the concentration approaches the limit for a given impurity, its further increase causes the formation of inclusions as a separate phase. At this stage, since local tension occurs around the inclusions, the built-in impurities are forced out from lattice positions into the area with higher tension. The lattice becomes more perfect and its absorption coefficient decreases, but now Rayleigh scattering takes place on the inclusions.[44c] Further increasing the impurity concentration produces visual effects and even degradation of the material.[50] More details about impurity effects and annealing are given in chapter 3.4.

Since the equilibrium between the amount of the impurity in the lattice and the formation of inclusions depends on temperature, thermal treatments of the host material are optimised for given impurities in order to maximise the optical transmittance.[44c] Instead of developing methods of material purification, this method is used in the industry for improving clarity of Tl halide optics. For example, several TlBr crystals used in our studies were grown with a temperature drop of about 100 degrees between liquid and solid phases.[51] These crystals

preserved the excess of impurities frozen in the lattice in a meta-stable state. More details about these crystals are given in chapter 3.3.2.2.

In general, TlBr crystals produced for optics do not fit to requirements of gamma-ray detectors because of impurities frozen in the lattice and strains caused by high temperature gradients during the solidification. TlBr purity and crystal quality are the most important characteristics for room temperature gamma-ray detectors, see chapter 2.2.2, above. In this work special attention was paid to these qualities and they were studied during TlBr purification, crystal growth and annealing as well during hydrothermal and aging treatments, as described in next chapter 3.

3 TlBr purification, crystal growth and annealing

3.1 TlBr raw material

Thallium halides are sparingly soluble in water (see Table 2), so the easiest way to obtain halides is a precipitation reaction between the cation Tl^+ and a corresponding anion A^-: $Tl^+ + A^- \Rightarrow TlA\downarrow$.[7a] With water solutions the method is quite flexible and widely used in industry. Soluble sulphate and nitrate of thallium are conventionally combined with a salt or acid of the corresponding halide. However, the routine operations removing by-product ions of the mother solution, such as a decantation or a filtration, are not sufficient for the production of optical grade material, because during the precipitation, thallium halides easily capture impurities of Ag, Pb, Cu and Cd.[52a] Water itself as an impurity influences the properties of Tl halides,[53] therefore, synthesis methods are often classified as “wet” or “dry” based on the presence or absence of water.

3.1.1 Wet method

In order to improve optical properties of Tl halides, it has been recommended that reagents of maximum purity be used for synthesis, for example, electrochemical grade Tl and its nitrate as precursors for the precipitation reaction.[52a] In the case of a reaction with acid, excess acid should be neutralised, for example, by alkali solution, but this increases the possibility of hydrolysis of Tl^+ to Tl^{3+} in subsequent operations, as described in chapter 2.1.1. The stability of TlBr detectors is a current problem, therefore the aging and precursor effects on stability of TlBr raw material were studied in this work.

3.1.1.1 Aging effects

Oxygen-containing anion impurities affect the properties of Tl halides and even cause visual degradation of the material.[53, 54, 50] The changes in optical attenuation with age are correlated with the physical properties of the material.[55] The prolonged decomposition of KRS-5 fibres under various environmental conditions has been studied using SIMS depth profile, powder neutron and X-ray diffraction, IR spectroscopy and EPR methods.[56] For aging over a two year period, illumination and darkness, and helium, argon, hydrogen, ammonia and air atmospheres, and also vacuum were used. The most common impurities were found to be H, C, N, O, Na, Mg, Al, Ca, Cu, Cl and Tl oxide. A high amount of hydrogen was confirmed as well by neutron scattering, and based on EPR data, the authors suggested that this impurity exists in the form of water. The annealed sample kept in a vacuum in the dark was found to undergo degradation to a lesser extent than other samples.[56]

Aging effects were observed as well in this work when commercial TlBr powder changed its colour from yellow to dark-red for several years. In Fig. 4, the powder diffraction patterns indicate the formation of new phases and the growth of their reflections during aging. The identification of extra peaks was difficult due to possible formation of intermediate compounds.

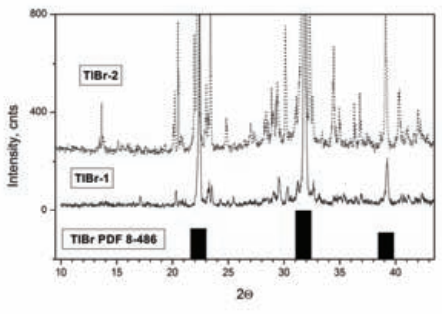

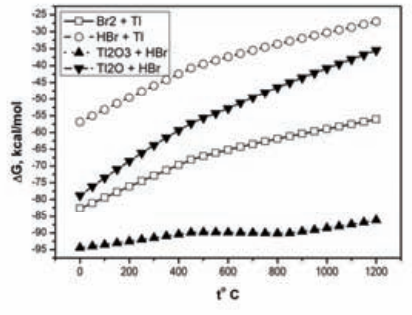

Fig. 4 (left) TlBr (CHEMPUR-99,999%) stored in the laboratory for ~2 years (TlBr-1, solid line) and ~4 years (TlBr-2, dotted line, offset 200 cnts), and reference pattern of TlBr (PDF 8-486), shown by bars.

Fig. 5 (right) Free energy ΔG for TlBr formed by reactions between Tl and Br_2 (open squares), Tl and HBr (open circles), Tl_2O_3 and HBr (solid triangles up), and Tl_2O and HBr (solid triangles down). The free energy ΔG was evaluated using HSC 5.1 software.[57]

3.1.1.2 Precursor effects

In order to elucidate the role of precursor in the process of ageing, soluble compounds of Tl, namely the carbonate, nitrate and sulphate, were chosen for precipitation reactions of TlBr. The Tl/Br ratio was varied from 1/5 to 5/1. All freshly precipitated products had a bright

yellow colour and their powder diffraction patterns were similar to that of TlBr, PDF 8-486. The powder products were stored in daylight, under both dry and wet conditions in laboratory atmosphere for about a month. They were annealed up to 200° C and, additionally, irradiated by UV-light under wet and dry conditions. No visual effects were observed in the case of samples produced from sulphate and nitrate. The product made from Tl carbonate became reddish after one month at laboratory conditions. Its powder diffraction pattern was similar to the TlBr-1 pattern shown in Fig. 4.

On the other hand, nitrate anion is a powerful oxidizing agent, and in hydrothermal experiments with $Ba(NO_3)_2$ the oxidation of Tl^+ to the oxide of Tl^{3+} has been observed. Therefore, in this thesis Tl sulphate was chosen for the synthesis of raw material by the hydrothermal method (see chapter 3.1.4). The sulphate anion has additional advantages that it can be found out by IR-spectroscopy (see chapter 5.2.1) and the sulphur content can be determined by ICP-MS.[I]

3.1.2 Dry method

Several possibilities for synthesis of TlBr using a waterless technique are illustrated in Fig Fig. 5. TlBr is obtained from Tl or its oxides using dry Br_2 or HBr. These reactions are thermodynamically favourable ($\Delta G < 0$) over a wide temperature range. A direct reaction between Tl metal and a halogen takes place at ordinary temperatures[11a] and produces a Tl halide material of low water content. If the thallium has been in air and corroded, the use of dry HBr is preferable, since impurities of thallium oxides can be avoided. An interesting setup for a direct reaction is used in GIREDMET (Russia), where bromine gas passes throughout the molten thallium (melting point 302 ^oC, density ~11.85[38a]) at a temperature slightly more than the melting point of TlBr (460° C). The product TlBr is collected from the Tl surface.

The dry method protects the product from water and ionic impurities that are typical for water solutions. However, Tl halides made by a dry method may contain oxides of Si, B, Na(K), Al, Zn, Ba, Ca, Pb, P and other elements that are characteristic of the material used for crucibles and glass.[58a] The purity can be improved by the sealing the reagents in optical quartz, but this limits the size of the batches to ampoule dimensions.

3.1.3 Method selection

In a dry method the limiting factor is the amount of product that can be made in one batch. This is restricted by the size of the corresponding reactor. Another disadvantage is the complicated apparatus needed for waterless purification of halogen or hydrogen halide gases.[59]

Thallium halides produced by wet methods are basically less clean than those made by dry methods. For example, removal of mother solution from the powder product includes filtration, decantation, washing and rinsing with pure water and organic solvents, then drying and re-loading. These routine operations that take away by-product ions add the impurities associated with ambient conditions (for example, dust) and instruments used. A second source of impurities is the precipitation process.[60] During the mixing of reagents, super-saturation with respect to solubility is created locally and randomly over the solution. Here, amorphous particles containing solution are formed in a local excess of ions. This charged and non-structured phase easily adsorbs by-product ions of the mother solution and other impurities. During nucleation the impurities are incorporated into the solid, and further crystallisation builds them into the host lattice. Thus, impurities and solvent appear to be captured by precipitated crystals, and this process is different from so-called co-precipitation, where impurity ions that are compatible with the corresponding host ions are built in the host lattice according to a distribution coefficient.

The first problem, contamination from vessels and air, can be diminished by the use of modern instruments developed for the semiconductor industry. Instruments made from plastics and ceramics, ultra-filtration of solutions, and clean room atmosphere help avoid ambient and instrumental impurities. The second problem, ions and water captured by precipitate, is mostly resolved by classical methods: by recrystallisation from water solution or by sublimation in a stream of dry N_2.[61] An attempt to solve both problems was made, as described below, by using hydrothermal synthesis.

3.1.4 Hydrothermal synthesis

In this work, the term 'hydrothermal' is applied to synthesis of TlBr because equilibrium for the synthesis reaction given in Eq. 3 was achieved under hydrothermal conditions. In Fig. 6, the solid reagents Tl_2SO_4 and NH_4Br were mixed inside a PTFE vessel in a clean glove box. The mixture was digested under hydrothermal conditions in pure water. The reagent quantities were selected so that the product TlBr was totally dissolved under the equilibrium conditions of the reaction

$$Tl_2SO_4 + 2NH_4Br \leftrightarrow 2TlBr + (NH_4)_2SO_4, \qquad \text{at } 150^oC. \qquad \text{(Eq. 3)}$$

The mixture was then slowly cooled to produce TlBr seed crystals inside the mother solution without amorphous phase formation so that impurity capturing by nucleation was minimised and only a co-precipitation of impurities and mother solution ions took place. After taking

solution and solid samples, Sm and S, the residual crystals were recrystallised in fresh pure water under similar conditions, and solution and solid samples, SRs and SR, were taken again.

Elemental analysis[I] for solid samples S and SR, and for single crystals, which were synthesised by the dry method and purified and grown with the melt technique,[51] showed that the sample S, just after synthesis, had twice the impurities of the average melt grown sample. The sample SR recrystallised from S was two times more pure than the average melt sample and only two times less pure than the cleanest melt sample. Thus, the relatively simple operation of a hydrothermal synthesis with recrystallisation produces high quality material, which can be just as pure as the material purified and grown by melt methods.

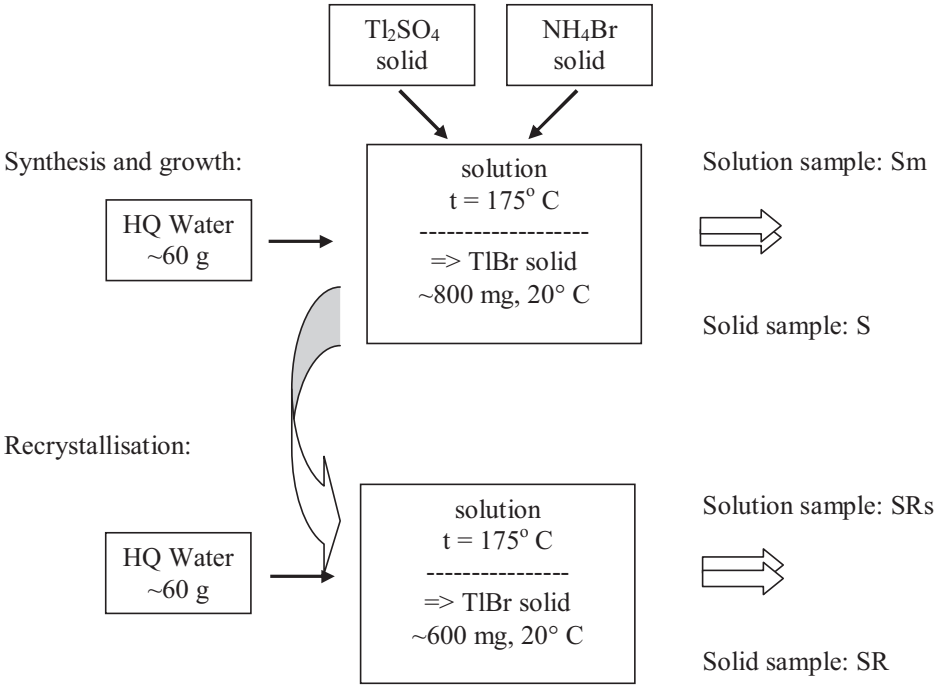

Fig. 6 Hydrothermal synthesis and recrystallisation of TlBr, and samples taken for trace element analysis.[I] Reagent's quality: Tl_2SO_4 - 99.995% and NH_4Br - 99.999% (CERAC). Abr.: HQ Water – high quality sub-boiled water.

3.2 Purification

The TlBr material synthesised needs further purification before it is suitable for detectors. Samples treated by 'dry' or 'wet' methods contain considerable mass amounts of S, P, Na, Si and Ca,[I] the elements being typical for both techniques. In this thesis the purification is studied by re-crystallisation of the host material from vapour (recrystallisation by sublimation), or from the molten state (by freezing), or from solution. Each recrystallisation

method is characterised by its own medium and temperature range, therefore, the extent of separation of the same component by different methods will be distinct.

3.2.1 Thermodynamics of separation and modelling

From classical thermodynamics[62] it follows that two phases (1 and 2) at equilibrium have equal chemical potentials, $\mu_1 = \mu_2$, for a given species. So

$$\mu_{o1} + RT \ln C_1 = \mu_{o2} + RT \ln C_2, \qquad \text{(Eq. 4)}$$

where μ_o is the standard chemical potential of the corresponding phase, depending on species, medium and temperature; and C is concentration of the species in mole per volume units, or its partial pressure in gas phase. Rearranging the equation gives

$$C_1 / C_2 = \exp[(\mu_{o2} - \mu_{o1}) / RT] = k(T), \qquad \text{(Eq. 5)}$$

where the coefficient k(T), known as distribution coefficient between two phases, depends on the standard conditions of given species and temperature. Thus, during the separation process at fixed temperature, impurity concentrations, C_1 and C_2, change in both phases so that one phase is depleted and the other is enriched with an impurity according to the constant ratio C_1/C_2.

For practical separation of impurities, the values of their distribution coefficients are needed in order to design a process in which the final solid will contain the impurities at acceptable levels. Experimental measurement of the ratio C_{solid} / $C_{liq.}$ is complicated because of the difficulty of directly measuring $C_{liq.}$ in the fluid, where diffusion and convection processes take place. And in a solid, the impurity is non-uniformly distributed along the ingot due to the collection or depletion process and, in addition, across the ingot due to radial gradients that exist at the crystallisation front. Therefore, modelling is the only method to estimate the distribution coefficient k. A 'simple' setup for sample growth and determination of k has been given by Pfann,[68a] where a series of C_{solid} values of impurities is determined by analysis of cross-section samples (thus, radial distribution is ignored). Then, k is deduced from the obtained C_{solid} and the original impurity concentration C_o:

$$C_{solid} = \text{Model}(k, C_o). \qquad \text{(Eq. 6)}$$

The measured value of k is affected by many factors. The impurity distribution depends on the rate of solidification,[69] which at large values destroys the equilibrium between solid and liquid phases. In a fluid, diffusion and convective mixing result in an effective distribution coefficient k_{eff}, which is between the equilibrium value and unity.[69, 70] The theory of contributions of fluid motion and diffusion to the distribution coefficient[71] and further its examination in Ge by a radioactive isotope method have showed that the incorporation of

solute elements into the crystal depends critically upon the transport processes occurring in the melt.[72] Thus, the value k_{eff} accounts mass transfer in the fluid, adsorption onto the surface of the growing solid and non-equilibrium action of the rate of solidification.[73]

The separation of two impurities with k values equal to 2 and 0.5 is modelled in Fig. 7 (left). For the calculations, the total volume of liquid is divided into 50 zones. Solidification starts in the first zone, where impurities are rejected into the solid or into the second zone of liquid, according to their distribution coefficients. Then, components of the second zone are 'mixed' with the residual part of the liquid in order to calculate new values of $C_{liq.}$ For the next cycle, the procedure starts again in the second zone and so on. As a result, the components initially distributed uniformly in liquid are collected at the ends of an ingot, and the extent of the separation increases with the number of passes, as shown in Fig. 7 (right).

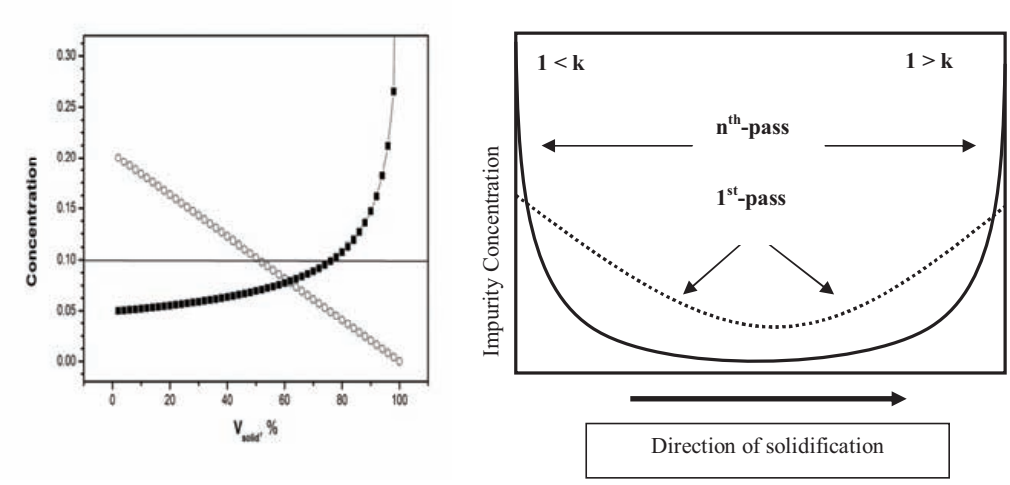

Fig. 7. Distribution of two impurities along a solidified volume of an ingot grown from liquid. On the left, the model is after one pass for a distribution coefficient $k = C_{solid} / C_{liq.}$ equal to 2.0 (open circles) and 0.5 (solid squares), full equilibrium between phases, initial concentration $C_o = 0.1$, and number of solidification steps n=50. On the right, schematic of separation of impurities with a distribution coefficient k of less and more than one.

The most common analytical form of the concentration of an impurity, C_{solid}, in a solid at the point where the mass fraction g of the fluid has solidified, is given by the Rayleigh equation[73]

$$C_{solid} = k_{eff}\, C_o\, (1\text{-}g)^{\,k_{eff}^{(Pf\,/\,Ps)-1}}, \qquad \text{(Eq. 7)}$$

where C_o is the original impurity concentration in the fluid; and Pf and Ps are fluid and solid densities, respectively. The equation (Eq. 7) can be applied to crystallisation from solution, as well.[73]

A single crystal growth can be used for purification, since the well-formed crystal is growing at equilibrium between solid-liquid phases, when k_{eff} is near the equilibrium value k. The single crystal is less contaminated by impurities than, for example, the powder crystals. This approach is widely used in Bridgman-Stockbarger[51] and zone refinement techniques for purification of TlBr from the molten state.

3.2.2 Recrystallisation from vapour

Solidification from vapour phase is an effective method for refining materials.[61] Dynamic distribution of impurities in condensed phase has been confirmed by fractional distillation of KCl.[63] Although, recrystallisation from vapour phase is seldom mentioned in the literature as a purification method of Tl halides, many impurities stemmed from wet and dry methods of TlBr synthesis can be easily removed by this method (see Fig. 8A).

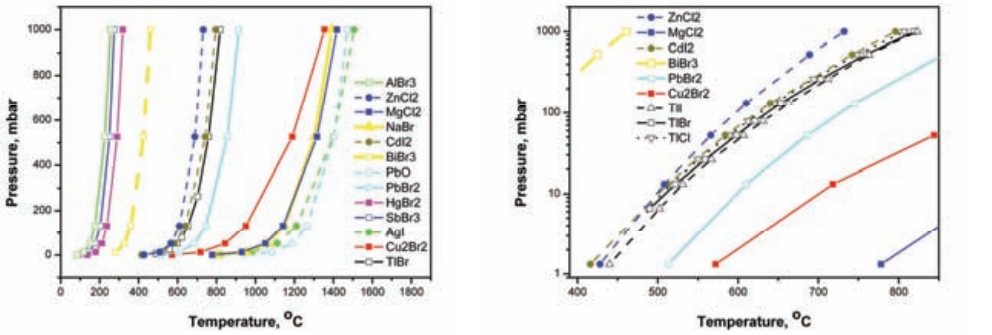

A B

Fig. 8. Vapour pressures of selected halides and PbO based on Refs.[38b, 44e] A: Data for TlBr and the most typical impurities in thallium halides. B: Overlapping between vapour pressures of halides of the thallium and impurity elements, Zn, Mg, Cd, Bi, Pb and Cu.

On the other hand, Tl halides have similar vapour pressure temperature curves, which overlap with that of $ZnCl_2$ and CdI_2, and partly with the other halides in Fig. 8B. Therefore, the separation of these halides from vapour phase is problematic. Also, the transfer of these halides through the vapour phase should be taken into account in horizontal processes with the molten state because of their relatively high vapour pressures at melting points of Tl halides.

The method of recrystallisation from the vapour phase in combination with crystallisation from the molten state has been applied to purification of TlBr material.[51] TlBr purified in this way was used as a raw material in this thesis and papers.[I-VII]

3.2.3 Recrystallisation from the molten state

In purification methods based on recrystallisation from the molten state, the host material serves as liquid solvent in the molten state and as solute in the solid state. Compatibility of impurities with liquid and solid host is a factor for impurity distribution between phases. Therefore, the radii of impurity ions and their oxidation states play a role in separation of impurities during recrystallisation from the melt. Possibly the first work and modelling on this topic was done in 1947, when rejection of K and Cu ions was studied during crystal growth of NaCl.[64] In alkali halide crystals, the enthalpy of mixing and anion environment of the first coordination sphere were the primary parameters affecting the distribution coefficient of Cd^{2+}, which was calculated and measured (experimental data in parentheses) in NaF – 0.006 (0.007), NaCl – 0.014 (0.017), NaBr – 0.10 (0.09) and NaI – 0.38 (ND).[65]

Data on distribution coefficients of different elements in Tl halides are limited. Average impurity distribution coefficients were found for TlCl and TlBr (in parenthesis) for the following elements: Cu – 0.009 (0.006), Ag – 0.004 (0.006), Pb – 0.04 (0.05), S (sulphate) - <1 (<1), O (Tl_2O) - <1 (<1), Fe – <1 (ND), Cd - <1 (ND). It was mentioned that Tl_2O moved to the end of an ingot less effectively than a sulphate impurity.[52a] Distribution of Li, Ca, Cr, Fe, Cu and Ba as impurities along a TlBr ingot purified by the zone refining technique was studied using ICP-MS in the work of Oliveira et. al.[66] From that data, the authors deduced distribution coefficients for Li (0.161), Ba (0.284) and Cr (0.238).[67]

3.2.3.1 Bridgman-Stockbarger method

In the Bridgman-Stockbarger method, the raw material is sealed into a quartz/glass ampoule with the appropriate inert atmosphere or vacuum. The seed crystal is located at the neck of the ampoule. A temperature stair with a gradient on the order of 10^{o}C/cm or steeper is created inside the vertical oven and the material inside ampoule passes several times from the molten to the solid state, the seed being always in the cold part of the oven.[74a]

The Bridgman-Stockbarger method is often called ‘directed crystallisation’,[51] when it is used for purification with higher rate of crystallisation than is needed for single crystal growth. The method can be used in horizontal setups as well. However, an optimal rate of crystallisation for Tl halides was 3 mm/h (typical for single crystals) and the best purification was obtained in vertical mode, which the authors explained as being due to the difference in density between the melt and foreign particles.[52a]

The distribution of an impurity along the polycrystalline ingot for one pass is illustrated in Fig. 9A, where water is collected by the melt and, therefore, is moved by the crystallisation

front to the ingot's end. It is notable that water-TlBr formation, with its characteristic IR band at 1627 cm^{-1}, is removed more readily than the band at 1608 cm^{-1}.

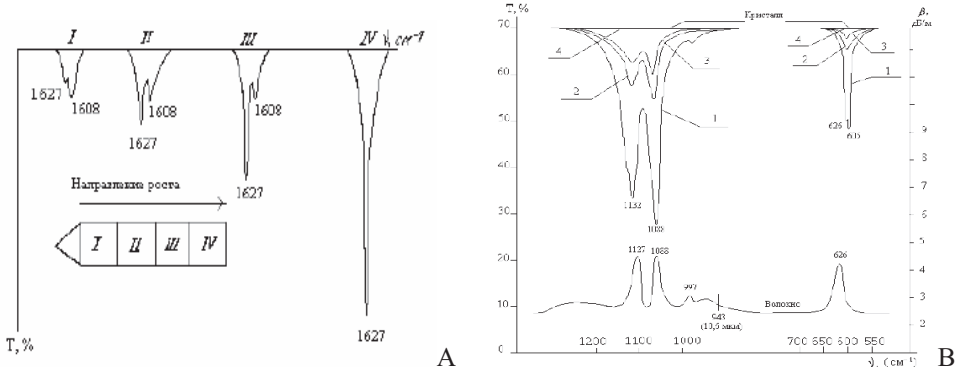

Fig. 9. A: The dynamics of water removal along the length of a TlBr ingot. The arrow shows the direction of growth.[53] B: (At top) transmittance spectrum (T) of a KRS-5 single crystal with the Tl_2SO_4 impurity (added concentration of SO_4^{-2} is 10^{-3} mas.%). In the figure, n for a plot corresponds to n-th directed crystallisation. (At bottom) absorption spectrum (β) of the fibre that was made from the crystal after the fourth directed crystallisation.[50]

The authors[53] explained this fact by association of the 1627 cm^{-1} band with polymeric water that is located at the crystal boundaries and between crystal grains. The band at 1608 cm^{-1} has been assigned to single water molecules, which are located in the lattice matrix and are removed less effectively than polymeric water. The purification effect of four passes is demonstrated in Fig. 9B for sulphate removal. However, the fibre extruded from the final crystal has, once again, sulphate IR bands. This effect could be explained by the change in measuring path of the sample, from 60 mm for the crystal to 1 m for the fiber.[50] Aging effects in Tl halide fibres[56] can not be excluded, however.

In general, a disadvantage of the Bridgman-Stockbarger method is that every new purification cycle requires reloading of the charge, cutting its ends enriched in impurities and melting of the residual middle part, as shown in Fig. 7, thus, averaging the result of the preceding purification over the total residual. The directed crystallisation technique[51] was used for purification of TlBr material, which was characterised and further purified by the hydrothermal method and zone refinement in our laboratory (see below).

3.2.3.2 Zone refinement

The best theoretical and practical illustration of the zone refinement method has been given by Pfann.[68] The technique is often named the travelling molten zone (TMZ)[75] method. In contrast to the Bridgman technique in this method, only a part of the charge (zone) is melted and travels along the ampoule in a horizontal direction. The size of a zone is on the

order of 1 cm, which is much less than the total length and, therefore, equilibrium is very rapidly achieved between solid and liquid phases. Due to the small volume of the liquid, the separation (difference between C_{solid} and C_{fluid}) is not as steep as in the Bridgman method. However, the highest purity can be achieved by multiple passes. Thus, from the purest commercially available germanium, Pfann produced material having less than 1 part of impurity per 10^{10} parts of Ge using only 6 passes.[68b] The method has vertical modifications[68c] and the cutting of the ends after every run is not obligatory.

In our laboratory, TlBr powder, ordinarily purified by the hydrothermal method, was degassed in vacuum at a temperature that was gradually increased to 300 ^{o}C, and under nitrogen flow up to 400 ^{o}C. Then the charge was loaded into a domestically made TMZ setup, as shown in Fig. 10. Optimisation of the rate of purification depends on the tube diameter and size of the molten zone. Typically, 5-7 passes of purification with the rate decreasing from 60 to 20 mm/h was sufficient to collect brown Tl oxide at the end of the ingot.

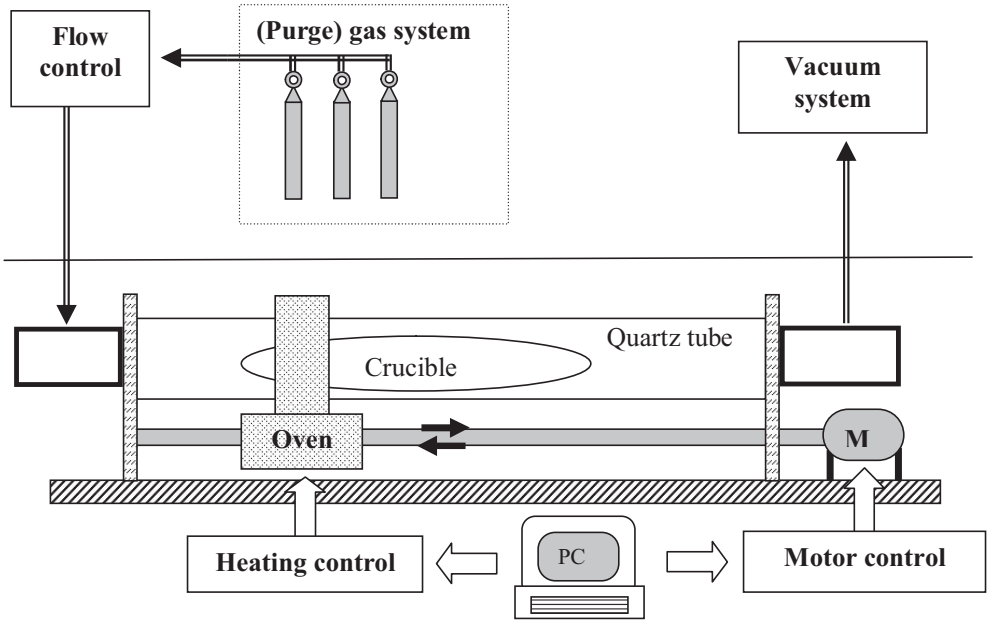

Fig. 10. TMZ set-up. The oven is driven by a motor M. The sample is in a crucible or quartz ampoule inside a quartz tube. A gas flow is controlled by MKS *Instruments*, Type 247D readout and Type 1179A controller. Oven's temperature and position are controlled through the PC by the LabVeiw/Tecono software. Quartz tube length – 600 mm. Temperature is controlled between 100 and 800 ^{o}C.

In the horizontal TMZ setup, free volume is usually formed above the melt. Thus, the gas phase takes part in the solid-melt equilibrium. In addition, more volatile components transfer through the vapour phase from the melt to colder solids before and after the molten zone.

Therefore, the free volume affects the distribution coefficient and modifies the composition of the charge. This disadvantage of horizontal TMZ is sometimes used for doping of TlBr, for example with Br_2[76] and I_2,[44a] in order to modify the electrical characteristics and hardness of the TlBr crystal, respectively.

3.2.4 Hydrothermal recrystallisation from solution

Hydrothermal recrystallisation of TlBr material is based on the increase in its solubility with temperature (see Fig. 11A). This separation method is the most effective for impurities that are difficult to remove by recrystallisation from vapour or molten states, and which solubilities are rather different from that of TlBr. This is illustrated in Fig. 11B, where solubilities of halides[34a] for elements, which separation is problematic by recrystallisation from vapour (see Fig. 8B) are compared. Only PbI_2 and TlBr have similar solubility-temperature curves (see Fig. 8A). As a result, Pb showed a separation efficiency ~1, when other elements of this series had relatively good efficiencies.[I]

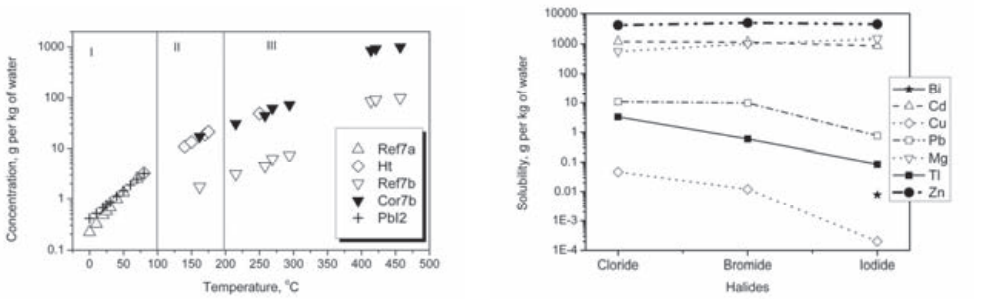

A B

Fig. 11. A: Solubility of TlBr and PbI_2 in water at different temperatures based on Refs,[38a, 38c, 34f, 52b] Ref7a/b,[100] and our data Ht, which were measured by the loss of nutrient weight after dissolution for 4 or more days. I - data for solubility below 100 °C. II - temperature range used for hydro-thermal re-crystallisation and crystal growth. III - high-temperature hydro-thermal range. Data of Ref7b were probably wrong retrieved from Ref.[177], and should be corrected by factor of ~10 (compare with Cor7b). B: Solubility of halides[34a] at 25°C for elements in Fig. 8B. (Solubility of halides of Tl and Cu, and BiI_3 are given at 20 °C.)

In this thesis, hydrothermal recrystallisation was carried out inside the reactor, so that TlBr (source) was dissolved in pure water at the hot part of the reactor, transferred through the reservoir to the cold part of the reactor, where it crystallised. During the transfer of TlBr, its impurities collected in solution. Recrystallised crystals gathered at the cold part of the reactor can be reloaded and recrystallised through the pure water again, and so on. Using this technique, two hydrothermal recrystallisation processes were studied for the purification of TlBr.[I]

During the first process shown in Fig. 6 a small amount of TlBr was totally dissolved at hydrothermal conditions. Recrystallised crystals were formed by cooling of the solution. In the second recrystallisation process a large amount of TlBr was transferred through the pure water due to the temperature gradient inside the reactor. The ratio of amounts of material in the second to the first process was ~10. Based on trace element analysis, the degree of purification obtained from the process was evaluated for separate element by the ratio of its concentrations before and after the process.[I] The efficiency of the overall process can be evaluated based on the ratio of the sums of concentrations of all elements. Evaluated in this way, the average purity of TlBr was improved by a factor of ~4 in the first process and by a factor of ~2 in the second process.

3.2.5 Combination of purification methods

The combination of purification methods allows acceleration of the refining process. For example, a sequence using distillation and solidification from melt has been used for purification of alkali halides[63] and Tl halides.[51] The efficiency of using a combination of different methods can be illustrated by Cl^- and I^- anions, which are hardly removed from TlBr during crystallisation, whether from the molten state or from vapour. Thallium halides have similar characters in molten and solid state, and easily form solid solutions with each other.[44a] These compounds have similar vapour pressure temperature curves, and therefore their separation from vapour phase is also problematic (see Fig. 8B). On the other hand, solubilities of TlCl and TlI are one order of magnitude greater and one order of magnitude less, respectively, than that of TlBr (see Table 2 and Fig. 11B). Therefore, during the recrystallisation of TlBr from water solutions, TlCl dissolves and remains in the solution, and TlI stays undissolved.

In this thesis, a combination of purification methods was applied to TlBr material, which was purified by 5-7 cycles of distillation and solidification from melt. Then, a single crystal was grown by the Bridgman method. This single crystal was hydrothermally recrystallised by dissolving it in pure water, then 5 purification runs were done using TMZ.

This sequence of purification steps and further crystal growth supplied the crystal with the mobility-lifetime product ($\mu\tau$) estimated as 3.3×10^{-4} cm^2/V (for electrons).[77] This value was one order of magnitude better than the value 3×10^{-5} cm^2 V^{-1}, which was obtained by Olschner et. al.,[6] for 200-300 passes of a molten zone.

3.3 Crystal growth

Crystal growth is an attractive subject for many researchers. It is an art and a science,[78] a laboratory practice[79] and an industry technique.[80] The growth can be done from solutions,[81] liquids,[82] melts,[83] high-temperature solutions[84] and in gels.[85] One of the best classifications of crystal growth methods is based on the medium from which the growth is carried out.[86] Thus, there are techniques for crystal growth from melt, vapour and solution.

3.3.1 Crystal perfection

Temperature has a primary effect on the quality of the growing crystal due to the entropy disordering factor S(->max):

$$G(->min) = H(->min) - T\,S(->max). \quad \text{(Eq. 8)}$$

The process of crystal structure formation (ordering) is characterised by the minimisation of enthalpy H and the minimum total gain in Gibbs free energy (G).[87a] Thus, ordering and disordering forces contribute to different extents to the process of crystallisation, resulting in the incorporation of point defects into the lattice:

$$n_{min} = N \exp(-E_d / kT), \quad \text{(Eq. 9)}$$

where N is the total number of possible sites, E_d is defect formation energy and n_{min} is minimum (or more) number of defects, the so-called *perfection limit*. The value n_{min} for TlBr plotted in Fig. 12 is about one order of magnitude higher for Schottky than for Frenkel point defects, although the latter should be corrected by the factor $\sqrt{n_{is}}$, where n_{is} is the total number of interstitial positions.[87a] The probability of defect formation by the Frenkel mechanism is low at low temperatures because the Tl halides have ionic radius ratios of cation to anion (R_c/R_a) close to the stability limit value[88] of 0.732 for CsCl-type structure: 0.878, 0.811 and 0.723 for TlCl, TlBr and TlI, respectively. So the CsCl-type structure becomes stable for Tl iodide only at temperatures higher than 168 ^oC (see Table 2).

During crystallisation at high temperatures a certain fraction of defects is frozen into the lattice due to the limitation of the diffusion rate.[87a] Thus, the plots in Fig. 12 determine the thermodynamic limits of defect concentration according to the crystal growth temperature. For example, accordingly to the Schottky defect values, the growth from solution at 100^oC and 200^oC is 40 000 and 400 times, respectively, more preferable than growth from melt. However, no crystal growth method for TlBr approaches the perfection limit due to the properties of TlBr and techniques used.

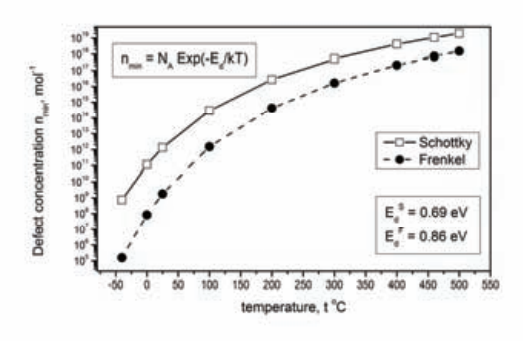

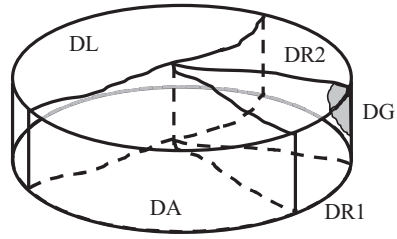

Fig. 12 (left). Temperature dependence of defect concentration, the thermodynamic 'perfection limit',[87a] calculated for one mole of TlBr using values for defect formation energy by Schottky (E_d^S) and Frenkel (E_d^F).[89] (N_A – Avogadro's constant).

Fig. 13 (right). A misty disk cut from an ingot of TlBr and annealed under hydrothermal conditions for ~40 days became separated by milky boundaries into four transparent blocks and one glassy piece DG. According to data from the X-ray rocking curve method, the blocks had different crystallographic orientations with respect to a cut surface: DA (110), DL – (210) and (211) reflection planes with deviations of 15.05° and –9.10°, respectively, from the disk surface. Crystalline blocks DR1 and DR2 were not identified, possibly due to a high deviation of reflection planes from the cut surface. The piece DG did not reveal any reflection planes in the range (100) – (220).

3.3.2 Crystal growth from melt

Melt growth techniques are very practical and widely used in industry. Among them, crystal pulling, the Bridgman method and zone melting are the most often used for crystal production.

3.3.2.1 Crystal pulling

The crystal pulling method is the most developed crystal growth method and it is easily controllable. A crystal pulled from the melt is the most pure and perfect, without any effect of the crucible walls.[87b] The Czochralsky method allows the growth of so-called 'dislocation free' crystals[86] and is widely used to produce halide crystals for optical components and scintillators.[87b] The Kyropoulos method for crystal pulling is characterised by the large diameter that can be achieved, however, the method is less effective than the Czochralsky method and tends to produce crystals with relatively high dislocation densities.[86] Unfortunately, pulling methods are not used for Tl halides because of their high vapour pressures (see Fig. 8) and toxity.

3.3.2.2 Bridgman method

The Bridgman method is widely used in laboratory practice and is the only method used for industrial growth of Tl halides. Purified halides are usually evacuated and sealed in a glass or quartz ampoule.[52a] Technical details of the method[86] and specific features related to Tl

halides[51] are well described. The growth rate depends on the minimum crystal dimension L as $1/L^n$, where n is between 1 and 2. For L~10 mm, rates are usually in the range of 1–10 mm/h, the values being larger for materials with higher thermal conductivity.[86] Several disadvantages of the method, however, are summarised below.

Many problems with the Bridgman method stem from the direct contact between the crystal and the crucible material.[87b] Adhesion and differences in thermal expansion coefficients produce stress in the growing crystal and initiate secondary grain nucleation on crucible walls,[37] resulting in the formation of separate crystals inside the ingot,[20] as shown in Fig. 13 for TlBr. Secondary nucleation and twinning can be minimised by the use of a horizontal method.[86] However, the extraction of the grown crystal from the crucible may result in its cracking.[87b]

The second problem is connected with purity requirements. The crucible selected must be appropriate and not produce contamination.[86] In the Bridgman method, impurity distribution is not uniform along the growing ingot (see in Fig. 7) and the problem is made worse by insufficient mixing in the molten zone.[87b]

The next problem is to obtain and maintain the desired temperature distribution. Thermal conductivity of the crucible should be less than that of the material grown.[86] Temperature gradients before the crystallisation front are responsible for the radial non-uniformity of a crystal, twinning and seed formation. The temperature in the liquid in front of the crystallising face is often locally increased by about 60 degrees[51] in order to improve solid-liquid equilibration by means of convectional mixing of the liquid. But this operation considerably increases the temperature gradient between solid-liquid phases, and creates laminar liquid flows that result in additional tensions in the cooling crystal. Defects, impurities and imperfections are more quickly frozen into the crystal lattice and number of defects in the lattice becomes further away from the perfection limit (Eq. 9).

In Fig. 14, the single crystal of TlBr is grown without the formation of separate crystals shown in Fig. 13. However, the irregular distribution of temperature, cooling tensions in the crystal and tensions stemming from the walls of the crucible result in strain and non-uniformity in the single crystal. Non-uniform zones can also be revealed by etching.[III] It should be noted that cutting and polishing effects are involved as well.

In general, non-uniformity in the Bridgman method originates from temperature gradients during the crystallisation and from the walls of the crucible during cooling. Adhesion of the crystal to the crucible material creates additional problems with blocking and cracking of the ingot. Recent attempts to decrease the adhesion and improve the crystallisation front shape

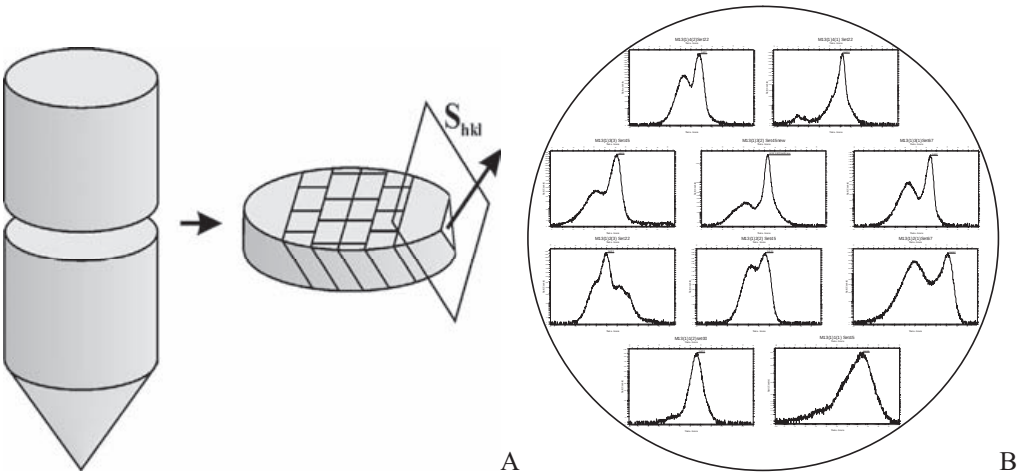

Fig. 14. TlBr wafer processing: an ingot is cut, the wafer is oriented and slices are made (A); a cross-sectional map of an ingot: slices are studied using the X-ray rocking curve method (B).

improved crystal quality, but simultaneously deteriorated the purity by dissolving of crucible components.[VII] Although these disadvantages of the Bridgman method diminish the purity and quality of the crystals, currently this is the only method by which large diameter ingots of Tl halides can be produced. The purity and quality of the crystals grown by this method can be improved by annealing[I, II] and etching,[III] as described below.

3.3.2.3 Zone melting

The zone melting method, typically used for purification,[68] is exploited for a crystal growth, as well. In the horizontal variant, the crystal experiences less influence from the crucible, since the top side of the charge is open and can release tension from the walls. In this case, however, the molten charge is in contact with the vapour phase, which is a particular disadvantage for Tl halides because of their high vapour pressure (~10 mbar) at melting temperature and volatile impurities (see Fig. 8B). A vertical variant of the zone melting method, the so-called floating zone method, might be used without a crucible or ampoule, but the method is difficult to realise technically. Its use for production of Si was mentioned in Ref.[86] For TlBr, the zone melting method is mainly used in Brazil, but for purification only,[66] and in Japan for both purification and crystal growth. Hitomi exploited the TMZ technique to grow TlBr crystals. The maximum size of the detector he fabricated is around 4x4x4 mm^3 with a working area of 3.8x3.8 mm^2.[90]

The rate of crystal growth is normally one order of magnitude less than the speed used for purification. In our experiments the crystal growth rate was 5-10 mm/h, in contrast to 20-60

mm/h used for purification. The maximum size of a detector fabricated in our laboratory was around 7x6x4 mm^3 with an electrode diameter of 3 mm.[77]

The smaller diameter of ingots grown by TMZ in comparison with the Bridgman method is a current disadvantage for TMZ. However, application of the floating zone method and development of a narrow zone heater might improve the purity and crystal quality of the TlBr to the extent that the total cross section of an ingot would be available for detector fabrication. This is supported by recent successful fabrication of a 4-mm detector[77, VI] and possibility to grow the ingot of high quality (see Fig. 29A) that is lower than industrial Si only by factor 3 (intensity: 34 vs 90 Kcnts; FWHM: 0.094 vs 0.034).[178]

3.3.3 Crystal growth from vapour

In general, crystal growth from vapour is more easily treated theoretically than crystal growth from a condense phase, since vapour comes more quickly than a fluid into equilibrium with a solid and the role of intermolecular forces in gas phase is negligible.[91] Crystals grown by this method should be free of effects from the crucible walls. For Tl halides, vapour growth is used for purification.[61, 51] There are no reports in the literature of growth of Tl halide single crystals from gas phase, possibly due to the lower productivity of this method in comparison with crystal growth from the melt.

However, the method is used for the production of Tl halide films. Kondo et al. have produced uniform amorphous TlBr[101] and TlCl[92] films condensed from gas phase on a metallic surface at cryogenic temperature, and they observed a well-defined transformation to crystalline phase at low temperatures. These films are clear and, therefore, the effect of crystallisation on their optical absorption near the UV fundamental edge has been studied.[93] In $TlCl_{1-x}Br_x$ films, crystallisation is affected by chemical disorder, as shown by UV absorption measurements.[94] A method for preparation of uniform amorphous films of mixed metal halides by means of two-source evaporation was recently described.[95] The thin films have a thickness of 300-500 nm and could be utilised for UV and soft X-ray detection.

In this work, condensation of TlBr vapour was studied on an Al surface heated to above room temperature. At temperatures below 150 ^oC, the crystalline films formed were uniform and transparent. If a sample was under a temperature gradient, the film had a thickness gradient that monotonically followed the temperature gradient of the substrate.

At temperatures above 150 ^oC, metallic Tl drops formed on Al surface that was confirmed by microscope and XRD studies. The corresponding reaction could be written as follows:

$$Al\,(metal) + 3\ TlBr\,(g) = AlBr_3\,(g) + 3\ Tl\,(dispersion) \qquad \text{(Eq. 10)}$$

with ΔG = -44.4 kcal at 150 °C.[57] The ΔG of this reaction becomes positive only at temperature above 900 °C, but the reaction below 150 °C is possibly inhibited by an Al oxide film on its surface. The ΔG of the reaction between the Al oxide and TlBr, given as follows:

$$Al_2O_3 + 6\ TlBr(g) = 2\ AlBr_3(g) + 3\ Tl_2O, \qquad \text{(Eq. 11)}$$

has reasonably positive values (184.6 kcal at 150 °C[57]). On the other hand, the reaction (Eq. 10) is 'accelerated' by $AlBr_3$, which easily escapes from the reaction zone because of its high vapour pressure, which is about 40 mm of Hg at 150 °C.[38b]

TlBr films grown from vapour on an Al surface are no thicker than ~500 nm. Prolonged growth results in the formation of an opaque polycrystalline layer on the Al surface. In general, the deposition of TlBr from the gas phase onto various metals is a useful technique for making TlBr (film) – metal interfaces.

3.3.4 Growth from solution

Solution growth techniques are attractive because of the low 'perfection limit' (see Fig. 12) and 'freedom' of the growth (compare with effects of crucible walls in the Bridgman method, Fig. 13 and Fig. 14B). Based on temperature and pressure used, the solution growth methods are conventionally divided into the low-temperature, hydrothermal and high-temperature methods. The first two are used in this work and discussed below. The high temperature method is sometimes called 'flux growth', because high temperature melts of salts are used as solvents. There are a few Tl halide – nitrate systems,[96] where the solubility of the halides is comparable to that in water. Liquid-phase epitaxy and electrolysis are typical solution methods.[86] Liquid-phase epitaxy has not been used for TlBr, whereas the formation of TlBr adlayers was observed and studied on Au, Ag and Pt electrodes.[97, 98, 99] Growth from gel can also be a promising method, since Tl iodide crystals with a size of ~1 mm grown by this method have been reported.[85]

A subsystem for classification of solution growth methods is often based on the method for achieving supersaturation of the solution: cooling, temperature gradient and solvent evaporation. The last technique is not suitable for Tl halides, since they are sparingly dissolved in water at room temperature, and therefore the productivity of this method is low.

Solubility is a necessary attribute for crystal growth by a solution method. The solubility of TlBr in water increases considerably with temperature: it is only 0.05% at 20 °C, 0.5% at ~94 °C and it is already about 5 % at 250 °C. The plot of solubility in Fig. 11A is divided in three parts: a low-temperature area below 100 °C (I) and a hydrothermal area with stable (II) and unstable (III) crystal growth of TlBr.

3.3.4.1 Low-temperature methods

In this work, the cooling method below 100 °C has only been used successfully for making small TlBr crystals, which were utilised as seeds in crystal growth by other methods. This is because a change of temperature, for example, from 80 ^{o}C to 30 ^{o}C, gives a total difference in solubility on the order of only 0.25%. Further growth using repetition of the cooling method produced twins, striations and new seeds joined with old ones.

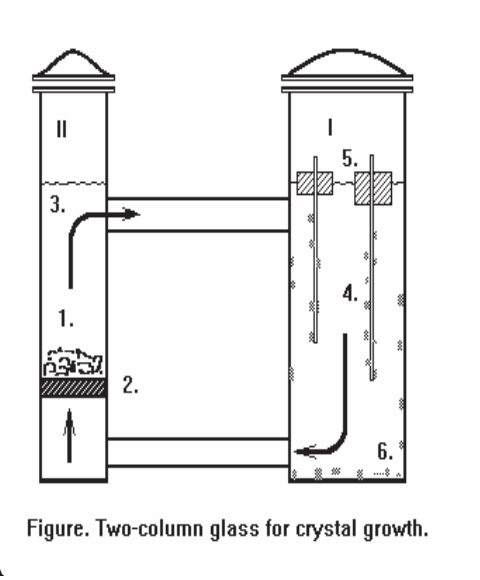

A

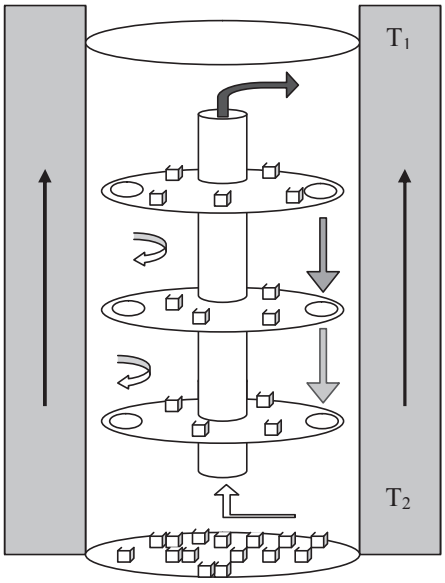

B

Fig. 15. A: Nutrients (1) on the glass filter (2) are dissolved and saturated solution rises to the top (3) of column II, which is at a temperature higher than that of column I. In column I the solution becomes supersaturated and crystals grow on the glass rods (4) attached to the floats (5). An excess of super-saturation is released on the formation of seeds (6) that fall down to the bottom of column II. B: A long column is heated by the outer shell. Nutrients on the bottom of the column are dissolved and saturated solution rises to the top, where it becomes supersaturated ($T_2 > T_1$). Crystals grow on the plates fixed to the column along its length.

The setups used in this work for crystal growth by the temperature gradient method are shown in Fig. 15. The first setup (A), with two glass columns, operates at a relatively small difference in temperatures between the columns, since a larger difference causes extensive formation of seeds that join to growing crystals. Over 1-2 months this technique produced a few crystals of about 0.5 mm in size. The crystals were clear and without striations.

The second setup allows an increase in the temperature, its gradient and, as a result, an increase in productivity of the process and convection flow of the solution. Several crystals were grown by this technique with a size of ~0.8 mm. Since the seeds in this method are firmly attached to the plates, they all have striations. The resistivity of the clearest crystal (0.4x0.4x0.4 mm^3) was ~1.5x10^{11} ohm·cm at room temperature at ± 60 V. The detector made

from this crystal by Bruker Baltic (Latvia) can resolve all necessary spectral lines, however its spectral characteristics are unstable.

3.3.4.2 Hydrothermal growth

The hydrothermal method allows water, high temperature and pressure to produce effects that are not attainable under ambient condition. The Earth itself is a huge high pressure and high temperature vessel,[102] in which diamonds, quartz and other crystalline minerals are synthesised and grown. A comprehensive review on the hydrothermal formation of silicates was published already in 1913.[103] Complete information on pressure-volume-temperature relations in water was given by Kennedy[104] in 1950. In this work, hydrothermal bombs were used in order to increase the solubility of TlBr above 100 ^{o}C. Maximum values of pressure and temperature were limited by the properties of the used bomb to ~ 25 bars and 225 ^{o}C at a bomb filling of ~60%.

Cooling and temperature gradient methods were used for achieving supersaturation of the solution. The seeds were placed on the levels above the solution, and after dissolving the nutrient and approaching the equilibrium state (for ~4-6 days) the bomb was inverted from top to bottom. Alternatively, overheating and cooling to the required temperature were used for seed formation. As shown in Fig. 11A, the optimal temperature range for crystal formation and growth was zone II, which is between 100 – 190 ^{o}C, since at higher temperatures the crystals grew easily with rounded shapes and faces, resembling more closely clear icicles than well shaped crystals. Also, the crystal quality of the 'icicles' was too low to create x-ray diffraction reflections. All crystals grown by the temperature gradient method had a large number of striations, like crystals grown at the low temperatures in Fig. 15B. Therefore, the method was used for recrystallisation (purification) purposes.

Crystals of better quality were grown from solution during prolonged crystal growth by the hydrothermal cooling method. In a typical example, saturated solution at 200 °C was slowly cooled to 180 ^{o}C, in order to form seeds and achieve supersaturation. Then prolonged cooling to 140 ^{o}C was done over the course of 40 days. At these conditions the concentration of TlBr changed from 2.3% to 1.1%, and the crystals grew to ~1 mm size and more. Unfortunately, the repetition of this technique gave striations on the crystals, or crystals that were joined, or crystals that looked like stairways. One of the crystals grown by this method (3x3x0.4 mm^3) had a resistivity of ~1.5x10^{11} ohm·cm at room temperature at +70 V. The detector made by Bruker Baltic from this crystal was able to count gamma-ray photons, but not to resolve, all spectral lines.

3.4 Annealing

Single crystals of TlBr grown from the molten state by the Bridgman method (chapter 3.3.2.2) are strained basically due to the effects of the crucible walls and the cooling regime. The applied stress easily generates dislocations in the cooling crystal. The motion of dislocation in shear (like the motion of a vacancy) is the movement of a corresponding line of atoms for only one interatomic distance or less. Thus, the stress required to move a dislocation is several orders of magnitude smaller than the stress required to shear one entire plane of atoms simultaneously over another in a perfect crystal.[105] The different dislocations accumulated during cold work create stress fields that interact strongly and lock the dislocations into metastable configurations. The crystal becomes harder, and externally applied stress should be sufficient to make dislocations move through the opposing stress fields of other dislocations.[105] The crystal has gained extra free energy from the work done on it. Metastable configurations undergo spontaneous changes to reduce the extra free energy, which is reflected, for example, in strain aging.[106]

Besides hardening, other properties, such as resistivity and rate of dissolution, are changed in worked material.[107] The broadening of X-ray diffraction lines in strained material has long been the only method for the study of worked material and its annealing on the micro-scale level. Annealing removes strains, improves the quality of the crystal and restores the properties of the material.[106] Annealing has a clearing effect on opaque crystals, shown for TlBr in Fig. 13, where the hidden block structure of an ingot becomes visible. In this thesis, effects of hydrothermal as well as various other annealing conditions on TlBr properties were studied in papers I – III.

3.4.1 Types of annealing

Annealing is known from ancient times and is widely associated with a heat treatment of a worked material in order to make it softer. In general, the process consists of heating the material to a definite temperature, keeping it at this temperature for the required time and cooling at a controlled rate. Sometimes annealing includes a thermo-treatment with the use of additional mechanical action. The result of the process is evaluated by measuring the materials or by observation under a microscope. During the last hundred years, development of X-ray diffraction methods has allowed the detection of fine effects of annealing and, thus, insights into its mechanism.[106] As a result, an understanding of the mechanisms of the annealing process became possible on the microscopic level. The action of annealing depends

on applied stress and the temperature regime. Both these factors can be used to differentiate the following types of annealing processes.[106]

Recrystallisation, or primary recrystallisation, is a process in which new crystals grow from nuclei and replace the strained ones. The orientations of these new crystals are independent of the strained crystals. Therefore, the growth is incoherent and results in the advance of large-angle boundaries separating the new crystals from their surroundings.[106]

When the growing crystals have consumed all the strained material, they continue to grow by consuming each other; this process is called *grain growth*. In specimens that have already undergone primary recrystallisation after severe cold working, *secondary recrystallisation* takes place at a higher temperature. During this recrystallisation a few grains grow abnormally rapidly and become many times larger than the average grain.[106]

Thus, recrystallisation is associated with large-angle boundaries and, in general, is observed to take place in a temperature range of 50 – 80 % of the melting temperature (T_{melt} K) of the material.[108] For example, for TlBr (T_{melt} = 733 K), this interval corresponds to 94 – 313 ^{o}C. In highly stressed KRS-5 material (T_{melt} = 683 K) made by extrusion to fibres, grain growth occurs with annealing above 50 ^{o}C,[47] which corresponds to 47% of T_{melt}.

Worked crystals can be repaired by the *recovery* process, preserving the orientation of the crystal without its recrystallisation. The structure of the material, the annealing temperature and the deformation type have primary effects on the recovery procedure. In cubic metals, recovery usually only partly removes the work hardening, while hexagonal metal crystals deformed in tension by basal slip can recover their original softness completely and do not recrystallised.[106] In general, recovery takes place at lower temperatures than recrystallisation. Since point defects (vacancies) are more mobile than dislocations, their role is more important at lower temperatures.[107] At higher temperature, appreciable diffusion occurs and allows the dislocations to move into a configuration of lower energy. Several dislocations will come together and annihilate one another or combine to form a single dislocation.[105] The energy per dislocation in a grain boundary is less than for isolated dislocations, therefore, the excess free energy of grain boundaries should be a driving force for crystallisation.[86]

The mechanism of dislocation movement and its elimination is explained by so-called the *strain-induced boundary migration*. The boundary, present initially in a lightly worked grain, migrates and causes the volume of material swept by it to become a strain-free continuation of the grain from which the boundary originated. The orientation of a strained crystal varies from point to point and so the strain-free additions which grow at different places along its

boundary have slightly different orientations from one another. As a result, when they join together small-angle boundaries are formed between them.[106]

Because various crystal imperfections affect to a different extent the properties of materials, the recovery of different properties with temperature occurs to different degrees and non-simultaneously. Non-completeness of a recovery is often reflected in its definition as the process of decreasing the amount and changing the distribution of point defects and dislocations.[107] In general, the recovery process is characterised by small-angle boundaries and lower temperatures than recrystallisation.[106] Therefore for TlBr, the recovery process can be observed at room temperature.

The process of *polygonisation* was first studied on bent single crystals of Zn, Al, Mg and NaCl. This process is characterised by small-angle grain boundaries and takes place in bent crystals at temperatures well above that at which the material softens. A bent crystal contains the excess edge dislocations of one sign[106] that are more or less uniformly distributed on parallel slip planes. In the process of annealing, dislocations on different slip lines line up one above the other and form a small-angle grain boundary. The energy per dislocation is reduced when the dislocations are so arranged.[105]

Polygonisation has features similar to recrystallisation in terms of the temperature, at which it can occur, and it is similar to the recovery process in the terms of the small-angle grain boundaries. However, polygonisation takes place only in bent crystals. In Tl halide ingots grown by the Bridgman method, there are several points on the cylindrical surface which are stuck to the walls of the crucible. The contraction forces create bent fields in 3D-space during ingot cooling. Thus, polygonisation can take place throughout the annealing of Tl halide crystals.

3.4.2 Processes associated with annealing

The variety of annealing processes based on applying mechanical stress and heat separately is enlarged by their combination, and/or by changing the environmental conditions (gas medium or solution), or by operation of external forces (for example, electric fields).

3.4.2.1 Strain-anneal method

A modification of the recrystallisation method as a *strain-anneal method* is used for so-called *solid-phase crystal growth* (compare with *strain-induced boundary migration*, above) The idea behind the method is to make the re-growth occurs inside the bulk of the material during annealing so that the inner single crystal experiences minimum contamination from crucible material and/or a reactive atmosphere. The material is heated to about half the

absolute melting temperature, where it is not brittle. Then, the material is subjected to strain on the order of 1 - 10%. Annealing is carried out in a temperature range of 50 – 95 % of T_{melt}, a temperature gradient across the sample being considered an advantage. The rates of growth are usually fast: 5 - 50 mm/h can be expected. The driving force for the process is the excess free energy attributed to dislocations or clusters of dislocations and grain boundaries.[86]

3.4.2.2 Annealing of amorphous materials

A solid in an amorphous (glassy) state has a higher free energy than in the form of a single crystal. Solid-phase crystal growth is the crystallisation of glassy material that can be accelerated by heating. The amorphous material is obtained, for example, from melt with a high temperature gradient by rapid quenching. The method used for production of films is known as *solid-phase epitaxy*. In films, selective crystallisation can be induced. Due to the amorphous starting state, the highest doping densities can be achieved by this method.[86]

In Tl halides, crystallisation from an amorphous state in films occurs at low temperatures. The amorphous phase is obtained on the substrate, which is kept at the temperature of liquid nitrogen or oxygen. During heating, the crystallisation observed by optical absorption spectroscopy takes place in a narrow temperature interval, near 95 K for TlBr,[101] 99 K for TlCl,[92] 120 K for TlI[93] and 138 K (maximum) for a mixture of TlCl (60 %) and TlBr (40%).[94] According to an electron diffraction study both, a normal structure of CsCl-type and abnormal structure of NaCl-type (rocksalt), were observed in TlBr and TlCl during heating. However, the abnormal structure disappeared well before room temperature was reached.[109]

3.4.2.3 Effects of impurities

During annealing, impurities are attracted to the region of tension around a dislocation and migrate to it, because distortion around the dislocation is reduced if host atoms stressed by dislocation are replaced by corresponding (larger or smaller) impurity atoms. The rate of the process is limited by diffusion and consistent with the Cottrell's time law of strain aging in the stress field.[105] Therefore, addition of impurities is often used in order to stop strain-induced boundary migrations during annealing and stabilise the material and avoid grain creeping during aging. On the other hand, grain growth can be expected if impurities are removed.[86]

Thus, during annealing, the impurities, dislocations and boundaries migrate outside the crystal, which become more perfect and clean inside. This effect has been described in plastically deformed crystals[105, 106] and, independently, in optical materials[44c] (see chapter

2.2.3). In TlBr, the crystal perfection effect of annealing has been shown in paper I, and the clearance of crystal blocks is illustrated in Fig. 13.

If a DC voltage is applied, *electro-annealing*, as solid-state electrolysis, removes impurities. Heating is applied to raise the sample temperature to 55-90 % of the absolute melting temperature. To be effective, solid-state electrolysis should involve large current densities (several amperes or even hundreds of amperes per square centimetre). The removal of impurities stimulates grain growth, rates of which can approach 3 – 50 mm/h.[86] The *electro-annealing* method seems to be effective for purity and crystal quality improvement of TlBr. However already at temperatures comparable with room temperature, the diffusion of own ions of TlBr becomes remarkable, and in a TlBr detector, the process produces aging[V] and polarisation[2, 40] effects, which are considered in chapter 4.5.6.

3.4.3 Annealing of single crystals of TlBr

In this thesis, annealing of single crystals of TlBr was studied in papers I-III and annealed crystals were used in IV-VII. The annealing process was limited to a temperature of 200 ^{o}C in vacuum and 300 ^{o}C under a protected atmosphere because some volatility of material was observed at higher temperatures. In pure water, annealing was restricted to 225 ^{o}C by the configuration of the hydrothermal system used. The lowest temperature of annealing was higher than 100 ^{o}C (51% of T_{melt}). Thus, thermal treatments took place in that temperature range where during the recovery process the recrystallisation was also possible.

The annealing effects were evaluated using the X-ray rocking curve method, IR transmittance and *I-V* measurements, and under polarised light. The effect of an Ar atmosphere and hydrothermal conditions on crystal quality was studied on the series of slices produced from the same ingot,[II] as shown in Fig. 14. Typically, annealing results in a decrease of FWHM of an X-ray reflection peak and elimination of the satellite peak that can be associated with deformation of the crystal (see Fig. 16a). Perfection of the crystal quality improves the electrical, optical and X-ray detection properties.[II] Annealing makes TlBr samples more transparent (see Fig. 13). Optically isotropic cubic TlBr crystals become anisotropic when under stress,[113c] therefore, removal of boundaries and non-uniformities can be observed directly under polarised light (see Fig. 17). Evaluation of annealing effects between different samples and types of annealing processes can be done using an *improving factor of annealing*, which is calculated as a ratio of FWHM before annealing to FWHM after annealing. In Fig. 16b, accordingly to the improving factors, annealing at higher temperature seems to be more effective for improving quality.

However, at higher temperatures the recrystallisation becomes more probable when material is stressed and contains impurities. Impurities are subtracted by the lattice and, being collected at boundaries, terminate the boundary's movement during the annealing (see chapter 3.4.2.3). For example, after annealing at 300 °C the TlBr samples, which contained impurities of Ca, Si and Cl, the rocking curves were resolved into several sharp overlapping peaks, IR absorption became abnormally large, and kaleidoscopic spots under polarised light were enlarged, but did not vanish.[VII] Thus, the annealing regime has to be optimised for every new series of samples.

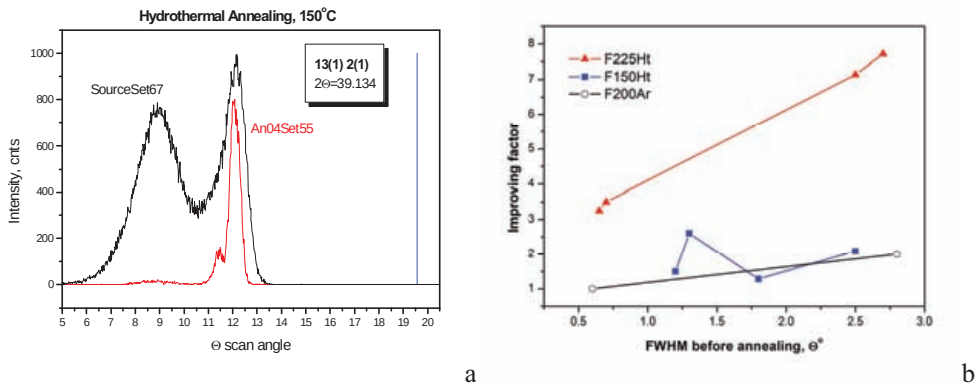

Fig. 16. Annealing effects on X-ray rocking curves of TlBr crystals. (a) Hydrothermal annealing in pure water for 5 days at 150 °C (represented by red curve) results in a decrease of FWHM of a broaden (111)-reflection and elimination of the satellite peak (black curve). (b) FWHM improving factors of annealing under Ar atmosphere (99,9999%, 1 bar, 200 °C – open black circles), or under hydrothermal conditions in pure water at 150 °C (closed blue squares) and 225 °C (closed red triangles).

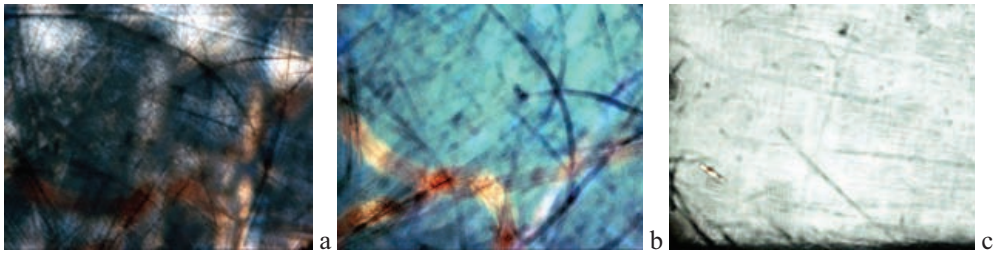

Fig. 17. Polarisation microscope images of machine polished sample. A non-annealed sample is intensely coloured and kaleidoscopic as indicated in semi-dark (a) and bright (b) positions during rotation under polarised light. The sample annealed at 200 °C is uniformly coloured without kaleidoscopic effects.

The sample actively interacts with the environment through the surface, so that doping of the material as well as its properties can be changed during annealing. For example, an iodine atmosphere increases the hardness of TlBr,[44a] and annealing under Br_2 changes the stoichiometry under the surface and, as a result, the electrical characteristics of the TlBr

crystal.[76] Annealing in pure water was more effective than annealing under Ar atmosphere,[II] since an impurity can move into solution due to the difference between its chemical potential in TlBr and in water. The removal of impurities through the sample surface was confirmed by IR reflection spectra.[I] This advantage of hydrothermal treatment over thermal annealing was often used for preparation of clean surfaces of the single crystal during annealing.

In general, annealing of TlBr contains the features of the recovery and recrystallisation processes, the latter being accelerated by high temperature and presence of strains and impurities. Recovery annealing decreases the strain and number of boundaries in the crystal and makes it more uniform and pure. Since these factors drastically affect the carrier transport characteristics of a crystal,[20] the proper annealing of a strained crystal can make it suitable for use in a radiation counter.[1]

4 TlBr detector fabrication

TlBr detector fabrication includes cutting the ingot into slices, polishing and etching, deposition of electrodes and packing of the detector into a safe case with a preamplifier and cooler. Crystal quality and electrical parameters of slices are controlled during the fabrication process. The operations are often followed by annealing. The detector fabrication was done in collaboration with GIREDMET (Russia), Bruker Baltic (Latvia) and Oxford Instruments Analytical Oy (Finland).

4.1 Slice preparation

The cutting and polishing operations during slice preparation damage the soft sample.[114] Different mechanical and chemical treatments of the TlBr wafer have been shown[115] to affect its performance as a radiation detector. Therefore, in this work, polishing and etching were carried out after cut operations in order to remove damaged material, and then an annealing was applied in order to eliminate strains introduced by the mechanical work.[I-III] The crystal and surface quality were tested by the X-ray rocking curve method, optical and SEM microscopy, and under polarised light. The effects of polishing and etching on the properties of TlBr single crystals were studied in paper III.

TlBr is extremely soft material (Knoop hardness of 12 kg/mm^2 – about the same hardness as refrigerated butter[2]) and the cutting operation deeply damages the TlBr crystal.[III] This problem is known for many soft materials, and different cut methods, including chemical methods, have been tested to try to solve the problem. One example is tellurium, which is harder than thallium bromide by factor ~4 (Mohs value of Te is 2.3, which corresponds to ~50

on the Knoop scale[38d]). Abrasive wheel, wire and airjet, and cleavage and spark discharge methods have all been tested for tellurium.[114] The first three methods produce considerable smearing of the diffraction spots in Laue back-reflection X-ray photographs. Cleavage causes much less structural damage, but this method can only be used for cleavage planes, which are not present in TlBr.[116] Spark cutting does not create noticeable structural damage, but the resulting surface is grooved and unsuitable for optical or electrical studies.[114] TlBr crystals are cut with a diamond saw,[66] razor blade[75] or wire saw,[117] which damages the surface layer to a minimal depth.[118]

Polishing is used in order to remove damaged material after cutting, to clean the surface of contamination and to flatten the surface. Since TlBr is a viscous, sticky material, during a mechanical treatment the slices are glued to a special hard substrate in order to avoid deformation,[118] and alumina abrasives are used for lapping and polishing.[117, 119] TlBr under moving abrasive resembles a viscous liquid. When the material is polished, areas of compression and expansion are formed in front of and behind the moving abrasive grain, respectively. TlBr particles, which are produced by polishing, stick to each other and to some grains. As a result, channels (see Fig. 17) and waves (see Fig. 18a) are formed on the surface of a crystal. Deep tracks and damaged areas that are most typical for machine polishing[III] can be avoid ed by manual polishing,[6] which was used in this work.

4.2 Chemical cutting and polishing

The process of making the TlBr slices with an abrasive results in deep structural damage to a depth of ~1.7 mm.[III] This destruction cannot completely be removed by heat treatment. Therefore, chemical procedures for cutting and polishing that have been developed for soft Te[114] were applied for TlBr. During a 'solvent cutting procedure', a horizontal thread impregnated with solvent was passed over the surface of the sample. Water, sulphuric acid, and a mixture of hydrogen bromide acid with hydrogen peroxide were used as solvents. Water, a weak solvent, was non-effective. Acids were aggressive to the thread, which was quickly torn.

For chemical polishing, a flat glass plate was placed in a Petri dish and covered with appropriate solvent. The sample was then moved continuously over the surface of the glass, the suede, cloth or filter paper. Pure water, ethanol solutions and a mixture of HBr with H_2O_2 were used as polishing solvents. This technique produced smooth surfaces without crowning and, in comparison to the mechanical treatment with abrasive materials, decreased the FWHM and increased the intensity of X-ray rocking curves by factors of ~6 and ~7, respectively.[III]

In general, slicing of TlBr using a solvent saw is currently limited by lack of a suitable thread and solvent. The solvents used are aggressive and their combination with TlBr is toxic. Chemical polishing procedures permit to avoid mechanical damage to the material and, in this work, these operations were used as a final phase after mechanical polishing.

4.3 Etching

Due to interaction of the sample with environment during annealing, the etching figures appear on the surface, revealing the dislocation lines, pits, surface imperfections and non-uniform areas.[III] Etching is used to remove contamination, by-products of the polishing and damaged parts of the crystal.[66, 117, 119, III] The dissolving activity of the solution determines the etching result. At high dissolving rates, parts of the surface that stand out in relief are dissolved more quickly than smooth and concave areas (*smooth etching*). As a result, the coarse surface becomes smooth and with appropriate reagents mirror-like faces can even be produced. Smooth etching is useful for finalising the slicing process before electrode deposition. In contrast, at law dissolving rates, parts of the material under different stresses or with different imperfections and deviations from stoichiometry are dissolved at different rates (*relief etching*). As a result, on the smooth surface the relief areas appear, if the sample is non-uniform.

Among the smooth etching agents, hot saturated nitric and sulphuric acids dissolve the Tl halides,[52b] the process being difficult to control. The oxidation process of Tl^{+} to Tl^{3+} with bromine is more easily managed. Bromine methanol solutions are often used during detector fabrication,[117, 119] since they produce smooth surfaces.[66] Another recipe is a freshly prepared mixture of HBr and H_2O_2 (5:1), which takes away the residual abrasive, removes the TlBr powder and smoothly dissolves as a damaged as well non-disturbed bulk layers. Chemical polishing and etching with this solution applied to a TlBr single crystal which has already been treated with abrasive materials increased the intensity of X-ray rocking curves by a factor of ~100.[III]

Decreasing temperature and/or dilution of the smooth etching solution slow down its activity and convert the process to relief one. The same effect is observed when a limited amount of etching solution is used (‘hungry etching’ shown in Fig. 18a). Also, less active solvents can be used for relief etching. Hot water and water-alcohol solutions readily dissolve TlBr. For example, sinking the crystal of TlBr into boiling water for several seconds causes the blocks and separate crystals to become visible in reflected light. In hydrothermal

annealing, the slightly dissolving conditions produce on the sample surface characteristic etching zones, channels and pits, as shown in Fig. 19.

Imperfections result also in higher volatility of areas adjacent to the imperfection. At moderate rates of sublimation, a pseudo-equilibrium exists between vapour and the sample, and the more damaged and imperfect areas of the material sublimate faster. This selective sublimation, called *thermal etching*, reveals the grain structure[120] and results in some quite characteristic figures being produced on the different crystallographic planes.[114, 121]

The symmetry of each etch figure appearing in a crystal face should conform to the symmetry elements of the point group normal to that crystal face. Furthermore, the relations between the shapes and positions of etch figures on the various faces of a crystal should conform to the symmetry relations of these faces.[122] The shapes and orientations of the etching pits might be used as hints to the internal symmetry.[123] The correct determination of the point group symmetry to which a crystal belongs can be often made if etch figures are carefully interpreted.[124] Several etching solvents at different concentrations should be used, as a single solvent may produce misleading effects. For the same reason, solvent molecules having only axial symmetry must be avoided.[123]

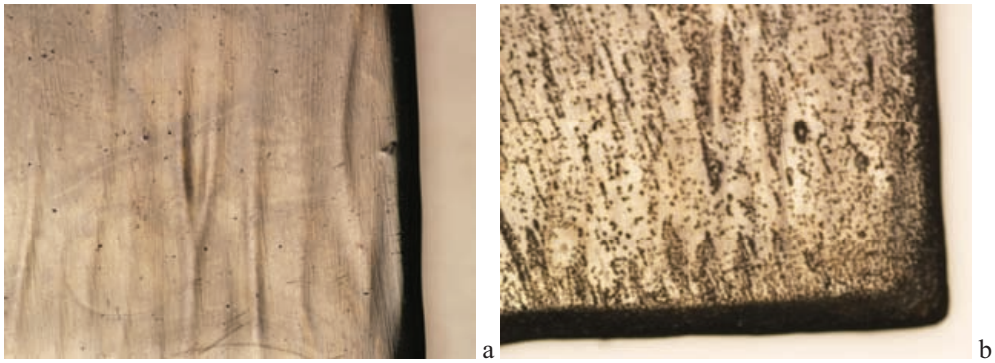

Fig. 18. (a) A worked TlBr crystal after smooth etching was additionally etched in ~0.5 ml of a mixture of HBr and H_2O_2 (hungry etching). (b) Then, thermal etching was carried out at 300 ^oC in N_2.

The final form of the pits has been explained by the difference in growth/dissolving velocities between the faces with various hkl indices.[122] This approach, based on descriptions of end forms of a crystal after dissolving,[81] does not provide a reason for the higher activity in the sample area (*cluster*) around the lattice imperfection. For example, when the crystal is etched by solvent, the cluster is dissolved slowly, the edges of the pits being sharp (Fig. 19B); in thermal etching, the cluster explosively sublimates and the edges of the pits are broken.[III]

Additional information about forms and symmetry of etching pits has been summarised by Buckley.[81]

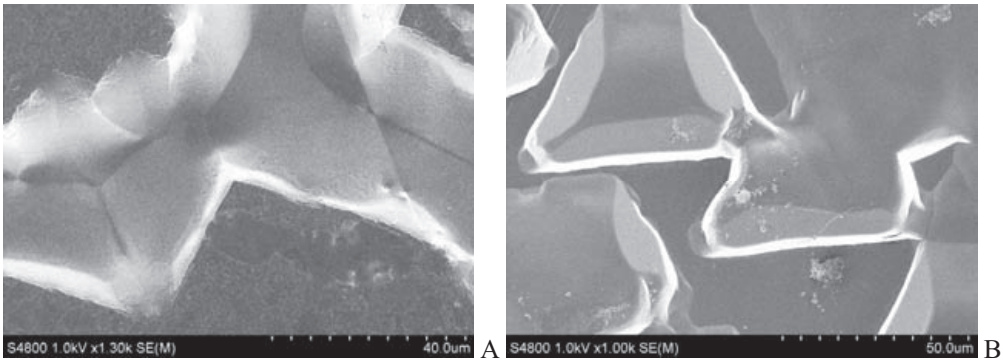

Fig. 19. Hydrothermal etching of the (111)-plane of TlBr: the formation of a channel (A) from a line of three-fold pits[III] (B).

A real view of the pit depends on the orientation of a crystallographic plane relatively to the sample surface, which cuts the cluster. Visual distortion also increases at higher indices of a cluster's face. As pits are formed at the sites of imperfections on the etched surface, the density of pits characterises the crystal quality.[114] The distribution of pits reveals a number of details about the nature of defect allocation,[125] so that the lines of etch pits are formed at the sites where dislocations meet the surface (see Fig. 18b).

In general, etching is used to remove surface contamination and damaged layers of the crystal. Relief etching of different planes of a crystal results in discovery of non-uniform areas and quite characteristic etch figures, whose shape, density and distribution over the surface can supply information about the quality of the crystal and the nature of imperfections. In this work, hydrothermal and thermal etching procedures were additionally used for identification of non-uniform areas of TlBr single crystals and characterisation of the symmetry of the etching pits.[III]

4.4 Crystal orientation

The drift velocity of carriers depends upon the orientation of the electric field relative to the crystal lattice.[32] Therefore, the slicing process requires a precise orientation of cut-off surfaces with respect to crystallographic axes of a single crystal. For the orientation of large ingots, mathematical approaches and machining techniques have been developed in the semiconductor industry.[87c] In research laboratories, several simple methods can be used for rapid orientation of a crystal before its cutting.

Since the rates of dissolution in non-equivalent directions are not the same, the *dissolution method* can be used for determination of the symmetry of the crystal and its orientation.[122] The method applied to a TlBr crystal shows development of the edge and faces of a cubic structure from the cylindrical form of the ingot (see Fig. 20). The second way by which dissolution of a crystal provides symmetry information is the etch figures considered in chapter 4.3. The axes and faces of the pits correspond to those of a crystal and, thus, the crystal can be properly oriented for slicing.

Fig. 20 The effect of the dissolution method on a TlBr ingot: the development of a cubic shape from the cylindrical ingot during dissolution under hydrothermal conditions in pure water for ~5 days.

Although many properties of cubic Tl halides are isotropic, the plastic properties and character of destruction depend on the crystallographic orientation of the crystal. In KRS-5 during compression of the crystal in the [100]-direction, the slip takes place along the (110)-planes.[44f] This anisotropic property of deformation is utilised for identification of the crystallographic plane on the surface of the crystal by the so-called *punch-pattern method*. In this method, the surface of a crystal is lightly pricked with a needle that produces the 'star' figures, which are specific for each crystallographic plane. The figures have been tabulated as patterns[126] that can be used for rough (5-10^{o}) orientation of a crystal.

Correct setting of the required crystallographic plane may be done using the *X-ray rocking curve method* that is described in chapter 5.3. A problem often arises from the large volume of the ingot that can not be freely positioned inside the diffractometer's compartment. In this case, dissolving or punch methods can be used for rough crystal orientation and making the wafers. The final slicing is done using precise determination of the orientation by the rocking curve method.

4.5 Electrode deposition

Properties of electrical contacts have a primary role in the performance of semiconductor gamma radiation detectors.[127] Metallisation of a dielectric TlBr material with different metals has specific features.[IV] Polarisation and degradation effects during prolonged detector biasing[V] and ageing processes[128, 129, 130] take place on electrodes. The processes associated with electrodes and their deposition are summarised below.

4.5.1 Electrode choice and design

The actual detector application determines the electrode materials. The detector can be equipped with ohmic or blocking (Schottky) contacts. The metal-semiconductor interface properties depend on the metal's work function, the semiconductor's band gap, and the type and concentration of major carrier. The barrier height between ionic compounds and metals was found to be directly proportional to the electro-negativity of the corresponding metal that would be used for the detector's design.[131]

By application of blocking contacts to a crystal with relatively high trapping, the leakage current can be decreased, which significantly improves the energy resolution of the device.[24] However, the depletion layer for such a device is on the order of a few hundred microns, so the device can not operate well for gamma rays, whose penetration into the detector is considerably deeper than this layer. Moreover, in blocking contact devices, there is practically no de-trapping mechanism for freeing charges within the forbidden band.[127]

For operation with gamma rays and, particularly, for hard gamma rays, ohmic contacts applied to high resistivity materials are an alternative to blocking contacts. The resistivity can be increased by application of materials with a higher bandgap and/or by the use of high-quality materials, i.e. materials with a high $\mu\tau$ (mobility-lifetime product) for both electrons and holes. In addition, p-type detectors have a higher resistivity than n-type detectors, due to the higher mobility of electrons than holes. In a p-detector with ohmic contacts, the holes freely enter and exit the bulk through the contacts, thus the leakage current is less noisy and the detector has higher resolution.[127]

In general, different electrode materials can be routinely used for making either ohmic or blocking contacts with either p- or n-type detectors. The final choice is based on the given application and existing equipment, so that for proper detector operation, different contact materials should be used for the positive and negative bias.[127] There is a thorough summary of contact resistance and Schottky barriers that can be used for detector design.[132]

4.5.2 Types of deposition

The way in which the electrode can be deposited depends on the nature of the electrode material. In general, chemical, physical vapour, metallurgical and glue methods of deposition are used for the metallisation of semiconductors. In the chemical method, a metal layer is formed on the substrate as a result of a chemical reaction. By this method, noble metals may be deposited as a thin film. For example, gold deposited on a TlBr slice from a chloroauric acid forms a 100–200 Å thick film.[118] The method is easily combined with chemical purification and etching of the surface, so that metal is directly deposited on the clean surface, the interaction with ambient atmosphere being excluded. However, the thinness of gold films obtained by this method has caused technological problems for wirebonding,[118] and application of the method to Tl halides is not much studied and has mostly been ignored by researchers.

Physical vapour deposition methods are the most common techniques used for making electrodes. Many metals form smooth metal films with a thickness of about 0.5 μm by the vacuum deposition method.[116] However, for gamma-ray applications, thinner metal layers are needed and, therefore, sputtering and electron beam (EB) deposition methods could be preferable for production of 10-100 nm thick films in a highly controllable manner. On the TlBr substrate, 20-50 nm Al, Cr, Ni, Pd and Ti can be easily deposited using an EB evaporator. The films are smooth and stable.[IV, V]

The metallurgical depositing methods can be applied with metals that have a melting point below that of TlBr, which is 460 ^{o}C. Actually, the limit is about 300 ^{o}C, above which the vapour pressure of TlBr has to be taken into account. The method has been used for making point contacts from In and Sn.[IV] The resulting films were thick but reliable. With an appropriate temperature and annealing time, a compound intermediate between the molten metal and the TlBr crystal surface can be formed (see chapter 4.5.5).

A glue method of electrode painting is convenient for rapidly producing contacts in cases where only an evaluation of crystal quality is of interest. The method is based on the gluing and protective properties of a third substance, which makes the mechanical contacts between the TlBr crystal and metallic particles spread inside glue. Several commercially available epoxy, polymer and paste mixtures with Al, Ag and graphite particles were used in this work. Additionally, conducting glue can be used for the protection of a deposited electrode[118] and fixation of a mechanical contact between an electrode and wire (wirebonding).

4.5.3 Surface quality

The metal-TlBr interface is formed due to adhesion, diffusion of metal and substrate, or formation of an intermediate compound.[IV] Formation of contacts strictly depends on the surface purity of the substrate and its crystal quality. For example, pre-treatment procedures before deposition typically included etching (chapter 4.3), washing with HBr and ethanol, and degassing under a vacuum of $5x10^{-6}$ - $5x10^{-7}$ mbar for 3 h or more.[IV, V] In case of impurities and incomplete degassing, TlBr interfaces with Fe and Ni quickly became black. In EB deposition, where a high vacuum is required, the use of metals with good gettering ability, such as Ti and Cr, gave smooth and bright layers.[IV]

Good crystal quality of the surface is important for adhesion and stability of the deposited layer. A cleavage method routinely used for preparation of clean and non-damaged crystal faces produces coarse torn surfaces in the case of Tl halides, even below room temperature.[116] For the study of adhesion and stability of metal electrodes, clean surfaces were produced by cut-off a layer less than 0.1 mm thick from a crystal directly under depositing metal vapour in a vacuum chamber.[116, 129] However, this operation could deeply damage the crystal, although it might improve adhesion[III] and should provide good ohmic contact due to high recombination rates.[132] But the damage also produces a net of deep splits that prevents the use of thin electrodes. Also, an electrode on damaged material and damaged material itself are less stable at ambient conditions.[128, 129, 130]

Thus, in the case of ohmic contacts a compromise between the extent of damage, stability and electrical requirements should be found. On the other hand, for the blocking electrodes the highest crystal quality is needed. In any case, the best surface purity and required crystal quality after mechanical treatments can be achieved by the use of chemical polishing and etching (chapter 4.2 and 4.3, respectively) and then by careful degassing.

4.5.4 Metal – Tl halide interactions

The adhesive interaction at the film-substrate interface can be mechanical, physical or chemical, accordingly to the nature of the binding forces. In mechanical joining, fluid material fills the trenches, holes or pores of a coarse substrate surface. After fluid solidification, the interface becomes mechanically anchored. The fluid and substrate work as a ‘key and lock’. When the interaction is physical, the adhesion (physiosorption) is realised by dispersive van der Waals forces between molecules with closed electronic shells. In addition, the formation of charges across the film/substrate interface and diffusion process can take part in the

physical interaction. In chemical interactions (chemisorption), primary covalent, ionic and metallic bonds contribute to adhesion.[133]

"Pure" mechanical, chemical and physical bindings are rarely achieved. For example, in a mechanical interaction, if the fluid material is a metal, a physical adhesion often takes place; if the fluid is glue, chemical bonding can occur, as well. Physical adsorption forces between metals and alkali-halides are usually weak, since ionic compounds have closed electronic shells. However, in the case of thallium (I) halides, the free inert electron pair of thallium tends to take part in covalent bonding (see chapter 2.1) and therefore, chemisorption phenomena contribute to physiosorption of different metals on a Tl halide surface.[116a]

A physical interaction is often observed between interface surfaces even in the case where chemical bonding is expected. In this case, chemisorption might be activated by the post-deposition annealing that is often used for improving interface quality. Since the melting point of Tl halides is around 450 ^{o}C (see Table 2), physical adhesion is expected with refractory metals.[IV] For example, gold metal, which is also resistant to ambient conditions, is widely used as an electrode for TlBr detectors.[39, 134]

Physical diffusion, accelerated by temperature and aging time, promotes the penetration of atoms of one material into another. The interface is spread out by inter-diffusion into the third dimension, and the boundary gets smeared. This type of film-substrate junction is known as a diffusion interface.[133] Due to the different inter-diffusion rates of atoms the interface shifts,[135] which is known as the Kirkendall effect.[133] In a chemical interaction, diffusion creates an intermediate compound layer or multilayer structure. The structure, being a separate phase under stress between the film and substrate, is often brittle.[133]

In turn, the nature of interface bonding is difficult to analyse because of the mixed character of the interactions involved, effects of temperature and aging. Moreover, approaches involving the nature of bonding are difficult to test because of the lack of a broadly applicable method for quantitatively measuring adhesion.[133] Element depth profiling might schematically supply information about the type of interaction across the metal–substrate interface.[IV] Several profiling techniques are available at this time. Starting from the work of Ziegler et al.,[136] neutron depth profiling (NDP) has been commonly used for characterising light element distribution near the surface. The Rutherford Back Scattering (RBS) method has been used for the determination of depth distributions of heavy elements in lighter compound semiconductors.[137] Dynamic Secondary Ion Mass Spectroscopy (Dynamic SIMS) is capable of profiling all elements[58b] and has been used for analysis of KRS-5.[56]

4.5.5 Metal – Tl halide interface stability

The study of the effect of adhesion on film quality, durability, and environmental stability has more pragmatic meaning than academic approaches based on the atomic binding energy.[133] Adhesion strength, intermolecular interactions, stability and ambient induced processes have been studied for different metal films on various halide crystals.[116, 129] In Tl halide interfaces, adhesion strength has been shown to depend on van der Waals interactions, chemisorption forces being added to this interaction when the free energy (ΔG) of the metal–Tl halide interface is positive.[116b] Unfortunately, crystal imperfections and surface contamination and defects have not permitted correlations between theory and experiment to be made.

The adhesion stability of metal films on a Tl halide crystal has been shown to correlate with the difference between the normal oxidation potentials of Tl and the electrode metal (M), ΔE(Tl, M).[129a, 138] In Table 4, metals are classified into three groups according to values of ΔE(Tl, M). In the first group, ΔE(Tl, M) is reasonably positive and metals react with halides during deposition just in vacuum. In the second group, ΔE(Tl, M) is around zero and interfaces are stable. Metals of third group have negative ΔE(Tl, M) values, but their interfaces, although stable in vacuum, are unstable at ambient conditions.[129a]

Instability in first group originates from direct chemical reactions between the metal (M) and TlBr (Eq. 12) when the corresponding free energy ΔG is negative:

$$M + nTlBr = MBr_n + nTl \qquad \text{(Eq. 12)}$$

The reaction with Mg and Mn, which standard ΔG^o is negative, takes place already during deposition. An ~500-nm thick layer of Al made by an electrically heated evaporator on the hot TlBr crystal (small positive ΔG^o) peels off just after deposition.[116] However, a 40-nm thick layer obtained by EB deposition on a TlBr substrate cooled to approximately room temperature is stable.[IV] Al-TlBr interfaces, which are prepared by TlBr vapour deposition on Al-foil at temperatures below 150 ^oC (see chapter 3.3.3), are also stable. TlBr thin films stick strongly to substrate and stay attached for several years. When the temperature of the substrate is above 150 ^oC, Al actively reacts with TlBr (see Eq.10). Thus, in case of the Al-TlBr interface, a variation in the process parameters (temperature, vacuum and layer thickness) gives different results: well-formed films with good adhesion or films that peel off, or a chemical reaction and total interface decomposition. In this work, both a TlBr film on Al substrate and an Al film on a TlBr crystal were stable, if they were obtained by EB deposition on the substrates at temperatures below 100 ^oC.

Table 4. Parameters of metals (M) on TlBr substrate.

Metal	mp, oC	EN	Tensile strength	Stability	Ox/Red	E, V	ΔE(Tl, M), V	M + nTlBr = MBr_n + nTl	ΔG^o	Additional Refs
Mg	649	1.31	X	Bad	Mg^{2+}/Mg	-2.372	2.036	Mg + 2TlBr = $MgBr_2$ + 2Tl	-169.989	138, 139
Al	660	1.61	Peel off	Bad (Good)	Al^{3+}/Al	-1.662	1.326	Al + 3TlBr = $AlBr_3$ + 3Tl	15.208	138, 139, IV
Mn	1244	1.55	X	Bad	Mn^{2+}/Mn	-1.185	0.849	Mn + 2TlBr = $MnBr_2$ + 2Tl	-35.294	138, 139
Ti	1660	1.54	18	Good				Ti + 4TlBr = $TiBr_4$ + 4Tl	80.918	139, IV, V
Zn	419	1.65	13		Zn^{2+}/Zn	-0.762	0.4258	Zn + 2TlBr = $ZnBr_2$ + 2Tl	25.25	
Cr	1857	1.66	14	Good	Cr^{3+}/Cr	-0.744	0.408	Cr + 3TlBr = $CrBr_3$ + 3Tl	131.196	138, 139, IV
Ga	29.8	1.81			Ga^{3+}/Ga	-0.549	0.213	Ga(l) + 3TlBr = $GaBr_3$ + 3Tl	143.636	
Fe(II)	1535	1.83	23	Good	Fe^{2+}/Fe	-0.447	0.111	Fe + 2TlBr = $FeBr_2$ + 2Tl	102.678	139, IV
Cd	321	1.69	36		Cd^{2+}/Cd	-0.403	0.067	Cd + 2TlBr = $CdBr_2$ + 2Tl	39.537	
In	157	1.78	18	Good	In^{3+}/In	-0.338	0.0022	In + 3TlBr = $InBr_3$ + 3Tl	137.803	138, 140, 139, IV
Tl	304	1.80		(Bad)	Tl^{+}/Tl	-0.336	0			111, 141, IV
Co	1495	1.88	22	Good	Co^{2+}/Co	-0.28	-0.056	Co + 2TlBr = $CoBr_2$ + 2Tl	134.5	138, 139
Ni	1453	1.91	22	Atm (good)	Ni^{2+}/Ni	-0.257	-0.079	Ni + 2TlBr = $NiBr_2$ + 2Tl	141.696	138, 139, IV
Sn	232	1.96	6	(good)	Sn^{2+}/Sn	-0.138	-0.1985	Sn + 2TlBr = $SnBr_2$ + 2Tl	107.328	140, IV
Pb	328	1.80	29		Pb^{2+}/Pb	-0.126	-0.2098	Pb + 2TlBr = $PbBr_2$ + 2Tl	75.079	140
Fe(III)	1535	1.83	23	Atm	Fe^{3+}/Fe	-0.037	-0.299	Fe + 3TlBr = $FeBr_3$ + 3Tl	265.745	139, IV
Cu	1083	1.90	24	Atm	Cu^{2+}/Cu	0.3419	-0.6779	Cu + 2TlBr = $CuBr_2$ + 2Tl	213.818	138, 139
Ag	962	1.93	27	Atm	Ag+/Ag	0.7996	-1.1356	Ag + TlBr = AgBr + Tl	70.97	142, 138, 143, 130, 144, 139
Hg	-39	1.90			Hg^{2+}/Hg	0.851	-1.187	Hg + 2TlBr = $HgBr_2$ + 2Tl	183.631	
Pd	1554	2.20		(good)	Pd^{2+}/Pd	0.951	-1.287	Pd + 2TlBr = $PdBr_2$ + 2Tl	247.087	77
Pt	1772	2.20			Pt^{2+}/Pt	1.18	-1.516	Pt + 2TlBr = $PtBr_2$ + 2Tl	277.26	
Au	1064	2.40	27	Atm	Au3+/Au	1.498	-1.834	Au + 3TlBr = AuBr3 + 3Tl	502.711	138, 139, 90, 39, 134

Comments. EN: Pauling's electronegativities.[34e] Tensile strength (MN/m^2) of 0.5-μm thick films was measured for the TlBr surface prepared by cutting in a vacuum.[116a]
Stability factors: Bad - chemical reaction (X); Good - stable; Atm - unstable under atmosphere[129] (in parentheses - results of this work and paper IV).
Ox/Red: oxidized/reduced M-species, normal potential of which is given under E, V[58c]; ΔE(Tl, M): difference between E(Tl) and E(M).
M + nTlBr = MBr_n + nTl: possible reaction for which ΔG^o, kJ/mol, is calculated.[57] Additional Refs are given for M deposited on halide crystals.
M – underlined metals are corroded under atmospheric conditions. Data for the most stable interfaces are shown in grey.

Metals of second group (shown in Table 4 in grey) have normal potentials around the Tl potential and a positive ΔG^o for reactions corresponding to Eq. 12. Therefore, the reactions are thermodynamically unfavourable, and M-TlBr interfaces are stable. These tendencies increase in the third group, where ΔG^o is more positive and ΔE(Tl, M) becomes more negative[129a] towards the end of Table 4. However, there are several possible reasons for interface instability under atmospheric conditions.

Firstly, there is the aging of the separate interface components, TlBr and metal itself, which are exposed to ambient conditions. The aging of TlBr gives the hydrogen and carbon oxide compounds described in chapter 3.1. Corrosion of the electrode metals Fe, Tl, Ni and Cu takes place under atmosphere conditions, thus the use of these metals is limited. Secondly, in so-called *ambient induced reactions*,[129] the electrode material of the third group participates in the interaction between atmospheric components and TlBr as a catalyst and/or forms intermediate compounds. The reaction products can include Cl, S and C from the atmosphere.[130]

In addition to the metals studied in Ref.,[116, 129] Ga, Tl and Hg are appended to Table 4 as metals able in the fused state to make contact with solid TlBr, and Pd and Pt are appended as alternatives to gold. In the deposition of metals in the molten state on a TlBr single crystal, indium and tin interfaces are stable. Thallium quickly forms a brittle intermediate layer.[IV] Pd-TlBr interfaces,[77] as well as those with Ni and Fe,[IV] are stable under ambient conditions if they are made and stored under clean and dry conditions.

In semiconductor devices, the intermediate layer is unique because it may provide a reliable and reproducible Schottky barrier.[131] In order to form intermediate compounds, In, Tl and Sn in the molten state at a temperature of ~310 ^oC were examined on the surface of TlBr single crystals.[IV] Indium easily develops an intermediate layer. The device shown in Fig. 21 after deposition of the opposite electrode at a lower temperature demonstrated rectifier properties. Thallium in the molten state forms on the surface of TlBr a dark-brown layer more readily than indium. However, all attempts to make a good contact by the melting method failed, because the layer was brittle. The prolonged annealing at 300 ^oC initiated TlBr evaporation and formation of a thick mixed Tl-TlBr compound with an extremely coarse surface. Molten tin forms good contacts with a TlBr crystal without formation of an intermediate layer. Therefore, low and high temperature contacts were similar and no rectifier effects were found in this case. Possibly a higher temperature is needed for Sn-TlBr intermediate compound formation, but this could stimulate TlBr evaporation.[IV]

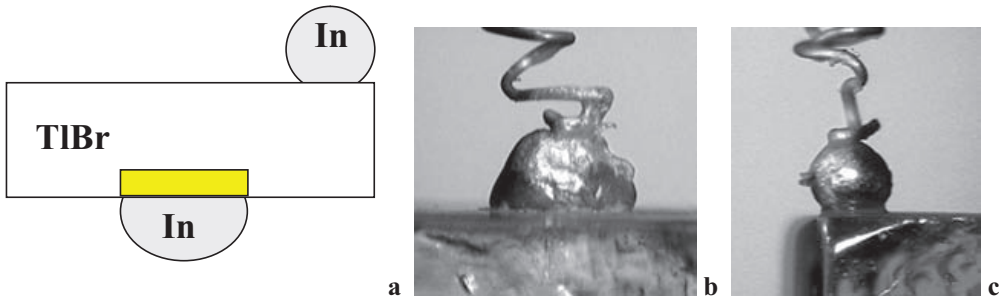

Fig. 21. Indium.-TlBr-Indium interfaces. Schematic view (a), Indium on the bottom side after annealing at 310°C (b). Indium-drop on the top-side of TlBr (c).

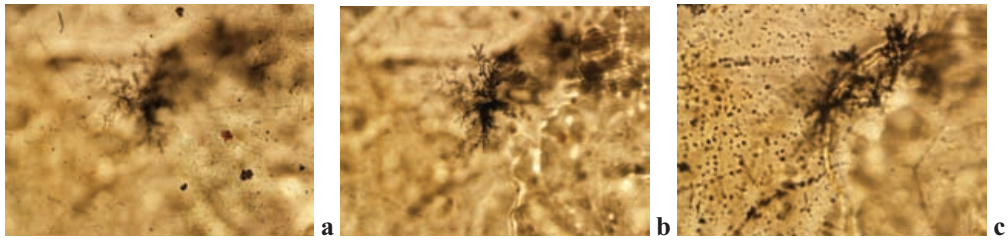

Fig. 22. Channel tree formation inside a sample under a prolonged electric field: focusing on the top (a), middle (b) and bottom (c) of the sample. Electric field of ~2 kV/cm, Ag-paste electrodes (magnification: 10x10, bright field.

In general, the interaction between a metal and substrate produces interfaces in which bonding of the surfaces occurs by mechanical, physical, chemisorption or diffusion mechanisms. A temperature increase can change the mechanism of primary bonding from one to another. Deposition at elevated temperatures and post-annealing used to improve adhesion and enforce diffusion can also initiate chemical reactions. If volatile products are formed, the film peels off. The metal-thallium exchange reaction Eq. 12 destroys the interface. A special case of chemical interaction is formation of an intermediate layer as a third phase between an electrode and substrate.

4.5.6 Electro aging of the metal-TlBr interface

The metal-TlBr interface becomes less stable under applied voltage. TlBr-based X-ray detectors tend to be short-lived. Time dependence of the electrical parameters of radiation detectors has been termed *detector polarisation*.[2, 40] The phenomenon is expressed as a steady drift of the peak position during the measurement of pulse–height spectra.[40] Suppressing polarisation phenomena improves detector performance in TlBr detectors.[141] The degradation of the metal-TlBr interface under prolonged biasing or 'electro aging'[V] has been studied by

electrical,[111] photoelectrical,[110, 145] XRD, SEM and EDS[V] methods. The polarisation problem may be considered on the following levels.

Firstly, a TlBr crystal, as dielectric material surrounded by electrodes, is a capacitor. Under applied voltage its plates collect negative and positive charges from the external circuit.[146] In a TlBr crystal, as in a semiconductor, the field induced inside it moves the holes and electrons towards the corresponding electrodes. An excess of electrons and holes at the electrodes creates a field which is opposite to the applied one, i.e. electrode polarisation, caused by the electrons and holes.

Secondly, degradation of the TlBr ionic crystal has been proposed to be caused by ionic current.[110] The corresponding activation energies determined from the pressure and temperature dependencies of the ionic conductivities[112] and from the temperature and frequency dependencies of resistance[111] are equal to 0.785 eV and 0.8 eV, respectively. The ionic current becomes noticeable at temperatures higher than 250 ^{o}K.[111] This temperature limit can possibly be increased for more pure TlBr, since impurities increase reasonably the level of conduction curves of alkali, silver and thallium halides.[17] Under applied voltage, Tl^{+} and Br^{-} ions are accumulated at the cathode and the anode in TlBr detectors, respectively,[141] and decrease the electric field inside the detector, i.e. create electrode polarisation caused by ions.

The contribution of cations and anions to conductivity is expressed in terms of *transport numbers*[148] (or *transference number* in electrochemistry[149]). Positive ions are found to account for most, but not all, of the conductivity of the alkali halides. The transport numbers are functions of temperature, and the role of negative ions increases with temperature. On the other hand, the positive ion transport numbers for silver halides are very close to 1.0 at room temperature and also at higher temperatures.[148] In thallium halides, the dominant charge carrier is believed to be the anion at temperatures of 350-700 K.[112, 150, 151] For pure TlBr, the anion transport number at 527 ^{o}K is 0.9 with the relatively great error (0.1) being due to the unfavourable mechanical properties of TlBr.[152] At the same time, during prolonged electro-biasing at temperatures below 330 ^{o}K, the total electric charge passing through the Al-TlBr-Tl-Al metal-insulator-metal system corresponds to the amount of Tl layer, which has been explained by the electro diffusion of the Tl^{+} ion as the primary carrier.[111] Therefore, it is quite rational to suggest that the role of cations and anions in TlBr changes with temperature as their mobility and transport numbers are different in different temperature regions. As a result, gram-equivalent concentrations of the movable ions in the vicinity of a cathode and anode are,

like in liquid electrolytes, not equal.[149] Thus, ionic polarisation of negative and positive electrodes is not equal, either.

Thirdly, the passage of the ionic current through the crystal is followed by electrochemical reactions with ion discharging. The Tl^+ cation takes an electron from external circuit through the cathode, giving a cation vacancy. The metallic thallium produced is collected at the cathode metal. Additionally, the anion vacancy of Br^- has been suggested to capture the cathode electron[141] which is, in fact, an electron trap. At the anode the Br^- ion can discharge giving bromine gas and an anion vacancy; also, the anode metal M can "be dissolved", producing an M^{z+} cation in the Tl^+ ion position (annihilation of cation vacancy) or in an interstitial location. Additionally, it is reasonable to suggest that the electron captured by the anion vacancy can be freed into the external circuit through the anode.

The device could be a reversible charge accumulator, but if gaseous Br_2 is formed, the anode peels off the crystal. Hopefully, discharge reactions take place with different potentials. For example, in aqueous solutions the reduction reaction for thallium $Tl^+ + e^- = Tl$, has a potential of -0.336 V, and for bromine the reaction $Br_2 + 2e^- = 2Br^-$ has a potential of + 1.0873 V.[34g] For this reason, bromine evolution is less probable and some kind of reversibility can be observed. If the applied voltage is switched off, the device works as a charged accumulator and an opposite current is registered for several days due to the reverse process, for example, $Tl \rightarrow Tl^+ + e^-$. In experiments on detector degradation, 46% of initial detector performance was recovered one hour after switching off the detector bias and removing the X-ray source.[40] Thus, the third type of electrode polarisation is caused, in fact, by electrochemical reactions.

Fourthly, passage of the current through the detector stimulates third party reactions. For example, a titanium cathode in a pair with metallic Tl formed during Tl^+ discharging is intensively oxidised.[V] The corrosion of Ti makes the degradation of the Ti cathode irreversible. Next, bromine, as a product of electrolysis, can form a compound with the anode metal, see for example Ref.[141] This precipitate decreases the contact area and, as a result, electrode performance. Material quality is very significant for electro aging. In Fig. 22, the chemical reaction starting at the crystal face penetrates into the bulk of the material probably along crystal block boundaries and imperfections in the direction of the applied electric field. The process path appears as a system of channels at different depths in the crystal.[110] The process is possibly similar to so-called electro-migration in semiconductors.[132] When a more perfect sample is employed, no indication of any burning effects are observed in TlBr even at higher electric fields.[IV] Thus, the formation of third party compounds at the metal-TlBr interface and inside the crystal cause irreversible degradation of the detector.

It is desirable to make devices equipped with electrodes that are free of chemical polarisation and electrode degradation. Inert electrodes such as Au and Pd are often used in order to avoid degradation reactions. However, the formation of gold bromine complexes at the anode was suggested by Hitomi.[141] In order to avoid polarisation associated with the passage of ionic current, Tl-electrodes have been used. The device in steady state collects the metallic Tl on the Tl cathode, when Tl^+-ions enter from the Tl anode into the bulk and discharge at the opposite Tl cathode.[141] The Tl electrode, in turn, is covered by Al[111] or Au[141] in order to protect it from oxidation. A reported Au-Tl-TlBr-Tl-Au device was free of significant polarisation phenomena for ~30 h, although the resolution was lower than for a less stable Au-TlBr-Au device.[141]

In order to suppress polarisation phenomena and Tl deposition on the cathode, Hitomi[153] changed alternatively the DC voltage. However, ionic current is similar to a hidden leakage current, which decreases the device resolution.[37, 127] Moreover, the devices are not protected against the anodic reaction

$$Br^- + Tl(anode) = TlBr(powder) + e, \quad \text{(Eq. 13)}$$

according to which the TlBr powder formed will destroy the Tl-anode – TlBr (single crystal) interface. Another approach to this problem is to increase crystal hardness by doping crystals with ingredients that can lock dislocations and vacancies in place. However, such an attempt with In^+ and Pb^{2+} led to degradation of the electrical, optical and detector properties of TlBr.[154] The use of the purest TlBr with the highest crystal quality and a lowering of the temperature of the device to below the level of noticeable ionic current seems to be the only solution to suppressing the polarisation effects associated with the ionic current and to make the gamma-ray detector more durable.

5 Characterisation methods

Several instrumental methods were used for optimisation of the single crystal manufacturing and detector fabrication. For evaluation and characterisation of the material properties, the following methods were most effective: imaging techniques using a light polarisation microscope and a Field emission scanning electron microscopy (FE-SEM); optical spectroscopy including ultraviolet and visible (UV-Vis) and Fourier transform infrared spectroscopy (FTIR); X-ray diffraction methods (XRD) including powder, rocking curve and single crystal diffraction techniques; electrical characterisation involving voltage-current (*I-V*), photocurrent, current-time, capacitance and electro-aging measurements; elemental

analysis with high-resolution inductively coupled plasma mass spectrometry (HR-ICPMS) and energy-dispersive X-ray analysis (EDS).

5.1 Microscope imaging techniques

Imaging techniques are powerful tools for visualising the details of an object. Due to focusing systems and the penetration ability of radiation, depth information is represented in images, as well. Topological contrast is achieved by shadowing using different modes of illumination/irradiation (incident angle) singly or in combination.[155a]

For routinely obtaining relief views of samples, LEITZ WETZLAR (Germany) and Nikon INSTRULAB (Japan) light microscopes were used with lateral illumination.[I-VII] A preliminary evaluation of the crystal quality was carried out using the polarisation microscope LOMO MPS-2U4.2 (USSR)[II-IV, VI] and OLYMPUS SYSTEM MICROSCOPE BX51 shipped with an OLYMPUS Digital SLR Camera E-500.[VII] The last device was used for preparation of the photos in this monograph. The surface morphology was examined in more detail with an electron microscope Hitachi S-4800 FE-SEM.[III, V, VII]

5.1.1 Light polarisation microscopy

In a cubic system, to which TlBr is assigned based on its CsCl-type lattice, the refractive index is the same along all directions of propagation.[113a] The high order of symmetry of cubic crystals results in cancellation of the directional effect of neighbouring dipoles, just as does the random arrangement in a liquid.[113b] However, solid isotropic media, when strained, acquire to some extent the optical properties of anisotropic crystals.[113c] If the sample is placed on a microscope stage between fully crossed polarisers and displays one or more colours, it has more than one refractive index. If the colours are spotty, the sample has some kind of strain birefringence or/and internal block disorientation. For anisotropic materials, stage rotation may show pleochroism, a change in the colour of the spots that is seen as bright flashes from separate areas of a crystal during rotation.[155b]

Strained Tl halides are coloured under polarised light, and this property has been used for determining the effects of annealing on strain in KRS-5.[1] A direct correlation made between strain fields and birefringence produced under a polarising microscope[47] has established the *stress-optical effect*, $\Delta n = q\sigma$, where Δn is the change in refractive index, q is the stress-optic coefficient and σ is the residual stress.[46] In this work, observations of TlBr under polarised light were used to determine the non-uniformities in samples during the total device process, as in the case of the abrasive treatment shown in Fig. 17, in which the morphological details, such trenches from polishing and their relative size, can be further evaluated.

5.1.2 Field emission scanning electron microscopy (FE-SEM)

The image in FE-SEM is produced by secondary electrons, which originate from the several upper tens of nanometres of the material under study. Due to the properties of electrons, not only crystal topology can be studied, but defects, magnetic domains, resistance and electrically charged regions can be revealed as well. The resolution in an FE-SEM image can be as low as 1 nm. FE-SEM images better represent the 3D-space (topology) of a specimen than optical images.[156a] The efficiency of topological contrast depends on the angle between the striking beam and the surface. If the instrument contains an energy dispersive X-ray spectrometer, the mapping of elements can be carried out. This additional information, covering a sample depth from several nanometres to the micrometer range, depends on the primary beam energy and particular physical process providing the contrast.[155a] Thus, FE-SEM has many advantages for uniformity analysis in semiconductors.

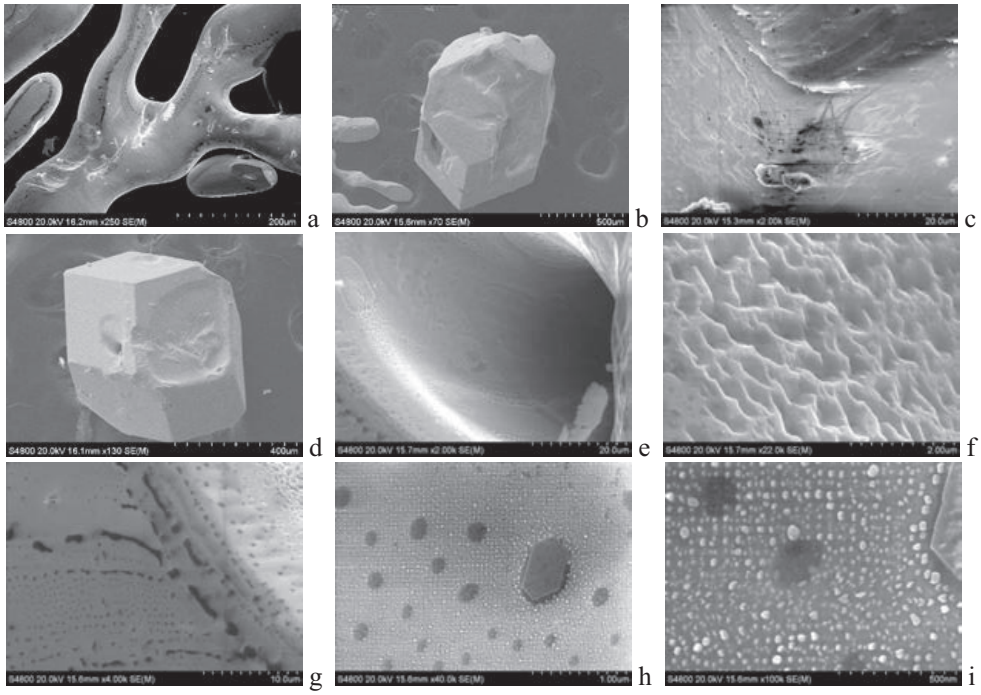

Fig. 23. SEM images of TlBr waste-material formed during the hydrothermal growth: (a) glassy TlBr material and (b) a broken crystal with rounded corner (c). (d) is another view of crystal (b) with a hole magnified in (e). View of the surface inside (f) and outside (g) the hole (e). Further magnification of (g): dark spots (h) surrounded by 'white' balls (i).

Conventionally, there are two types of images in the SEM: secondary electron (SE) and backscattered electron (BSE) images. The SE is scattered by an inelastic mechanism at energies less than ~ 50 eV. The elastic scattering is responsible for the production of BSE at

energies greater than 50 eV and comparable to the energy of the primary beam. The probability of backscattering grows with atomic number Z, thus increasing the brightness of the BSE image.[155c]

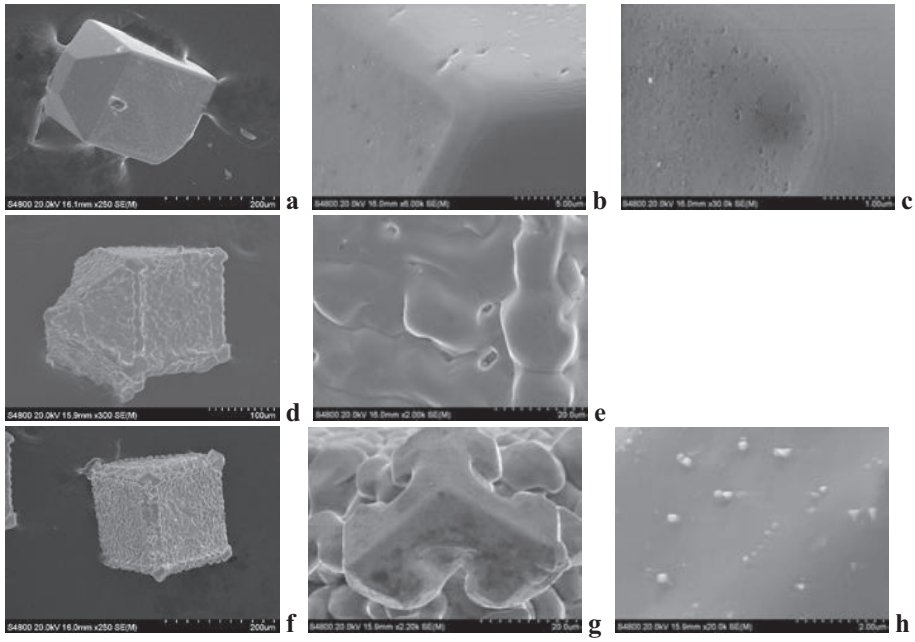

Fig. 24. SEM images of crystals grown by the hydrothermal method in solution supersaturated with Tl bromide and iodide. A 'yellow' crystal (a) and one corner magnified (b) and (c). A 'green' crystal (d) and its edge magnified (e). Another 'green' crystal (f) and magnification of a skeleton corner (g) and (h).

The origin of elastic (for BSE[156b]) and inelastic (for SE[156c]) scattering allows the separation of emitted electrons based on the energy[155c] or the angle distribution. Practically, it can be done with a detector that treats both signals, or with a detector that is selective for one of the signals.[156d] The proper combination of two SE detectors located at the side of the sample and above it produces images with good contrast and a deep depth of information. This method was used to study the effects of polishing and etching on TlBr single crystals,[III] degradation of the TlBr crystal and Ti electrode under prolonged bias voltage[V] and discovering the foreign phases inside the sample.[III, VII]

Several illustrations of the combination of two SE detectors are given in Fig. 23, Fig. 24 and Fig. 25. In Fig. 23, glassy material and broken crystal are examined. These by-products were formed between dissolving and growth zones inside a bomb during hydrothermal crystal growth. Yellow crystals, which are normal for TlBr, and green ones are formed in solution supersaturated with Tl bromide and iodide. The crystals are examined in Fig. 24. Another example in Fig. 25 is TlI grown by the hydrothermal cooling method. TlI is rhombic at room

temperature and cubic above 168 °C.[11a] The process started at a temperature of 180 °C produces amorphous products, triangle plates (a)-(e), and dendrite and broken crystals (f) that are similar to the TlBr broken crystals in Fig. 23b.

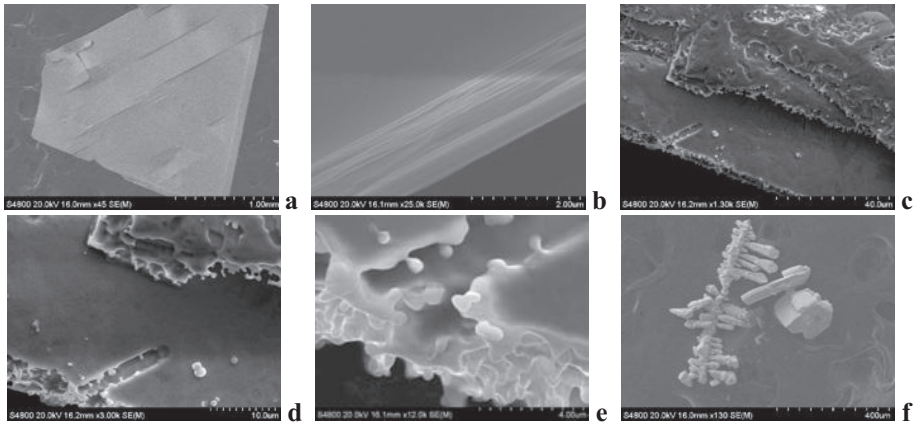

Fig. 25. SEM images of TlI crystals synthesised and grown under hydrothermal conditions. A triangle plate crystal (a) with a manually broken edge (b) and its own edge (c), shown magnified in images (d) and (e). Dendrite and broken crystals (f).

The samples in SEM examination have to be vacuum compatible and either conducting or coated with a thin conducting layer.[155a] TlBr single crystals studied in this work with SEM were mostly conducting, although more pure samples, being more resistant, would probably require conducting coating.

5.2 Optical spectral methods

Optical spectra provide information about the short and long wavelength limits of transmittance, absorption, and optical losses, which are associated with composition, impurities, crystal defects and imperfections, as well surface quality. TlBr is a transparent material over a wide optical range: 440 nm (~22730 cm^{-1}) – 48 μm (~208 cm^{-1}). The UV and IR limits of transmittance are determined by the electronic structure of TlBr and vibrations of the crystal lattice, respectively.[44d] The exact limits of UV[157] and far IR[44c] transmittance are sensitive to impurities and structural defects in the crystal, as has also been confirmed for TlBr.[158, 159]

The transparency of a material over a transmittance region depends on the size of particles, imperfections and non-uniform areas inside the material. When the size of these objects is comparable to the wavelength of light, elastic scattering takes place. For particles smaller than the wavelength of the incident light, it is known as Rayleigh scattering.[160] The more general Mie approach[161] treats all possible ratios of particle diameter to wavelength. The

result of scattering is directly observed in a baseline of optical spectra as deviations from 100% of transmittance. Since polishing of the surface can be controlled to within several nanometres, the effect of surface roughness is larger in UV-Vis than in IR spectra. This is particularly valid for TlBr materials, whose softness does not permit to produce crystal faces of high quality, and therefore, transmittance of TlBr samples in the visible region is decreased. In Fig. 26, the effect of transmittance reduction is much greater for Vis than for IR spectra. The transmittance UV-edges of the samples match each other, since the crystals have been cut from the same part of an ingot. However, their base line levels vary considerably due to low surface quality, as also indicated by the Vis-reflectance spectra.

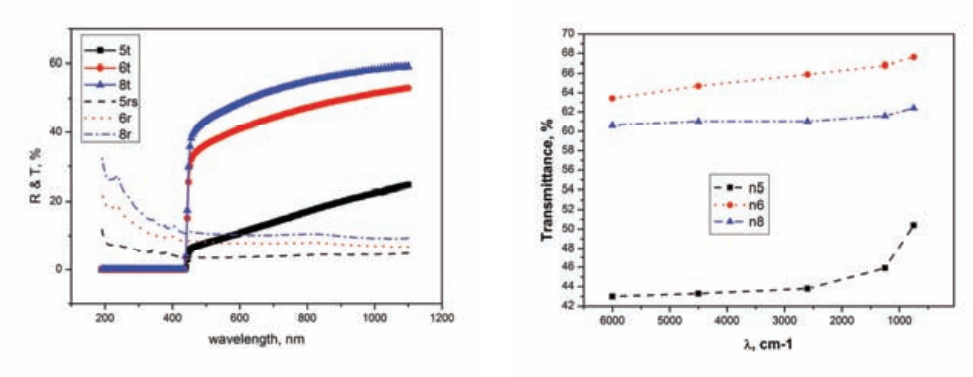

Fig. 26. Transmittance (T, thick lines) and reflectance (R, thin lines) UV-Vis spectra (left) and IR transmittance base line (right) of TlBr crystalline samples of series Lis27.

In this thesis, the quality of the TlBr samples was examined by UV-Vis transmittance and reflectance spectra recorded using a HITACHI U-2000 Spectrophotometer.[VII] Transmittance and impurity control in the IR range was done by measuring spectra with a Perkin Elmer Spectrum One spectrometer equipped with a Universal ATR Diamond/ZnSe unit[I] and Perkin Elmer FT-IR system Spectrum GX.[VII]

5.2.1 FTIR spectra

A second phenomenon affecting transparency is absorption due to impurities built into the lattice. When the impurity is a molecule or anion, it has absorption bands that are specific to that group, which can be easily determined by the IR spectroscopy.[162] Transmittance spectra are used for quantitative determination of relatively large amounts of impurities distributed over the material bulk. The attenuated total reflectance (ATR) technique allows determination of trace amounts of impurities. The physical basis of ATR leads to a limited penetration of the

radiation (a few microns) into the sample.[163] Therefore, the ATR method is more suitable for investigation of the surface and a volume of material close to its surface.

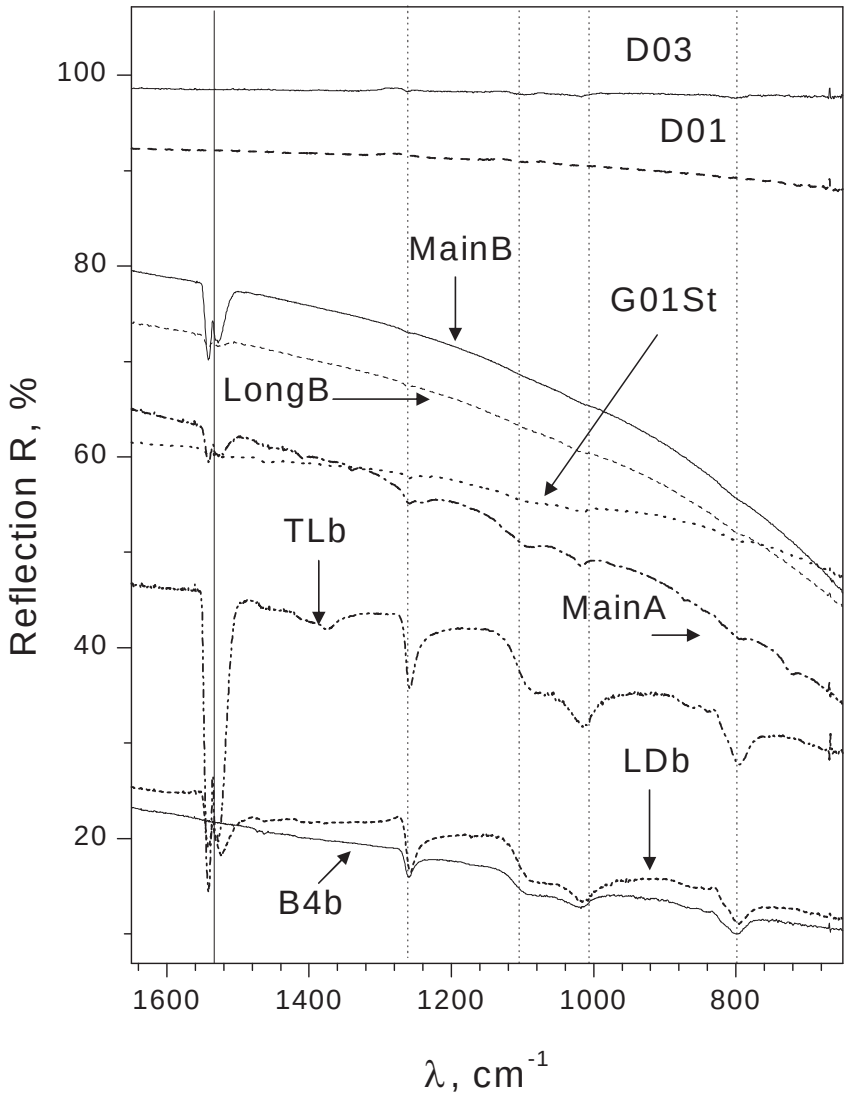

Fig. 27. ATR FTIR spectra of TlBr samples manufactured in different ways. B4b, LDb, TLb and MainA crystals are grown from melt. MainB and LongB are additionally hydrothermally annealed. G01St is several crystals grown by the hydrothermal method. D01 and D03 are dendrite crystals obtained after first and third hydrothermal recrystallisations, respectively. All samples are in a contact with diamond under fixed pressure. Dashed vertical lines mark the position of sulphate bands in TlBr. The solid vertical line corresponds to CS_2 liquid, which is added for better contact between the sample and the diamond.

Interpolation of ATR results to the whole sample volume should take into account any possible impurity depth profile near the surface, for example, due to aging.[56] In Fig. 27, the ATR FTIR method is used for qualitative characterisation of TlBr samples made by different methods. The samples are dissimilar as shown by base level behaviour, as well as by sulphate content. However, the origins of these differences, whether they be crystal growth, treatment or aging, is not clear, because the method only characterises the material near its surface.

Due to impurities inside the lattice of a Tl halide, the experimental value of the coefficient of bulk absorption (10^{-5} cm^{-1} at λ=10,6 μm) is three order less than the theoretical value.[53] The key impurities, which are introduced by the manufacturing processes, decomposition reactions of by-product and ageing, are oxides of sulphur, carbon, nitrogen, chlorine and hydrogen. Their typical IR frequencies are 1200 and 620 cm^{-1} (for SO_4^{-2}), 1400-1500 cm^{-1} (for CO_3^{-2}), 2100 cm^{-1} (for NCO^-), 960 cm^{-1} (for ClO_3^-), 1380 and 830 cm^{-1} (for NO_3^-), and 1600-1700 cm^{-1} and 3200-3600 cm^{-1} (for H_2O).[44c] Sulphate,[50, 164] nitrate[54] and water[53] impurities, and their derivatives are considered the most deleterious with respect to the transparency of Tl halides and their aging. Due to the effects of the crystal field,[162] the absorption bands may split, or become hidden; lines active only in Raman spectroscopy often become active in IR spectra, and vice versa. For example, the orientation effects of a nitrate group inside the lattice can change the intensities and appearance of the bands in an IR-spectrum after annealing.[54] The absorption bands of water, as well as nitrate and sulphate ions, in different solids are summarised in Table 5, Table 6, Table 7. Assignments used for the bands are made according to Nakamoto.[162]

In general, water in lattices absorbs at 3550-3200 cm^{-1} (symmetric ν_1 anti-symmetric ν_3 OH stretching) and at 1630-1600 cm^{-1} (HOH bending ν_2).[162b] Additional bands at ~600 cm^{-1} and ~500 cm^{-1} observed in Tl halides are suggested to be caused by Tl_nO_m impurities formed by the reaction of water with the Tl halide.[53]

Table 5. Vibrational frequencies of water (C_{2v}) in solid crystals.

Crystal	**ν_1**	**ν_3**	**ν_2**	**(?Tl_2O)**	**(?Tl_4O_2)**	**Ref**
Solid	3400	3220	1620			162a
TlCl	3345		1641	644	-	53
Tl(Cl,Br)	3344		1644	645	507	53
TlBr	3370		1630	604	469	53
Tl(Br,I)	3380		1628	594	462	53

In sodium and potassium nitrates, the nitrate ion is planar.[162c] By analogy with the lattices of NaCl and CsCl, in which the impurity NO_3^{1-}-ion has been studied, the impurity bands in TlBr can be assigned. Additional bands at 1190 cm^{-1} and 824 cm^{-1} observed in TlBr are

suggested to be caused by either NO_2^{-1} or by the formation of complexes that are more complicated than the NO_3^{1-}-ion. The intensity of the ν_4 band is proposed to be small.[54]

Table 6. Vibrational frequencies of the nitrate ion (planar) in solid crystals. Frequencies ν_1 and ν_2 are Raman (R) and IR active, respectively.

Crystal	IR/R	$\nu_1(A_1')$	$\nu_2(A_2'')$	$\nu_3(E')$	$\nu_4(E')$	Ref
$Na[NO_3]$	IR		831	1405	692	162c
$Na[NO_3]$	R	1068		1385	724	162c
$K[NO_3]$	IR		828	1370	695	162c
$K[NO_3]$	R	1049		1390	716	162c
TlBr	IR		835	1373	weak?	54

Impurities of sulphur and its compounds (S, S^{2-}, SO_3^{2-}, SO_4^{2-}) are often found in optical materials, since source materials and reagents used during the manufacturing process, as well as air, contain them. The most probable form of sulphur in Tl halides is the sulphate ion.[50] The free sulphate ion has the symmetry point group T_d. Only ν_3 and ν_4 frequencies are IR-active. However, a reduction of the symmetry, for example by coordination,[162e] inside the lattice can cause the vibrations to degenerate and activate Raman modes in the infrared spectrum. The appearance of additional lines and their splitting is explained by the formation of pairs between sulphate ions and a metal, defect or impurity.[164] The process may be dynamic, since the number and intensity of the bands is not reproduced from sample to sample with the same composition.[50]

Table 7. Vibrational frequencies of sulphate ion (tetrahedral) in solid crystals. Only frequencies ν_3 and ν_4 are IR active.

Crystal	ν_1	ν_2	ν_3	ν_4	Ref
$[SO_4]^{2-}$	983	450	1105	611	162d
TlCl-TlBr	~960, 997		1090, 1130	626	50*
TlBr-TlI	997		1106, 1149, 1163	628	44c*
TlBr	800		1010, 1100, 1260		Fig. 27

* - assignments were not made

5.3 X-ray diffraction methods (XRD)

Material characterisation by the use of X-ray diffraction methods has been known since the discovery of the wave character of X-ray radiation by Max von Laue in 1912.[165] The powder diffraction method was devised independently in 1916 by Debye and Scherrer and in 1917 by Hull.[166] After Klug and Alexander,[124] the powder diffraction method became a routine technique for identification of compounds and impurities and their quantification. Data collection has been considerably simplified by computer-based instruments, which are supplied with software packages for rather tedious data reduction. Instrumentation and

experimental procedures have been widely developed for different forms of substances, i.e. for single crystals,[125] powders[167, 165, 166] and thin films.[168]

In this work, a Philips powder diffractometer (PW1710/00) supplied with PC-APD software (PW1877/42) was used for phase purity testing of TlBr,[I] the identification of reaction by-products and localisation of impurities forming their own phases.[IV, V] A D8 Advanced Bruker X-ray diffractometer was used for the orientation of single crystals of TlBr and their quality control by the rocking curve method.[I-VII]. For 2Θ-Ω scans was used a PANalytical X'Pert Pro MPD X-ray diffractometer.[178]

5.3.1 Penetration depth

X-rays are absorbed in materials by photo-electric effect, and are scattered by elastic Rayleigh and inelastic Compton mechanisms. As in optics, total attenuation follows the Bouguer–Lambert–Beer law for a given wavelength λ: $I(d) = I_o \exp(-\mu \rho d)$, where d is the length of the path of the X-rays inside the material, ρ is its density and μ is the mass attenuation coefficient. The coefficient μ can be computed from the composition of the material: $\mu = \sum c_i \mu_i$, where c_i is the mass proportion of a chemical element i, and μ_i is its attenuation coefficient.[169]

The significance of absorption coefficients to diffraction experiments is that only a part of the material is represented in diffraction patterns. The thickness of the 'work' layer (penetration depth) depends on the wavelength of the X-rays and the angle at which the incident beam strikes the sample (θ). Penetration depth P_d of TlBr in the range 20° - 70° of 2θ is 2.5 μm and 8.2 μm for reflections from (100)- and (300)-planes, respectively (Table 8). Thus, as in the case of ATR FTIR, XRD methods can characterise a relatively thin layer of the TlBr crystal, in which surface effects have a clear contribution.

Table 8. X-ray penetration depth P_d (μm) for 98% contribution to the diffracted beam ($I(d) / I_o$) for TlBr, TlI and, for comparison, for Si and some metallic electrode materials. Cu-radiation (Kα1) at incident angle θ. Calculations performed using the program Diffrac-plus, AbsorbDX V.1.1.4 (Bruker Advanced X-ray solutions).

2θ	P_d (TlBr)	P_d (TlI)	P_d (Si)	P_d (Pd)	P_d (Au)	P_d (Ti)	P_d (Al)
20	2.450	1.922	24.370	1.397	0.863	4.647	26.180
45	5.399	4.235	53.070	3.080	1.902	8.037	57.690
70	8.093	6.347	80.490	4.616	2.851	12.050	86.460
90	9.977	7.825	99.230	5.690	3.515	14.850	106.600
150	13.630	10.690	135.600	7.773	4.801	20.290	145.600
180	14.110	11.070	140.300	8.048	4.971	21.000	150.700

5.3.2 Data collection and specimen displacement

The collection of the data with a counting detector, which sums the integer number of counts per fixed time interval, follows the probability distribution p of the Poisson random variable n: $p(n, \mu) = \exp(-\mu)\ \mu^n / n!$, where n (here) is number of counts and μ is the average number of counts or a signal level. In a Poisson distribution, the statistical standard deviation σ is directly connected with the mean μ: $\sigma^2 = \mu$.[170] So, a relative error is about $\sigma/\mu = \mu^{-1/2}$. Thus, in order to decrease the relative error by factor K, the signal level μ or time of the data collection should be increased by factor K^2. Although modern searching programs can find peaks on a coarse background with criteria less than 1σ, Poisson's approach helps with planning the data collection experiment in order to have reliable peaks.

For XRD data reduction the programs require precise values, for example, of peak positions, with an error often less than a scanning step (0.02^o of 2Θ in the indexing program TREOR). Approximately half of the error in peak location is due to instrumental error.[171] The discrepancy in 2Θ peak position, the specimen-displacement error, is by far the largest of the errors found in XRD powder data.[167a] Even in the case where the sample holder itself can be accurately referenced to a machined surface on the goniometer, due to the different attenuation coefficients of the sample and reference material it is difficult to set the sample into the correct position. Since a Si-standard is commonly used for instrument alignment, for TlBr samples this creates a problem, because the penetration depth for TlBr is ten times smaller than for Si (Table 8).

The specimen-displacement error can be expressed as follows[165a]: $\Delta(2\Theta) = 2\ S \cos(\Theta) / R$, where S is the displacement of the specimen from the focusing circle with radius R. The error can be eliminated by the use of an internal standard. A typical procedure includes the fitting of peak positions of the standard, and then correction of the sample pattern using the S value obtained.[172] However, for a slice of a single crystal of TlBr, for which only one of a few reflections can be registered, the only way to decrease the effect of the specimen-displacement error is careful instrument alignment followed by variation of its Z (vertical) - coordinate.

5.3.3 Full width at half medium FWHM

The width of the peak characterises crystalline quality of the crystal. The origins of the broadening of peaks are crystallite domains (whose size is designated τ) and strain (ε). The first term is usually associated with variation in the domain sizes and their disorientation. Lattice strain ε represents variable displacements of atoms from their sites in the idealised

crystal structure caused by dislocations, vacancies, interstitials, foreign atoms and similar defects. Strained crystals are often composed of elastically strained micro-domains separated by plastically-deformed regions of high defect density.[167b] Two determination methods for the line broadening β have been described: (1) $\beta + b = B$ and (2) $\beta^2 + b^2 = B^2$, where b is instrument broadening and B is the width of the observed diffraction line at its half-intensity maximum, also known as FWHM. The first definition (1) is often associated with size effects, while the second is related to the strain.

The crystalline size broadening β_τ is expressed by the Scherrer equation: $\beta_\tau = K \lambda / (\tau \cos \theta)$, where K is the domain shape factor, λ is the wavelength, τ is the average crystallite size, and θ is the Bragg angle. The peak breadth β_ε due to stress is related to the residual strain ε by $\beta_\varepsilon = 4\varepsilon \operatorname{tg} \theta$.[165b] The strain ε can also be expressed as mean lattice distortion Δd/d, where d is the lattice parameter.[173] The difference in angular dependence of size and strain broadenings is the basis for size-strain analysis, which assists in separation of β_τ and β_ε fractions in the common broadening (B – b). For slices of TlBr single crystals, this analysis is difficult to carry out since only one or a few reflection planes (for example, (110) and (220)) are detected in a 2Θ-scan. Actually, disorientation between cut-off surface and reflection plane complicate this problem. Therefore, in this work, crystal quality was mainly studied by the rocking curve method.

5.3.4 Rocking curve method

The broadening effects, both due to size and strain, generally produce a symmetric broadening around the original peak position.[165b] This permits study of how perfect the stack of hkl-planes of a given reflection over the sample is by scanning with the X-ray tube and detector fixed relative to each other at the original $2\Theta_{hkl}$ angle (see Fig. 28). This is done for every turn of the sample around the z-axis in the xy-plane. When, after a sequence of turns around the z-axis, a scattering vector S_{hkl} reaches the yz-plane, the intensity maximum of the original peak will be recorded during the Ω-scan (Fig. 29A).

If the stack of planes is broken (domains) or/and bent (strains), the local disorientations of planes of the stack will produce a splitting of the original peak and redistribution of its intensity over the Ω-scan (Fig. 16 and Fig. 14B). Thus, step rotation over the z-axis and Ω-scans result in the detection of several peaks, each having its the own δ- and φ- orientation with respect to the xyz-system. In fact, the δ-angle characterises the deviation of a reflection plane from the slice's surface during the cutting and polishing procedures. Both φ- and δ-angles characterise the disorientation between S_{hkl}-vectors in 3D space. The rocking curve

method (Ω-scan) can be enhanced by variation of 2Θ that is the same as 2Θ-scans with series of Ω fixed (see Fig. 29B).[178] Thus, information about a domain size and strain in a crystal can be extracted (compare chapter 5.3.3).

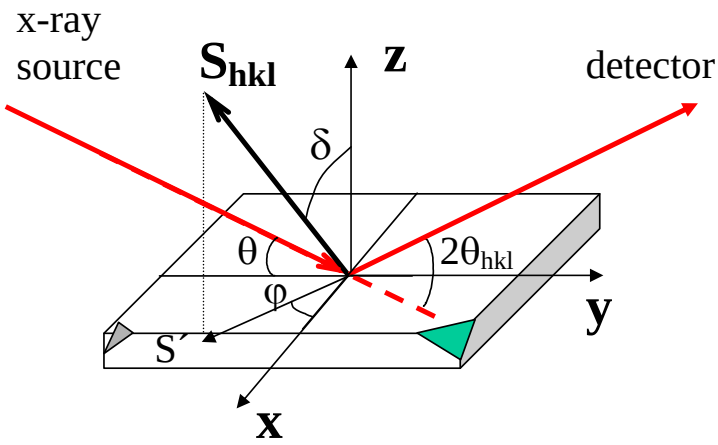

Fig. 28. Bruker setup for recording X-ray rocking curves, the xy-plane is fixed on a work table. The sample is positioned on an xy-flat surface of the diffractometer. A scattering vector S of a reflection hkl-plane forms a δ-angle to the z-axis and its S´-projection onto the xy-plane forms the φ-angle to the x-axis. The X-ray source tube and detector fixed at $2\theta_{hkl}$ are scanned over the angle Ω in the yz-plane (rocking curve Ω-scan).

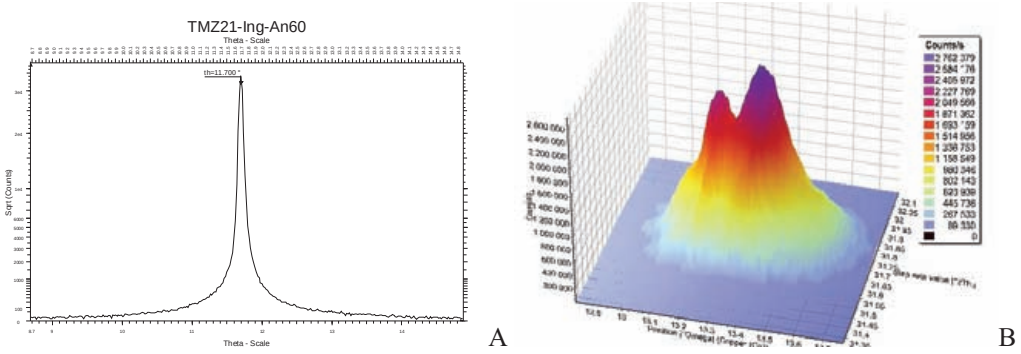

Fig. 29. An X-ray study of a crystal grown by the TMZ method.[178] (A) A rocking curve of the ingot's area, which is free of strains [FWHM(Ω) = 0.1]. (B) 2Θ-Ω scans of the slice N11 that was polished, etched and annealed [FWHM(Ω) = ~ (0.2+0.3)].

The X-ray rocking curve method has several limitations. The first is related to the penetration depth, which is shown for several substances in Table 8. Secondly, the irradiated area of the sample varies with Ω-scan as w/sin(Ω), where w is the beam thickness. Thirdly, an Ω-scan is limited by geometry to angles of 0^o to $2\Theta^o$ (see Fig. 28), and the diffractometer construction often decreases additionally these limits.

5.4 Electrical characterisation

For improving the performance of the TlBr detector, preliminary electrical characterisations of TlBr crystals are carried out in order to establish electrical parameters (resistivity, capacitance, leakage current and temperature limits) for future use of the crystals as detectors. There are two factors to be taken into account. The first one is quality of the surface and electrodes, since they serve as the current supply, signal collectors and radiation window. The interactions between the TlBr surface and metallic electrode are considered in chapter 4, and the effects of metallisation[IV] and degradation[V] on TlBr single crystals have also been studied. The second factor is related to the TlBr crystal electrode system, which is a capacitor and therefore a time delay is used during the voltage sweeping.

For the electrical characterisation a Keithley 2400 Series Sourcemeter [I-V] and Agilent/HP 4155A semiconductor parameter analyzer[VII] were used. Frequency dependence of capacitance and C–V curves were measured with a Precision LCR Meter HP4284A (Hewlett Packard).[III, V] Beckman (Modell 2400) or Perkin Elmer MPF-44A spectrophotometers were used for obtaining a photo-response from crystals.[II, III, V] The X-ray response of the TlBr crystals was studied using Cu-radiation from a Philips X-ray diffractometer, PW1710/00.[II, IV] MULTI-POWER/SPECTRUM (Bruker Baltic)[147] was used for characterisation of the TlBr crystals as detectors.[VI, VII]

5.5 Elemental analysis

An inductively Coupled Plasma Mass Spectrometry (HR-ICPMS ELEMENT, Finnigan MAT, Bremen/Germany, equipped with a microconcentric nebulizer MCN-100, CETAC Tech., Omaha/USA) was used for the trace element analysis. The method permitted simultaneous determination of Al, As, Bi, Ca, Co, Cr, Cu, Fe, Mg, Na, Nb, Ni, P, Pb, Pd, Pt, S, Sb, Si, V and Zn in crystals of TlBr and its solutions.[I] The analysis was done by totally dissolving the samples. The sample preparation steps and subsequent measurements were performed under clean room conditions. The detection limits were between 0.001 and 0.01ng/ml, depending on the element, with a dynamic range of more than eight orders of magnitude. The details of trace element analysis with ICPMS have been described in Ref.[174]

The elemental composition was also studied by energy-dispersive X-ray spectroscopy (EDS) analysis using an Oxford INCA350 EDS connected to a Hitachi S-4800 FESEM.[III, V, VII] The instrument is supplied with software for spectrum collection, peak identification and quantitative analysis. The instrument allows point analysis, line scanning and elemental mapping of the image obtained by SEM. Since chemical analysis is performed by measuring

the energy and intensity distribution of the x-ray signal generated by a focused electron beam, the depth depends on the energy and incident angle of the beam, properties the material being examined and energy of the X-ray radiation (see Table 8). The minimum size for point analysis is associated with a minimum probe current. For example, a 20-nm probe diameter has been estimated for conventional 20 kV voltage and a minimum 10 pA probe current.[156f], The EDS system coupled with SEM was used in this work to provide information concerning non-uniformity of the sample on the elemental scale.[III, V, VII]

Conclusion

In the field of gamma-ray detection there is a great need for high performance detectors that work at ambient conditions. The applications that need these detectors range from medical and military to astrophysical. A single crystal of TlBr is a promising candidate for gamma-ray detection at room temperature because of its high stopping power, density and wide bandgap (chapter 2). However, this material has less developed technology for crystal growth and purification than, say, that for Si and Ge detectors. As a result, purity and crystal quality are the main problems of TlBr crystals as detectors.[I, II] Therefore, the technological processes for TlBr detector manufacturing were studied with respect to obtaining the best purity for TlBr and the highest quality of TlBr crystals.

The improvement of purity and crystal quality was the central topic in published papers[I-VII] and in chapters 3 and 4. In chapter 3.1, wet and dry methods of synthesis of TlBr, as raw material, were studied and compared. Precursors were shown to have the drastic effects on quality of material and its aging. The hydrothermal method for TlBr synthesis was proposed for better purity[I]. Purification methods by recrystallisation from vapour, molten state and water solutions[I] were considered in chapter 3.2. A combination of wet (hydrothermal) and dry (Bridgman and TMZ) methods of purification was shown to be successful for obtaining high quality crystals.[77, VI]

Various methods for crystal growth were summarised in chapter 3.3. Crystals grown from water solutions by the hydrothermal method were small, but available for production of the counting gamma-ray detectors. The crystal growth from melts currently is the only method by which large ingots of Tl halides can be produced. Bridgman and TMZ methods were studied and used for growth of large crystals of TlBr. Basically, non-uniformity of TlBr crystals grown from melt was shown to stem from the walls of the crucible. In Bridgman method, recent attempts to decrease the adhesion by increasing the temperature of melt deteriorated also the purity of a crystal by dissolving the crucible components.[VII] Thus, the problem of

interaction of an ingot and crucible material persists. In the horizontal TMZ method, crystals grown were less stressed than in the Bridgman method possibly due to releasing tension from the walls through the top surface which was open.[178] Crystal quality can be improved by annealing[I, II] (chapter 3.4). Various annealing processes were used in this work to decrease the strains and number of boundaries in the crystal and make it more uniform and pure. The annealing improved electrical characteristics as well.[II]

During TlBr detector fabrication (chapter 4) cutting and polishing the crystals were showed to make pronounced and deep structural surface damage.[III] Chemical polishing and etching were used and chemical cutting was proposed in order to avoid mechanically damaging the material and to clean its surface. Metallisation effects were demonstrated to depend on the metal and deposition conditions.[IV] The stability of TlBr-metal interfaces was influenced to much extent by an ionic current, which produced degradation of the TlBr crystal and metallic electrodes.[V] The use of the purest TlBr of highest crystal quality and lowering of the temperature of the device below the level of noticeable ionic current seems to be the only solution for suppressing the polarisation effects associated with an ionic current and making the gamma-ray detector more durable.

In this thesis, the technological stages, such as preparation of TlBr raw material, crystal growth, annealing and detector fabrication, were optimised using various instrumental characterisation methods (chapter 5). Different technological processes were studied by elemental analysis of corresponding samples using HR-ICPMS.[I] The FTIR method was reviewed and used to determine the impurity molecules or anions that were built into the lattice. The ATR-FTIR technique was applied for qualitative characterisation of raw material and single crystals of TlBr.[I] Also, FTIR base lines were used for the characterisation of quality of the samples.[VII, 178] A polarisation microscope was used to determine the extent of non-uniformity in crystals.[II-IV, VI, VII] The study of the surface morphology was carried out with SEM, and the elemental composition of irregularities observed was studied using an EDS system.[III, V, VII] The phase purity characterisation of TlBr was done using X-ray powder diffraction.[I, IV] The effects of technological operations on the quality of single crystals were studied by the X-ray rocking curve method.[I-VII] Characterisation of electrical properties of TlBr single crystals was carried out by measuring *I-V* curves, photocurrent, current-time (electro-aging) and capacitance characteristics.[I-V, VII] Final qualitative characterisation of a crystal as a detector was done using gamma ray spectroscopy methods.[77, VI, VII]

The central concept for this thesis was to recrystallise TlBr from water solution in a chain of routine purification methods. This significantly improved the detector performance. A

second approach was the use of annealing methods for improving the crystal quality and purity. The innovation in this thesis was the use of the hydrothermal method for the synthesis, purification, annealing and crystal growth of TlBr. These techniques allowed detector-grade TlBr single crystals to be produced.[77, VI] The best crystal had parameters, the mobility-lifetime product for electrons of 3.3×10^{-4} cm^2/V and resistivity of 2.9×10^{12} Ω cm (at -20 °C), which were approached using only hydrothermal recrystallisation and seven TMZ passes.

Looking ahead, the crystal growth, annealing and TlBr detector fabrication techniques could be developed for making non-strained and pure crystals of TlBr. Future steps should solve the existing problems such as adhesion to crucible material, strain-less treatment of samples, and develop new technological stages, for example to use the electrochemical methods for purification. The study of non-stoichiometry in TlBr and its doping will allow to make p- and n-type materials that could be used in a creation of diode structures, and thus, to decrease the leakage current in TlBr detectors. The other problem is an ionic current and its interaction with electrode material. The formation of barriers to the ionic current and electrochemical reaction on the electrode could make the TlBr detector more durable.

References

Ref. Num.	Publication
1	R. Hofstadter, Thallium Halide Crystal Counter, Phys. Rev. 72(11) (1947) 1120.
2	A. Owens, A. Peacock, Compound semiconductor radiation detectors, Nucl. Instr. and Meth. A 531 (2004) 18.
3	R. Hofstadter, Crystal counters - II, Nucleonics 4(5) (1949) 29.
4	F. Olschner, M. Toledo-Quinones, K. S. Shah, J. C. Lund, Charge carrier transport properties in thallium bromide crystals used as radiation detectors, IEEE Trans. Nucl. Sci. 37(3) (1990) 1162.
5	K. S. Shah, F. Olschner, L. P. Moy, J. C. Lund, M. R. Squillante, Chracterization of thallium bromide nuclear detectors, Nucl. Instr. and Meth. A 299 (1990) 57.
6	F. Olschner, K. S. Shah, J. C. Lund, J. Zhang, K. Daley, S. Medrick, M. R. Squillante, Thallium bromide semiconductor X-ray and gamma-ray detectors, Nucl. Instr. and Meth. A 322 (1992) 504.
7	P. J. Durrant, B. Durrant, Introduction to advanced Inorganic chemistry, Longmans, (1962): a - p. 487; b - p. 557; c - p. 558; d - p. 561.
8	F. A. Cotton, G. Wilkinson, C. A. Murillo, M. Bochmann, Advanced inorganic chemistry, 6th ed., John Wiley & Sons, Inc., (1999), p. 175; b - p. 204 and ibid.
9	N. V. Sidgwick, Variable valence, Inst. intern. chimic Solvay (1928).
10	A. J. Downs (ed.), Chemistry of Aluminium, Gallium, Indium and Thallium, Blackie Academic & Professional, London, 1993: a - pp. 11-12, 39-46, 111-118.
11	H. Remy, Treatise on Inorganic Chemistry, v. 1, Elsevier Publishing Company (1956): a - p. 381 and ibid.; b - p. 385 and ibid.
12	W. C. Price, W. F. Sherman and G. R. Wilkinson, Infra-red studies on polyatomic ions isolated in alkali-halide lattices, Spectrochimica Acta, 16 (1960) 663.
13	John Courtney Decius and Robert Maurice Hexter, Molecular Vibrations in Crystals, McGRAW-HILL INTERNATIONAL BOOK COMPANY, New York, 1977: a – p. 289 and ibid.
14	Alan F. Clifford, Inorganic Chemistry of Qualitative Analysis, Prentice-Hall, Inc., Englewood Cliffs, N. J., 1961, p. 81 and ibid.
15	F. A. Cotton and G. Wilkinson, , Advanced inorganic chemistry (a comprehensive text), Advanced inorganic chemistry, 2nd ed., Interscience Publishers, John Wiley & Sons, New York, London, Sydney, 1968: a - p. 453; b - p. 467; c - p. 495.
16	Per Kofstad, Nonstoichiometry, diffusion and electrical conductivity in binary metal oxides, New York : Wiley, 1972
17	W. Lehfeldt, Electric conductivity of single crystals, Z. Physik 85 (1933) 717.
18	W. Lehfeldt, Electron conduction in crystals of silver and thallium halides, Nachr. Ges. Wiss. Gottingen Math. physik. Klasse, Fachgruppe II (1935), 1 1711.
19	P. J. Van Heerden, The crystal counter, Dissertation, Utrecht University, 1945.
20	R. Hofstadter, Crystal counters - I, Nucleonics 4(4) (1949) 2.
21	J. Bardeen and W. H. Brattain, The Transistor, A Semi-Conductor Triode, Phys. Rev. 74(2) (1948) 230.
22	W. H. Brattain and J. Bardeen, Nature of the forward current in germanium point contacts, Phys. Rev. 74(2) (1948) 231.

23 W. Shockley and G. L. Pearson, Modulation of conductance of thin films of semi-conductors by surface charges, Phys. Rev. 74(2) (1948) 232.
24 K. McKay, A Germanium Counter, Phys. Rev. 76 (1949) 1537.
25 M. B. Prince, P. Polishuk, Survey of materials for radiation detectors at elevated temperatures., IEEE Trans. Nucl. Sci. NS-14 (1967) 537.
26 D. S. McGregor, H. Harmon, Room-temperature compound semiconductor radiation detectors, Nucl. Instr. and Meth. A 395 (1997) 101.
27 L. Strüder, High-resolution imaging X-ray spectrometers, Nucl. Instr. and Meth. A 454 (2000) 73.
28 G. W. Mayer, Search for semiconductor materials for gamma ray spectroscopy, in Ref.[30], p. 445
29 G. Dearnaley and D. C. Northrop, Semiconductor Counters for Nuclear Radiations, Wiley, New York (1966)
30 G. Bertolini and A. Coche (eds), Semiconductor detectors, North-Holland Publishing Company, Amsterdam (1968)
31 G. Armantrout, S. Swierkowski, J. Sherohman, J. Yee, What can be expected from high-Z semiconductor detectors?, IEEE Trans. Nucl. Sci. NS-24 (1977) 121.
32 G. Ottaviani, C. Canali and A. A. Quaranta, Charge carrier transport properties of semiconductor materials suitable for nuclear radiation detectors, IEEE Trans. Nucl. Sci. NS-22 (1975) 192.
33 M. Schieber, H. Hermon, M. Roth, Physical-Chemical Considerations for Semiconductor Room-Temperature Radiation Detectors, Mat. Res. Soc. Symp. Proc. 302 (1993) 347.
34 CRC Handbook of Chemistry and Physics, 87th edition (2006-2007) by D. R. Lide (Ed.) , published June 26, 2006: a - Ch. 8, p. 118 and ibid.; b - Ch. 12, p. 11 and ibid.; c - Ch. 4; d - Ch. 10; e - Ch. 9, p. 77; f – Ch8, p112 and ibid.; g – Ch8, p20 and ibid.
35 K. S. Shah, J. C. Lund, F. Olschner, L. Moy, M. R. Squillante, Thallium bromide radiation detectors, IEEE Trans. Nucl. Sci. 36(1) (1989) 199.
36 P. R. Bennett, K. S. Shah, L. J. Cirignano, M. B. Klugerman, L. P. Moy, F. Olschner, M. R. Squillante, Characterization of polycrystalline TlBr films for radiographic detectors, IEEE Trans. Nucl. Sci. 46(3, Pt.1) (1999) 266.
37 P. J. Sellin, New Materials for Semiconductor Radiation Detectors., PSD7 Abstracts, 7th International Conference on Position Sensitive Detectors, University of Liverpool, 12-16 September 2005, p. 40
38 C. D. Hodgman (ed.-in-ch.) , Handbook of Chemistry and Physics, Chemical Rubber Publishing Co, 37-th ed., 1955: a - p. 606 and ibid.; b - p. 2150 and ibid.; c - p. 1604 and ibid.; d - p. 1992.
39 A. Owens, M. Bavdaz, G. Brammertz, V. Gostilo, N. Haack, A. Kozorezov, I. Lisjutin, A. Peacock, S. Zatoloka, Hard X-ray spectroscopy using a small-format TlBr array, Nucl. Instr. and Meth. A 497(2-3) (2003) 359.
40 K. Hitomi, M. Matsumoto, O. Muroi, T. Shoji, Y. Hiratate, Thallium bromide optical and radiation detectors for X-ray and gamma-ray spectroscopy, IEEE Trans. Nucl. Sci. NS-49 (2002) 2526.
41 R. Farrell, F. Olschner, K. Shah, M. R. Squillante, Advances in semiconductor photodetectors for scintillators., Nucl. Instr. and Meth. A 387(1.2) (1997) 194.
42 K. Hitomi, O. Muroi, T. Shoji, Y. Hiratate, Promising blue sensitive photodetectors using thallium bromide crystals., Rev. Sci. Instrum. 71(1) (2000) 322.

43 K. Hitomi, O. Muroi, T. Shoji, Y. Hiratate, H. Ishibashi, M. Ishii, Thallium bromide photodetectors for scintillation detection., Nucl. Instr. and Meth. A 448(3) (2000) 571.
44 S. V. Bogdanov (ed.), Crystals of Thallium Halides (Production, properties and application), "Nauka", Sibirskoe otdelenie, Novosibrsk, 1989: a - p. 20; b - p. 29 and ibid.; c - p. 31 and ibid.; d - p. 45 and ibid.; e - p. 8; f - p. 19; g - p. 66.
45 D. A. Pinnow, A. L. Gentile, A. G. Standlee, A. J. Timper, L. M. Hobrock, Polycrystalline fiber optical waveguides for infrared transmission, Appl. Phys. Lett. 33(1) (1978) 28.
46 J. A. Harrington, A. G. Standlee, Attenuation at 10.6 um in loaded and unloaded polycrystalline KRS-5 fibers, Appl. Opt. 22(19) (1983) 3073.
47 A. L. Gentile, Infrared Fiber Optical Materials, in Fiber Optics: Advances in Research and Development, B. Bendow and S. S. Mitra, Eds (Plenum, New York, 1979) 105.
48 M. E. Lines, Scattering losses in optic fiber materials, I. A new parametrization, J. Appl. Phys. 55(11), 1 June (1984) 4052.
49 M. E. Lines, Scattering losses in optic fiber materials, II. Numerical estimates, J. Appl. Phys. 55(11), 1 June (1984) 4058.
50 I. S. Lisitskii, V. F. Golovanov, V. G. Plotnichenko, Effect of oxygen-containing anion impurities on spectral transparency of thallium halogenide crystals, Part III. sulfate ions, Tsvetnye Metally 11 (2001) 73.
51 M. S. Kouznetsov, I. S. Lisitsky, S. I. Zatoloka, V. V. Gostilo, Development of the technology for growing TlBr detector crystals, Nucl. Instr. and Meth. A 531 (2004) 174.
52 K. A. Bolshakov (ed.), Chemistry and technology of rare and scattered elements, 2-nd ed., Visshaja Shkola, Moskva, 1 (1976): a - p. 359 and ibid.; b - p. 332.
53 I. S. Lisitskii, V. F. Golovanov, A. B. Chapyzhnikov, V. G. Plotnichenko, Effect of oxygen-containing anionic impurities on spectral clarity of thallium halogenide crystals, Part I. Water molecules, Tsvetnye Metally 8 (2001) 79.
54 I. S. Lisitskii, V. F. Golovanov, V. G. Plotnichenko, A. B. Chapyzhnikov, The effect of oxygen-containing anionic impurities on spectral clarity of thallium halogenide crystals, Part II. Nitrate ions, Tsvetnye Metally 9-10 (2001) 66.
55 J. A. Wysocki, R. N Schwartz, A. G. Standlee, R. G. Wilson, A. R. Williams, Aging effects in extruded polycrystalline thallium bromo-iodide fibers, Proc. SPIE-Int. Soc. Opt. Eng. 843 (1988) 94.
56 J. A. Wysocki, R. G. Wilson, A. G. Standlee, A. C. Pastor, R. N. Schwartz, A. R. Williams , G.-D. Lei, L. Kevan, Aging effects in bulk and fiber TlBr-TlI, J. Appl. Phys. 63(9) (1988) 4365.
57 HSC Chemistry 5.1 for Windows, Chemical Reaction and Equilibrium Software with Extensive Thermochemical Database, ver. 5.1 , Outokumpu Research Oy.
58 D. R. Lide (ed.-in-ch.) , CRC Handbook of Chemistry and Physics, CRC Press, 82-nd ed. (2001-2002): a - Ch12-p. 228 and ibid.; b - Ch12-p. 1; c - Ch.8 p.21 and ibid.
59 G. MULLER und G. GNAUCK, Reinste Gase, VEB Deutscher Verlag der Wissenschaften, Berlin 1965 (in German).
60 U. G. Frolov, Course of the colloid chemistry, Kemia, Moskva, 1982, p. 270 and ibid. (in Russian).
61 G. Brauer, Handbuch der Präparativen Anorganischen Chemie, Ferdinand Enke Verlag Stuttgart (1954), p. 654 and ibid.

62 J. Waser, Basic Chemical Thermodynamics, W.A. Benjamin, Inc., New York (1966), p. 145 and ibid.
63 H. Kanzaki, K. Kido, Purification of Alkali Halide Crystals through Fractional Distillation and Normal Freezing, J. Phys. Soc. Japan 15 (1960) 529.
64 R. McFee, Foreign Ion Rejection in the Growth of Sodium Chloride Single Crystals from the Melt, J. Chem. Phys. 15 (1947) 856.
65 O. L. Kreinin and K. M. Rozin, Distribution coefficients of divalent impurities in alkali halide crystals, Crystallography 18(2) (1973) 432 (in Russian).
66 I. B. Oliveira, F. E. Costa, J. F. D. Chubaci, M. M. Hamada, Purification and preparation of TlBr crystals for room temperature radiation detector applications, IEEE Trans. Nucl. Sci. 51(3, Pt. 3) (2004) 1224.
67 C. H. Mesquita, I. B. Oliveira, J. F. D. Chubaci, M. M. Hamada, Multielementar segregation coefficient of thallium bromide impurities from inductively coupled plasma mass spectroscopy measurements, (un-published).
68 W. Pfann, Zone melting, John Wiley, New York (1966): a - p. 18; b - p. 100; c - p. 48.
69 W. A. Tiller, K. A. Jackson, J. W. Rutter, B. Chalmers, The Redistribution of Solute Atoms during the Solidification of Metals, Acta Met. 1 (1953) 428.
70 W. G. Pfann, Comment on paper by Tiller, Jackson, Rutter and Chalmers, Acta Met. 1 (1953) 763.
71 J. A. Burton, R. C. Prim, W. P. Slichter, The Distribution of Solute in Crystals Grown from the Melt. Part I. Theoretical, J. Chem. Phys. 21 (1953) 1987.
72 J. A. Burton, E. D. Kolb, W. P. Slichter, J. D. Struthers, Distribution of Solute in Crystals Grown from the Melt. Part II. Experimental, J. Chem. Phys. 21 (1953) 1991.
73 B. L. Karger, L. R. Snyder, C. Horvath, An Introduction to Separation Science, A Wiley-Interscience publication, John Wiley & Sons, Inc. (1973), p. 312.
74 C. Berry, W. West, F. Moser, Silver Halides, in Ref. [78] p. 214; a - p. 227.
75 K. Hitomi, O. Muroi, T. Shoji, T. Suehiro, Y. Hiratate, Room temperature x- and gamma-ray detectors using thallium bromide crystals., Nucl. Instr. and Meth. A 436(1.2) (1999) 160.
76 H. Kitaguchi, K. Amemiya, K. Yokoi, Y. Ueno, K. Tsuchiya, N. Yanagita, S. Kojima, K. Hitomi, T. Shoji, Semiconductor Radiation Detector and Radiation Detection Apparatus, US Pat. Appl. 2006/0065847 A1.
77 V. Kozlov, H. Andersson, M. Leskelä, H. Sipilä, Improved Process for the Detector Grade TlBr Single Crystals, 2006 IEEE Room-Temperature Semiconductor Detector (RTSD) Workshop, October 30 - November 3, San Diego, CA, US, R06-27.
78 J. J. Gilman (ed.), The Art and Science of Growing Crystals, John Wiley & Sons, Inc. (1963).
79 I. Tarján and M. Mátrai (eds.), Laboratory manual on crystal growth, Akadémiai Kiadó, Budapest (1972).
80 K. Nassau, Crystal growth techniques (in Technique of inorganic chemistry), John Wiley & Sons, Inc. (1968).
81 H. E. Buckley, Crystal Growth, John Wiley & Sons, Inc., New York, Chapman & Hall, Ltd., London (1951), p310 and ibid.
82 J. C. Brice, The growth of crystals from liquids, Amsterdam : North-Holland (1973).
83 J. C. Brice, The growth of crystals from the melt, Amsterdam : North-Holland (1965).

84 D. Elwell, H. J. Scheel, Crystal Growth from High-Temperature Solutions, Academic Press, London, New York, San Francisco (1975).
85 H. K. Henisch, Crystal Growth in Gels, The Pennsylvania State University Press.
86 J. C. Brice, Crystal Growth, Ullman's Encyclopedia of Industrial Chemistry, 5-th Ed, VCH A8, p. 99.
87 H. J. Scheel, T. Fukuda, Crystal Growth Technology, John Wiley & Sons Ltd (2003): a - p. 16 and ibid.; b - p. 511 and ibid.; c - p. 548 and ibid.
88 H. Krebs, Grundzüge der Anorganischen Kristallchemie, Ferdinand Enke Verlag Stuttgart, 1968.
89 A. K. Shukla, S. Radmas and C. N. R. Rao, Formation energies of Schottky and Frenkel defects in thallium halides, J. Phys. Chem. Solids, 34(4) (1973) 761.
90 K. Hitomi, O. Muroi, M. Matsumoto, T. Shoji, Y. Hiratate, Large-volume thallium bromide detectors for gamma-ray spectroscopy, IEEE Trans. Nucl. Sci. NS-48 (2001) 2313
91 N. Cabrera and R. V. Coleman, Theory of Crystal Growth from the Vapor, in Ref. [78] p. 3.
92 S. Kondo, T. Iton, T. Saito, M. Mekata, Well Defined Amorphous to Crystalline Transformation of Cold Condensed TlCl Films, Solid State Communications, 78(6) (1991) 557.
93 S. Kondo and M. Nakano, Optical Absorption near the Fundamental Edge in Amorphous Thallous Halides, J. Phys. Soc. Japan, 61(11) (1992) 4255.
94 S. Kondo, N. Yamagishi, T. Saito, Effects of Chemical Disorder on Crystallization Behavior in Amorphous TlCl1-xBrx Films Studied by UV Absorption Measurements, J. Phys. Soc. Japan, 67(1) (1998) 353.
95 S. Kondo, H. Tanaka, T. Saito, A simple method for preparing uniform amorphous films of mixed metal halides by means of two-source evaporation., Journal of Physics D: Applied Physics 33(22) (2000) 2973.
96 E. A. Secco, Heats of solution of TlI in TlNO3 and TlBr in TlI crystals. Phase diagrams of TlNO3-TlI and TlBr-TlI systems., Solid State Communications 115(8) (2000) 397.
97 R. R. Adzic, J. X. Wang, Bromide Adsorption Induced Formation of Thallium Bromide Adlayers with Varying Composition and Structure on the Au(111) Electrode Surface., J. Phys. Chem. B 102(33) (1998) 6305.
98 R. R. Adzic, J. X. Wang, Structure of Active Phases during the Course of Electrocatalytic Reactions, Journal of Physical Chemistry B 104(5) (2000) 869.
99 R. R. Adzic, J. X. Wang, Structures of surface adlayers and oxygen reduction kinetics., Solid State Ionics 150 (2002) 105.
100 A. Seidell (ed.) , Solubilities of inorganic and metal-organic compounds, 3-rd ed., D. Van Nostrand company, Inc. Vol.1 (1940) 1538, p. 1538.
101 S. Kondo, T. Iton, T. Saito, M. Mekata, Amorphous to Crystalline Transformation of Cold Condensed TlBr Films, J. Phys. Soc. Japan, 60(8) (1991) 2764.
102 M. Takano, Y. Takeda, O. Ohtaka, High pressure synthesis of solids, Encyclopedia of Inorganic Chemistry, p. 1372.
103 G. W. Morey, P. Niggli, The hydrothermal formation of silicates, J. Am. Chem. Soc. 35 (1913) 1086.
104 G. C. Kennedy, Pressure-Volume-Temperature relations in water at elevated temperatures and pressures, Am. J. Sci. 248 (1950) 540.
105 W. T. Read, Dislocations in Crystals, McGraw-Hill Book Company, Inc., 1953.

106 A. H. Cottrell, Dislocations and Plastic Flow in Crystals, in The International Series of Monographs on Physics, Oxford, at the Clarendon Press, 1958, p. 180 and ibid.
107 Recovery of metals, article in, Dictionary of Physical Encyclopaedia, v. 3, Soviet Encyclopedia, Moscow, 1963 (in Russian).
108 P. I. Poluhin, G. Ja. Gun, A. M. Galkin, Resistance of metals and alloys to plastic deformation (handbook), 2nd ed., Moskva, Metallurgija, 1983, p. 9 (in Russian)
109 M. Blackman and I. H. Khan, The polymorphism of thallium and other halides at low temperatures, Proc. Phys. Soc., London PPSOA, 77 (1961) 471.
110 J. Vaitkus, V. Gostilo, R. Jasinskaite, A. Mekys, A. Owens, S. Zatoloka, A. Zindulis, Investigation of degradation of electrical and photoelectrical properties in TlBr crystals, Nucl. Instr. and Meth. A 531 (2004) 192.
111 J. Vaitkus, J. Banys, V. Gostilo, S. Zatoloka, A. Mekys, J. Storasta, A. Zindulis, Influence of electronic and ionic processes on electrical properties of TlBr crystals., Nucl. Instr. and Meth. A 546(1-2) (2005) 188.
112 G. A. Samara, Pressure and temperature dependences of the ionic conductivities of the thallous halides TlCl, TlBr and TlI, Phys. Rev. B 23(2) (1981) 575.
113 N. H. Hartshorne, A. Stuart, Crystals and the Polarising Microscope , Edward Arnold (Publishers) Ltd., London 4-th ed. (1970): a - p. 19; b - p. 138; c - p. 101.
114 M. El Azab, C. R. McLaughlin, C. H. Champness, Preparation and characterization of tellurium surfaces, J. Crystal Growth, 28 (1975) 1.
115 I. B. Oliveira, F. E. Costa, P. K. Kiyohara, M. M. Hamada, Influence of crystalline surface quality on TlBr radiation detector performance, IEEE Trans. Nucl. Sci. (2005), 52(5, Pt. 3), 2058.
116 S. A. Varchenya, A. A. Simanovsky, S. V. Stolyarova, G. P. Upit, Adhesion phenomena on metal film /halide crystal (juvenile contact), I. Adhesion strength and intermolecular interaction, Latv. PSR Zinat. Akad., Fiz. Inst., Preprint LAFI-067, Salaspils (1984) 1-38 (in Russian): a - p. 11 and ibid.; b - p. 30.
117 K. Hitomi, M. Matsumoto, O. Muroi, T. Shoji, Y. Hiratate, Characterization of thallium bromide crystals for radiation detector applications., Journal of Crystal Growth 225(2-4) (2001) 129.
118 V. Gostilo, D. Gryaznov, I. Lisjutin, Technological limitations and processing-generated defects at the development of pixel and strip arrays, Nucl. Instr. and Meth. A 487(1-2) (2002) 13.
119 K. Hitomi, T. Murayama, T. Shoji, T. Suehiro, Y. Hiratate, Improved spectrometric characteristics of thallium bromide nuclear radiation detectors., Nucl. Instr. and Meth. A 428(2.3) (1999) 372.
120 G. V. Bunton, S. Weintroub, Chemical and thermal etching of antimony, J. Crystal Growth 2(2) (1968) 91.
121 S. Ahmed, S. Weintroub, The chemical and thermal etching of tellurium single crystals, J. Crystal Growth, 8 (1971) 299.
122 Martin J. Buerger, Elementary crystallography , John Wiley and Sons, Inc. (New York London Sydney), 3d ed., 1965, p 176 and ibid.
123 C. W. Bunn, Chemical Crystallography, 2nd ed., Oxford University Press, 1961, p. 55.
124 Harold P. Klug and Leroy E. Alexander. , X-ray diffraction procedures, John Wiley & Sons, Inc., 1954 (new ed.: 1974, Wiley, New York) pp. 47-48.
125 C. Giacovazzo (ed.), Fundamentals of crystallography, International Union of Crystallography, Oxford, University Press (1992) p. 624.

126 A. Smakula, M. W. Klein, The Plastic Deformation and Crystal Orientation of Thallium Halides, Journal of the Optical Society of America 39(6) (1949) 445.
127 U. Lachish, The role of contacts in semiconductor gamma radiation detectors, Nucl. Instr. and Meth. A 403 (1998) 417.
128 A. A. Simanovsky, S. V. Stolyarova and G. P. Upit, Ambient-induced diffusion in metal film/halide systems, Thin Solid Films 97 (1982) 301.
129 S. A. Varchenya, A. A. Simanovsky, S. V. Stolyarova, G. P. Upit, Adhesion phenomena on metal film /halide crystal (juvenile contact), II. Adhesion stability and ambient induced processes, Latv. PSR Zinat. Akad., Fiz. Inst., Preprint LAFI-068, Salaspils, 1984 (in Russian): a - p. 38 and ibid.
130 S. V. Stolyarova, A. Simanovskis, V. N. Kovalev, S. Varchena, Ambient-induced interface reactions and adhesion failure in the silver/thallium monobromide-thallium iodide system., Thin Solid Films 177 (1989) 181.
131 S. M. Sze, Physics of Semiconductor Devices, 2nd ed., John Wiley and Sons, Inc., 1981, p. 276 and ibid.
132 D. K. Schroder , Semiconductor Material and Device Characterization, 2nd ed., John Wiley & Sons, Inc., 1998, p. 133 and ibid.
133 Milton Ohring, Materials Science of Thin Films / Deposition and Structure, 2nd ed., Academic Press, 2002, p. 764 and ibid.
134 T. Onodera, K. Hitomi, T. Shoji, Spectroscopic performance and long-term stability of thallium bromide radiation detectors, Nucl. Instr. and Meth. A568(1) (2006) 433.
135 A. D. Smigelskas, E. O. Kirkendall, Zinc diffusion in a brass., Am. Inst. Mining Met. Engrs., Inst. Metals Div., Metals Technol. (1946), 13(No. 7, Tech. Pub. No. 2071).
136 J. F. Ziegler, G. W. Cole and J. E. E. Baglin, Technique for determining concentration profile of boron impurities in substrates, J. Appl. Phys., 43 (9) 1972 p. 3809-
137 Jonatan Slotte, Diffusion of impurities and vacancies in compound semiconductors, Acta Polytechnica Scandinavica No.222 (1999) 67.
138 A. A. Simanovsky, S. V. Stolyarova and G. P. Upit, Adhesion stability of thin metal film-thallium bromide-iodide systems, Poverkhnost 11 (1985) 58 (in Russian).
139 S. Stolyarova, A. Simanovskis, Y. Nemirovsky, Degradation mechanisms and stability forecasting for adhesion contacts of metal films with binary dielectric substrates., Proceedings of the Annual Meeting of the Adhesion Society (1996), 19th 218-221.
140 J. Maniks, A. A. Simanovskii, Joining of optical materials with metallic coatings used as the bonding layers, Adgez. Rasplavov Paika Mater. 24 (1990) 61.
141 K. Hitomi, T. Shoji, Y. Niizeki, A method for suppressing polarization phenomena in TlBr detectors, Nucl. Instr. and Meth. A 585 (2008) 102.
142 S. V. Stolyarova, A. A. Simanovskii, M. Lubane, G. Upit, Atmosphere-induced adhesion failure of silver films on thallium bromide iodide., Latv. PSR Zinat. Akad. Vestis, Fiz. Teh. Zinat. Ser. (1982), (5) 34.
143 S. V Stolyarova, Effect of the crystal surface state on the development of diffusion and adhesion processes in the silver condensate-thallium bromide-thallium iodide system. , Latv. PSR Zinat. Akad. Vestis, Fiz. Teh. Zinat. Ser. (1984), (5) 32.

144 S. V. Stolyarova, A. A. Simanovskii, S. Varcena, Adhesion and solid-phase reactions at the silver condensate interface with thallium bromide iodide., Adgez. Rasplavov Paika Mater. 18 (1987) 19.
145 V. Kazukauskas, A. Jurgilaitis, A. Ziminskij, V. Gostilo, M. Shorohov, Photoelectrical properties of TlBr related to ionic transport and presence of defects, Abstract Book, The 10th International Workshop on Radiation Imaging Detectors, June 29 -July 3, 2008, Helsinki, Finland, p 60.
146 S. Dimitrijev, Understanding Semiconductor Devices, Oxford University Press, 2000, p.73
147 http://www.bruker-baltic.lv/spectrometric_device_multispectrum_eng.html
148 F. C. Brown, The physics of solids / Ionic crystals, lattice vibrations, and imperfections , New York Benjamin, 1967, p. 300 and ibid.
149 S. Glasstone, Textbook of Physical Chemistry, D. Van Nostrand Company, Inc., 2nd ed., 1946, p. 910.
150 R. J. Friauf, Diffusion Process in TlCl, Z. Naturforsch., 26a (1971) 1210
151 R. J. Friauf, Ionic conductivity of Thallium Chloride, J. Phys. Chem. Solids, 18 (1961) 203.
152 P. Herrmann, Fehlordnungserscheinungen in festem Thalliumbromid, Z. Phys. Chem. (Leipzig), 227 (1964) 338.
153 K. Hitomi, Y. Kikuchi, T. Shoji, K. Ishii, Improvement of Energy Resolutions in TlBr detectors, Abstract Book, The 10th International Workshop on Radiation Imaging Detectors, June 29 -July 3, 2008, Helsinki, Finland, p 58.
154 Y. Dmitriev, L. J. Cirignano, K. S. Shah, The effect of doping on X-ray response of TlBr crystals, Nucl. Instr. and Meth. A 594(2) (2008) 206.
155 C. R. Brundle, C. A. Evans, Jr., S. Wilson (eds), Encyclopedia of Materials Characterization (Surfaces, Interfaces, Thin Films), BUTTERWORTH-HEINEMANN - MANNING, 1992: a - p. 57 and ibid.; b - p. 65; c - p. 72.
156 J. I. Goldstein, C. E. Lyman, D. E. Newbury, E. Lifshin, P. Echlin, L. Sawyer, D. C. Joy, J. R. Michael, Scanning Electron Microscopy and X-Ray Microanalysis, 3rd ed., Springer Science & Business Media, Inc., 2003: a - p. 2 and ibid.; b - p. 75 and ibid.; c - p. 97; d - p. 125 and ibid.; f - p. 297 and ibid.
157 M. V. Kurik, Urbach Rule, Phys. Stat. Sol. A8 (1971) 9.
158 L. Grigorjeva, D. Millers, M. Shorohov, I. S. Lisitskii, M. S. Kuznetsov, S. Zatoloka, V. Gostilo, Optical investigations of TlBr detector crystals, Nucl. Instr. and Meth. A 531 (2004) 197.
159 M. Shorohov, L. Grigorjeva, D. Millers, Optical properties and spectrometric performance of TlBr detector crystals, Nucl. Instr. and Meth. A 563(1) (2006) 78.
160 S. Chakraborti, Verification of the Rayleigh scattering cross section, American Journal of Physics 75 (2007) 824.
161 M. Mishchenko, L. Travis, A. Lacis, Scattering, Absorption, and Emission of Light by Small Particles, Cambridge University Press, 2002.
162 K. Nakamoto, Infrared and Raman Spectra of Inorganic and Coordination Compounds, A Wiley-Interscience Publication, John Wiley & Sons, New York, Chichester, Brisbane, Toronto, 3rd ed. (1978): a - p. 119; b - p. 227; c - p. 129; d - p. 142; e - p. 239.
163 Joachim Oelichmann, Surface and depth-profile analysis using FTIR spectroscopy, Fresenius Z. Anal. Chem. 333 (1989) 353.

164 L. Grigorjeva, J. Zakis, D. Millers, K. Preceniece, Thermal processing and irradiation influence to SO4-2 -ion vibration spectra in thallium halides, LATVIJAS PSR ZINÄTNU AKADEMIJAS VESTIS 3 (1988) 50.
165 R. Jenkins and R. L. Snyder, Introduction to X-ray Powder Diffraction (in series of Chemical Analysis, v. 138), John Wiley & Sons, Inc., New York, 1996: a - p. 194; b - p. 89 and ibid.
166 J. I. Langford and D. Louêr, Powder Diffraction, Rep. Prog. Phys. (printed in the UK) 59 (1996) 131.
167 D. L. Bish & J. E. Post (editors), Modern Powder Diffraction, Reviews in Mineralogy, vol.20, Mineralogical Society of America, Washington, DC, (1989): a – Ch. 2, R. Jenkins, Instrumentation, p. 26 and ibid.; b – Ch. 7, D. K Smith, Computer analysis of diffraction data, p. 203.
168 Václav Holý, Ullrich Pietsch, Tilo Baumbach, High-Resolution X-Ray Scattering from Thin Films and Multilayers, Springer, Verlag, Berlin, Heidelberg, New York, 1999.
169 Leonid V. Azároff, Elements of X-ray crystallography, McGRAW-HILL BOOK COMPANY, 1968, p. 95 and ibid.
170 Ronald E. Walpole and Raymond H. Myers, Probability and statistics for engineers and scientists, The Macmillan Company, 1972, p. 95 and ibid.
171 R. L. Snyder, X-Ray diffraction, in: "Materials Science and Technology - a Comprehensive Treatment", R. W. Cahn, P. Haasen, and E. J. Kramer (Eds), VCH Verlagsgesellschaft mbH, Weinheim, FRG. (1992), vol. 2, Ch. 4, p. 316.
172 V. Kozlov, M. Leskelä and I. Mutikainen, Peak Position Correction using Specimen-Displacement Approach in Bragg-Brentano Powder Diffractometer Environment , The 9th symposium on Inorganic and Analytical Chemistry, Helsinki (1996), Programme and Abstracts, p. 38.
173 Topas, ver. 2.1 (software), User's Manual, Diffrac-plus, Bruker advanced X-ray solutions, p. 69 and ibid.
174 C. Latkoczy, T. Prohaska, G. Stingeder, W. W. Wenzel, Simultaneous multi-element analysis of trace elements in soil samples by means of high-resolution inductively coupled plasma sector field mass spectrometry (SF-ICP-MS), Fresenius J. Anal. Chem. (2000) 368:256-262.
175 N. N. Greenwood and Earnshaw, Chemistry of the elements, 2nd ed., Butterworth-Heinemann (1998): a - p. 241.
176 P. J. Sellin, Thick film compound semiconductors for X-ray imaging applications, Nucl. Instr. and Meth. A 563 (2006) 1-8.
177 A. Benrath, F. Gjedebo, B.Schiffers and H. Wunderlich, Über die Löslichkeit von Salzen und Salzgemischen in Wasser bei Temperaturen oberhalb von 100^{o}. I., Z. Anorg. Allg. Chem. 231 (1937) 285.
178 V. Kozlov, P. Kostamo, M. Leskelä, H. Lipsanen, Improved purification and TlBr single crystal growth for the detector applications, Book of Abstracts, 11th International Workshop on Radiation Imaging Detectors, June 28 – July 2, 2009, Prague, Czech Republic, p. II-65.